

Structure and Surface Study of Hydroxyapatite-Based Materials: Experimental and Computational Approaches

Guylène Costentin, Christophe Drouet, Fabrice Salles, Stéphanie Sarda

▶ **To cite this version:**

Guylène Costentin, Christophe Drouet, Fabrice Salles, Stéphanie Sarda. Structure and Surface Study of Hydroxyapatite-Based Materials: Experimental and Computational Approaches. Design and Applications of Hydroxyapatite-Based Catalysts, 2022, 10.1002/9783527830190.ch3 . hal-03727861

HAL Id: hal-03727861

https://hal.sorbonne-universite.fr/hal-03727861

Submitted on 19 Jul 2022

HAL is a multi-disciplinary open access archive for the deposit and dissemination of scientific research documents, whether they are published or not. The documents may come from teaching and research institutions in France or abroad, or from public or private research centers.

L'archive ouverte pluridisciplinaire **HAL**, est destinée au dépôt et à la diffusion de documents scientifiques de niveau recherche, publiés ou non, émanant des établissements d'enseignement et de recherche français ou étrangers, des laboratoires publics ou privés.

Chapter 3. Structure and Surface Study of Hydroxyapatite-Based Materials: Experimental and Computational Approaches

By *Guylène Costentin*[1], *Christophe Drouet*[2], *Fabrice Salles*[3], and *Stéphanie Sarda*[2,] *

Affiliation

[1] Sorbonne Université, CNRS, Laboratoire de Réactivité de Surface (LRS), 4 place Jussieu, 75005 Paris, France

[2] CIRIMAT, Université de Toulouse, CNRS, Université Toulouse 3 Paul Sabatier, ENSIACET, 31030 Toulouse, France)

[3] ICGM, University of Montpellier, CNRS, ENSCM, 8 Rue de l'École Normale, 34090 Montpellier, France

* Dr. Stéphanie Sarda. Corresponding-Author

[2] CIRIMAT, Université de Toulouse, CNRS, Université Toulouse 3 Paul Sabatier, ENSIACET, 31030 Toulouse (France)

Keywords: Catalysis, Hydroxyapatite, Structure, Surface, Advanced Characterization

Abstract:

In addition to designing catalytic materials ever more active and selective, the emergence of new classes of greener catalysts remains very challenging. The apatite family system with hydroxyapatite (HA) structure appears as a good candidate for catalysis due to its eco-compatibility properties, its sorption ability toward organic molecules, and its tunable composition resulting into modulation of its surface properties. Depending on their mode of preparation, these inexpensive and environment-friendly apatitic calcium phosphates exhibit properties of relevance to catalysis, such as large surface area and various morphologies. However, most studies focused so far on the catalytic performance of these compounds, while the study of structure–reactivity relationships required for rationalized optimization remains rather limited. This chapter aims at providing tools to help understand the catalytic behavior of apatite compounds, giving details about their structure, surface properties, and reactivity; this will include both stoichiometric and nonstoichiometric compounds, sometimes biomimetic and potentially substituted. A special attention is dedicated to recent advances in the characterization of their structural properties (bulk and surface/interphase) that have a strong impact on their reactivity, through both experimental and computational approaches to study the mechanisms occurring in the structure or at the crystals surface, as well as thermodynamic and dynamical properties. Remaining characterization challenges for apatite-based catalysts will also be discussed.

1. Introduction

Heterogeneous catalysis plays a key role in the development of green and sustainable chemistry. It appears as an alternative method in organic synthesis as it presents several advantages over homogeneous processes, including simple product isolation while allowing catalyst separation and recycling. Beside the design of catalytic materials always more active and selective, the emergence of new classes of greener catalysts remains very challenging. Due to their eco-compatibility (low production costs using green chemistry in aqueous medium and excellent storage abilities) and their sorption ability toward organic molecules and ionic species selected to tune surface properties, the apatite family system was investigated as catalysts from the 1960s [1-3], but their increasing attractiveness appeared essentially from the 2000s, as illustrated by the growing number of publications dedicated to the use of this type of calcium phosphate as heterogeneous catalyst [4-6], **(Figure 1)**.

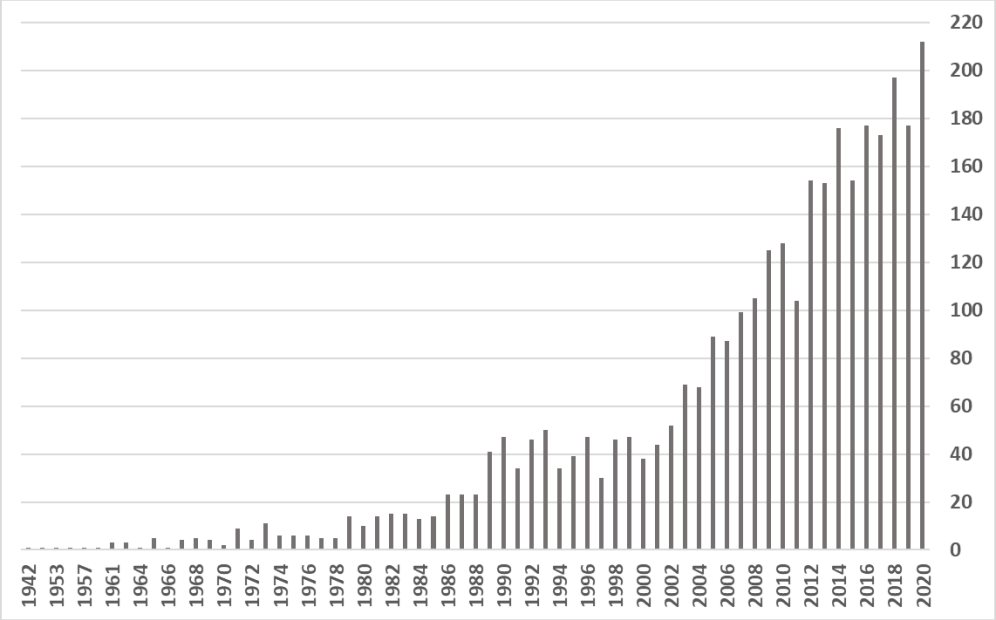


Figure 1. Referenced publications per year for "hydroxyapatite and catalysis" (data from SciFinder Source, 2020).

Such inexpensive and environment-friendly apatitic calcium phosphate as hydroxyapatite (HA, $Ca_{10}(PO_4)_6(OH)_2$) and their non-stoichiometric and/or substituted counterparts can develop large surface areas and various morphologies, depending on their mode of preparation. HA (in its stoichiometric form) is not only stable in aqueous medium (typically above pH ~ 4.5) but also at high temperature [7-9] and can thus operate in large condition ranges, being of interest for both liquid medium (aqueous [10-14] or solvent free [15-

17]) and gas phase reactions [18-20]. Moreover, it was reported to be stable over time on stream, resistant to sintering [18, 21-23] and to leaching [10, 12, 24-29], and recyclable [11, 17, 23, 25-27, 30-40]. Also, as mentioned above, several subtypes of apatitic compounds (stoichiometric or non-stoichiometric, nanocrystalline or not, substituted or not, surface-grafted or not) may be obtained depending on the mode of preparation, thus providing samples with different features of relevance to catalysis.

One of the most interesting characteristics of apatitic calcium phosphates is their surface reactivity. The great modulation of composition by substitution on both its cationic and anionic sites offers endless opportunities for the design of calcium phosphate compounds with the apatite structure, eventually modified by heteroatoms, to be used by themselves as bulk tunable active phases [8], or as suitable supports for the controlled surface deposition of highly dispersed catalytic metallic centers [10, 15, 18, 30, 41-47]. Such an amazing tunable composition ability, including its non-stoichiometry properties, confers to the apatite system a very unique property: it is a rare example of metallic oxide surface exposing not only several types of acid sites, both Brønsted PO-H (proton donor groups) and Lewis (coordinatively unsaturated cationic metallic centers: Ca^{2+} or other exchanged or anchored cation) but also of efficient basic sites, which nature will be discussed in this chapter. Their relative density and strength are tunable by synthesis and activation conditions. Moreover, the substitution ability participates to the adjustment of the acid-base balance properties [48, 49]. Also, when associated to transition metal modification, it also provides additional redox properties [19, 48, 50-58], making of this catalytic material a multifunctional very powerful and tunable system efficient for many classes of catalytic reactions, including C-C formation [14, 59] (Knoevenagel [11, 15, 17, 60], Claisen-Schmidt [61, 62], Michael [47, 63, 64], Guerbet [8, 20, 59, 65-76] reactions...), cycloaddition [77], N-Arylation [78], epoxidation [79, 80], selective [19, 26, 50, 53-55, 81-83] or total [51, 84-88] oxidation, hydrogenation [56, 89], dehydrogenation [90-93], dehydration [2, 56, 91, 94-99], water gas shift [23, 43, 100], reduction of NO_x [52, 57, 58, 101], steam reforming [102], dry reforming [18, 30, 103-105] etc. Despite being thus of prime interest to answer the challenges or many societal issues, going from organic syntheses [14, 32, 60, 106], to environmental reactions (for depollution [6, 10, 12, 52, 57, 58, 84-86, 101, 107] or valorization of bio-sourced molecules [35, 56, 93-95, 108-111]) and reactions for energy [27, 34, 36, 65, 89, 107, 112] etc.), most of the studies essentially focused so far on the catalytic performances, while structure-reactivity relationship approaches needed for rationalized optimization still remain quite limited, especially in the case of liquid phase reactions.

In this view, this chapter aims at providing tools to help rationalizing the behavior of apatite-based catalysts. We will give details about the HA structure, surface properties and reactivity of apatitic compounds, whether stoichiometric or non-stoichiometric and potentially substituted or biomimetic. A special attention will be dedicated to the latest progress in the characterization of their structural properties (bulk and surface/interphase) which have a strong impact on their reactivity, through both experimental and computational approaches. By combining molecular simulations and experiments, the elucidation of the mechanisms occurring in the structure and at the surface as well as the thermodynamic and dynamical properties (in order to take into account the chemical versatility) are also considered to provide quantitative structure-properties relationships [113, 114]. Remaining characterization challenges for apatite-based catalysts will also be discussed.

2. Structure and surface properties of hydroxyapatite: overview

Apatites are crystalline ionic compounds that share common structural features to which the term "apatite" refers [115] – although some local modifications may arise depending on their exact chemical composition [116]. We will focus in this chapter on phosphate apatites, but it may be mentioned that the apatite family also encompasses vanadates, arsenates, silicates and sulfates among other minerals [117]. The generic formula often encountered nowadays for apatites is of the form:

$$M_{10}(XO_4)_6Y_2 \quad (1)$$

where M represents a metal cation, X stands here for phosphorous, and Y refers typically to a monovalent anion such as OH^-, F^- or Cl^-. In these conditions, there is one formula unit per unit cell (Z = 1). In some domains as in mineralogy, however, the notation $M_5(XO_4)_3Y$ is otherwise frequently used. In this case, the atomic arrangement remains of course unchanged, but Z = 2. Although, strictly speaking, the notation in M_5 is more straightforward from a crystallographic point of view, the M_{10} notation is easier to handle when tackling possible non-stoichiometry aspects (*section 2.2*), HPO_4^{2-}-for-PO_4^{3-} substitutions or else hydrolysis-bound transformations into apatite from possible precursor phases like amorphous calcium phosphate (ACP) or octacalcium phosphate (OCP). Therefore, this convention will be used in the following.

Depending on the conditions of preparation and/or of post-treatments, a large variety of apatitic compounds can be obtained, thus exhibiting different features. The term "apatite" thus refers in fact to a large family of compounds with some specificities. Stoichiometric apatites should in particular be distinguished from non-with surface properties which could present

interesting features for catalysis applications. Apatites may also be classified on the basis of the size of their constituting crystals, nanocrystalline apatites exposing a larger contact surface area than micron/millimeter-sized crystals. A sub-category of apatites that cumulate both the non-stoichiometry and the nanocrystalline character is found in biomineralizations as in bone or dentin, but may also be obtained synthetically at low temperature (e.g. near room temperature) and can be referred to as "biomimetic" apatites – although applications of use may extend way beyond the biomedical field. Also, apatite can be substituted with various cations and anions which may confer additional properties, e.g. in terms of catalytic activity. Finally, by way of adsorption of molecular species, it is possible to expose on the surface of the nanocrystals some functional groups, e.g. exploiting the exchange capacity of surface ions.

In the following, we will first address stoichiometric apatites and present the main characteristics of the apatite structure (*section 2.1*). We will then discuss the cases of non-stoichiometric and/or biomimetic apatites (*section 2.2*).

2.1. The apatite structure and model studies

Most apatites crystallize in the hexagonal system (typically in the $P6_3/m$ space group) [115, 116], although a few apatite compounds such as chlorapatite and hydroxyapatite [118] exhibit a monoclinic structure. **Figure 2** represents the typical crystallographic/symmetry features of hexagonal calcium hydroxyapatite (HA) $Ca_{10}(PO_4)_6(OH)_2$. For HA, typical unit cell parameters are a = 9.418 Å and c = 6.881 Å, leading to a theoretical density of *ca*. 3.16 g/cm^3 [119, 120]. Using molecular simulations, both the hexagonal and monoclinic structures have been determined as well as the theoretical localization of the OH^- ions localized along the c-axis [113, 121]. The hexagonal and monoclinic symmetries are in fact strongly linked: starting from the hexagonal symmetry $P6_3/m$, the requirement to access the monoclinic structure is first to fix the position of OH^- groups in a channel along the c-axis, limiting the symmetry of the solid to $P6_3$ by losing the mirror between the OH^- ions, and then by doubling the unit cell and imposing the alternation between 2 adjacent channels for the orientation of OH^- ions, leading to the $P2_1$ type of symmetry [122].

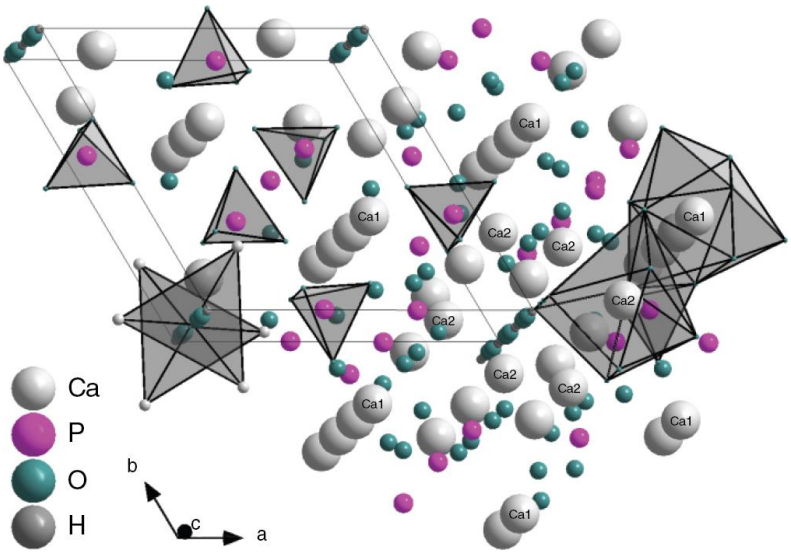


Figure 2. Representation of the hydroxyapatite structure (projection on the (a,b) plane) , evidencing the crystallographic sites Ca1 and Ca2. Source: [117]. Adapted with permission of IntechOpen.

Beside Ca^{2+} and OH^-, a wealth of other cations (such as Mg^{2+}, Sr^{2+}, Cu^{2+}, Zn^{2+}, Na^+, Pb^{2+}, Cd^{2+} etc.) and anions (F^-, Cl^-, CO_3^{2-} etc.) can also be accommodated, at least to some extent, in the apatite structure which is known to be very "open" to many substituents, thus exhibiting a high chemical versatility [117, 123]. Such substitutions may occur either at the time of synthesis (in dry or humid conditions) or during subsequent steps. For example, upon heating HA at high temperature (typically in the range 900-1200°C depending on external conditions [124]), HA dehydroxylation leads to oxyapatite $Ca_{10}(PO_4)_6O$ where one O^{2-} ion "replaces" two OH^-. It may also be mentioned that some end-members can be called using another terminology than "apatite"; one typical example being pyromorphite for designating chlorinated lead apatite.

The three-dimensional cohesion of the structure is ensured by strong electrostatic interactions between the constitutive anions (here essentially the large phosphate ions) and cations – therefore lower stability is to be expected in the case of nonstoichiometric apatites (*section 2.2*). The determination of partial charges by quantum calculations also confirmed that the interaction between phosphate and calcium ions is mainly ionic [125] and that the monoclinic structure seems only slightly more stable than the hexagonal one [126], even if the resulting energy difference is not enough for some authors to affirm a particular preference. Concerning the structure, it has been shown that the coordination number of the different elements plays an important role in the structure. For instance, the different calcium sites have

an influence on the charges carried by the cation and on the related strength of the Ca-O interaction [127], which results in different adsorption properties with guest molecules. To go further, quantum calculations coupled with NMR (Nuclear Magnetic Resonance) results showed the impact of the presence of OH^- ions on the migration of Ca^{2+} as well as the rotation of PO_4^{3-} groups [128]. In the hydroxyapatite structure, phosphate ions PO_4^{3-} are the largest components of the structure. As such, they provide a primary backbone via 3D compact-like piling, generating interstitial sites for the other ions of the structure. Metal cations such as Ca^{2+} occupy two types of crystallographic sites, denoted Ca1 (4 sites per unit formula) and Ca2 (6 sites per unit formula), see **Figure 2**. Ca1 sites are localized along the trigonal axis with the coordinates (1/4, 3/4, 1/2) and (3/4, 1/4, 1/2), forming linear columns along the c-axis. Ca2 sites in contrast form equilateral triangles at z = 1/4 and z = 3/4 on the sixfold screw (senary) 6_3 axes. Adjacent Ca1 and Ca2 sites are linked through shared oxygen atoms from PO_4 tetrahedra. Ca1 sites generate (distorted) polyhedra where the metal ion is in ninefold coordination, while in Ca2 sites it is in sevenfold coordination.

The Ca2 triangles contribute to delimit so-called "apatitic channels" where ions such as OH^- are axially located (**Figure 3**) [116, 120]. In calcium hydroxyapatite, the Ca2 triangular sites correspond to the narrow portion of the channels with a diameter of *ca*. 2.73 Å. At z = 1/2, the channels are delimited by a distorted hexagon of oxygen atoms from PO_4^{3-} ions, thus slightly enlarging the channel diameter (2.85 Å) [129]. The approximate "volume" of the channel in calcium hydroxyapatite may be evaluated to roughly 28 $Å^3$ [130], but the channels should better be seen as a linear series of ovoid cavities rather than straight cylinders [131]. A modulation of unit cell parameters *e.g.* by substitution of calcium/phosphates with other larger/smaller ions may modify the dimensions of these channels by either expanding or compressing the lattice (*e.g.* [132]). For instance, A-type carbonation increases the "a" unit cell parameter and slightly decreases the "c" parameter compared to raw HA [133]. The existence of these channels may allow the exchange of channel ions such as OH^- if adequate conditions are in place (*e.g.* substitution during the synthesis or if enough energy is provided to the system for example by heating). This explains why these compounds are sometimes compared to zeolites [134], although in apatites the channels remain rather small and monodimensional. Besides ions like Cl^-, F^-, OH^-, A-type CO_3^{2-} (i.e. substituting OH^- ions), etc., small molecular species can also be incorporated in these channels such as peroxide, glycine, acetate etc. There are essentially two processes by which molecular species may be entrapped into apatitic channels: *via* the intracrystalline decomposition of unstable lattice ions (*e.g.* molecular oxygenated species) and by synthesis/treatment in the presence of molecular entities to be incorporated [134].

Chemical exchange capabilities involving channel entities may prove helpful for catalysis purposes for providing active species (if conditions allowing the exchange and related ionic mobility are verified). Also, chemical substitution in the apatitic network itself can be another strategy for conferring/improving catalytic properties (*e.g.* vanadate substitution for the oxidative dehydrogenation of propane [135]). It may also be noted that proton diffusion along the channels may come into play in some conditions, allowing the transport of protons across the OH^- channels [131, 136].

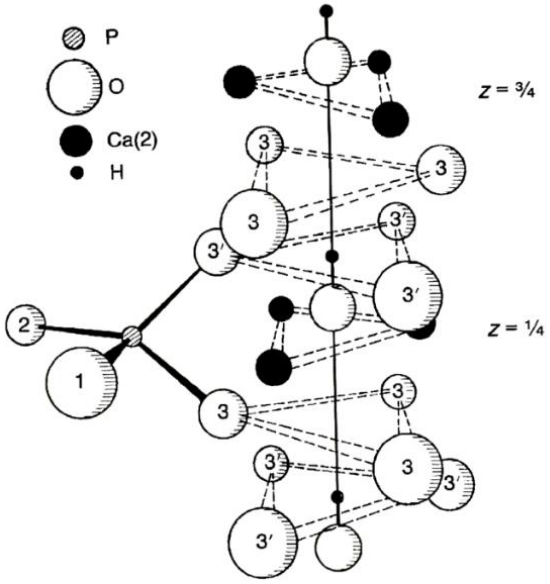


Figure 3. Detail of the hydroxyapatite structure: apatitic channels along the c-axis, hosting the OH^- ions and partially delimited by Ca2 sites. Source: [115]. Adapted with permission of Elsevier Science BV.

Due to the substitution capabilities of apatites, molecular simulations are a relevant complementary tool to determine expected structural changes and the evolution of the unit cell parameters for a large range of compositions, and then compare with experimental data such as XRD (X-Ray diffraction). This is the main validation for force-fields specifically developed for stoichiometric apatites, and, simulation conditions are validated, thermodynamic, dynamic or mechanical properties induced by substitutions can be calculated [137, 138]. In the case of non-stoichiometric samples, it is required to localize the position of the charge deficit (vacancies) and try to compensate the charges in order to obtain a neutral structure. This last situation is more difficult to address due to the models issued from the numerous substitution possibilities [139]. Some theoretical results have shown that, for non-stoichiometric apatites, the vacancies are most probably situated in Ca2 sites with a charge compensation resulting from the

incorporation of H in the structure (H_2O instead of HO^- and HPO_4^{2-} instead of PO_4^{3-}). Such calculations thus concluded that hydration has a strong impact on the apatite structure [140].

After understanding the structure of HA as a reference apatitic compound, the description of the substitution positions (in simple cases where only ions with similar charges are considered) or several substitution-charge compensations concerted mechanisms have been elucidated using molecular simulations. This is the case of carbonate ions (CO_3^{2-}), one of the main substitutions occurring in apatites, either on purpose (precipitation in the presence of a source of carbonates) or by contact with atmospheric CO_2 in some preparation conditions. Carbonate ions can be found in substitution of hydroxyl groups (type A defaults) or phosphate groups (type B defaults). Quantum calculations have determined that substitutions could occur in both default sites, strongly modifying the electrostatic potential of the solid and therefore the adsorption performances [141, 142]. In addition, the corresponding charge compensation mechanisms were investigated by invoking the presence of supplementary OH^- groups or the substitution of Ca^{2+} by alkaline ions [143, 144] (**Figure 4)**. As a typical illustration, the interaction between Na^+ and CO_3^{2-} seems to play an important role in the limitation of structural distortion. From the comparison between calculations with substitutions in A, B or simultaneously in A and B sites (see *section 2.2*) , it appeared that occupancy of CO_3^{2-} in both sites could result as a configuration with a minimum energy [143], confirming that this mechanism is plausible while other authors have shown that other configurations (involving only sites A or B) are preferential. This discrepancy is mainly based on the chosen charge compensation mechanisms [142, 145]. The substitution of OH^- groups by halogens (F^-, Cl^-, Br^-) has also been the subject of many theoretical studies. In particular, fluorapatite was widely investigated, demonstrating that the structure is essentially ionic in this case [146]. In addition, the transport of F^- ions in the structure seems to impose a concerted mechanism along the c axis, implying both framework and interstitial sites: one interstitial site replaces an ion in a structural site, which can replace an interstitial [147], and so on. Regarding mixtures of halogens (F^- and Cl^-), the most stable structure was defined by distinct channels containing either F^- or Cl^-, with an equimolar composition. In the case of combined F^-/CO_3^{2-} substitution, the fluoride ions preferentially adopt interstitial positions [127].

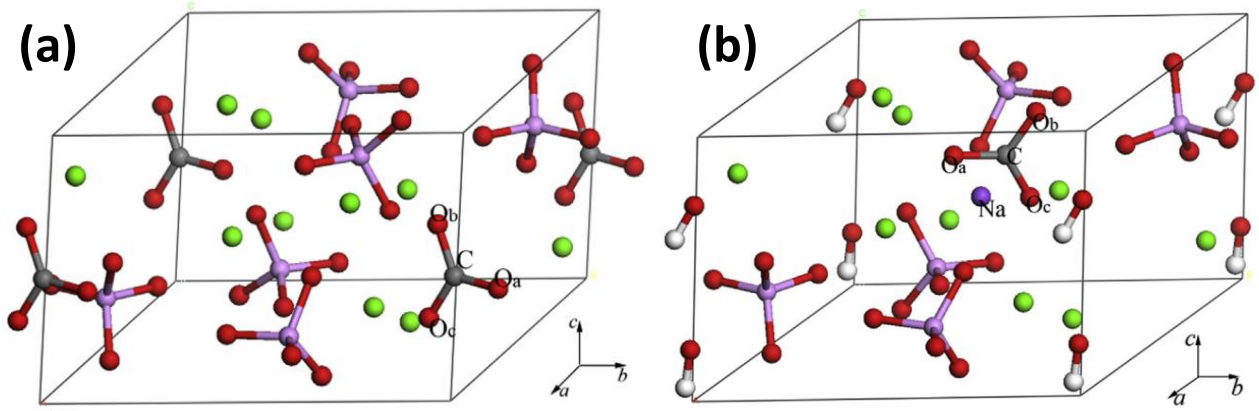


Figure 4: Illustration of the most energetically favoured configuration for type-A carbonated apatite (a) and the most stable structure of type-B carbonated apatite with charge compensation by co-substituting a Na^{+} ion for a Ca^{2+} ion (b), after geometry optimization. Source: [144]. Adapted with permission of Elsevier.

The substitution of Ca^{2+} by other divalent cations has also been characterized by molecular simulations in link with the possibility to enhance the catalytic properties [148]. From molecular simulations, it has been concluded that the position of the substituents is strongly dependent on the nature of the cation (mainly its charge, radius and electronegativity) and on the spatial constraints: for instance Zn^{2+} preferentially occupy the Ca 2 sites (see **Figure 5** as a typical illustration), which is less obvious for Mg^{2+} [122, 127, 149, 150], In contrast, substituting Sr^{2+} cations are preferentially situated in Ca 2 sites for an amount above 10 at.% but in Ca 1 sites below 5 at.% [151], even if some authors proposed a different threshold value between the two preferential sites (e.g. 20at. %) [152]. A similar behaviour was observed for Ba^{2+} [153]. In the case of Pb^{2+}, a reorganisation of the oxygen atoms around the cations was observed (in both Ca1 and Ca2 sites) and the substitution energy appears strongly impacted by the formation of covalent-like bond between divalent cations and oxygen [153]. Finally, few studies have focused on the co-doping for cations [149] or cations and anions [154]. The doping in Ag^{+} and Sr^{2+} has for example been investigated from a modelling point of view and, while the two cations individually replace Ca^{2+} in sites 2, the mixture has a different behaviour with Sr^{2+} placed in Ca1 sites and Ag^{+} in Ca2 sites [155].

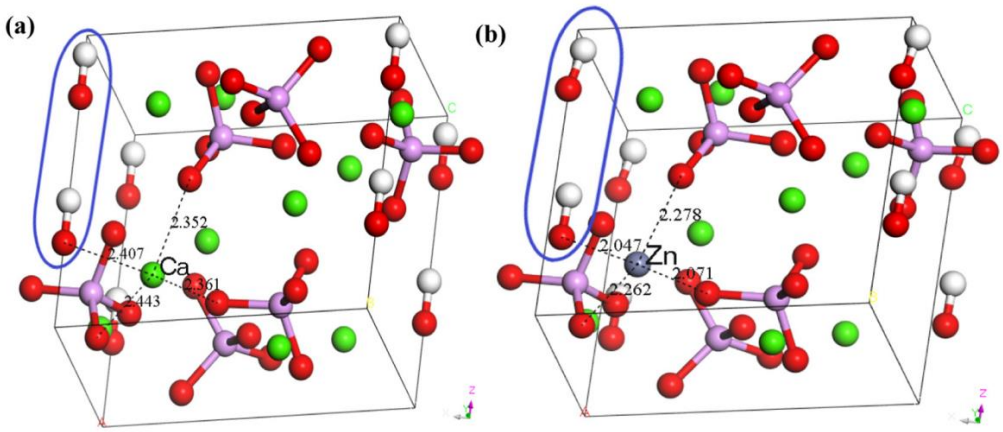


Figure 5: DFT-optimized structures for (a) HA and (b) Zn-doped-HA. Source: [156]. Adapted with permission of Elsevier.

Although progresses have been made in the last decades on the modelling of apatite compounds, additional work is needed in this field. Due to the numerous possibilities of substitutions and therefore compensation mechanisms (vacancies for OH^- and Ca^{2+}, substitution of Ca^{2+} cations, substitution of PO_4^{3-} by other anions etc.) combined with different database sets and approaches, theoretical calculations have sometimes led to very different results considering the same apatitic compounds [142, 143, 145]. It is therefore still necessary to clarify the mechanisms involved during these substitutions by coupling experiments and theoretical calculations in order to fix the conditions leading to the calculated results and better ascertain their accuracy.

Knowing the bulk structure, the determination of the surface structure(s) is of primary relevance in the catalysis field, so as to be able to analyse the surface activity. Then, the elucidation or prediction of the ionic conductivity and polarisation mechanisms can be of great importance to better apprehend the catalysis activity of doped apatites. For that purpose, molecular simulations should bring appropriate solutions to clarify the different components present in the solid phase and involved in the catalytic mechanisms. However, to date, few simulations have been performed in this way [157]. Indeed, while the simulation of apatitic structures doped with trace elements has already allowed adjusting the mechanical or antibacterial properties of apatites for biomedical applications, similar calculations to extract the electronic properties and potential interactions should be proposed for catalysis systems [158, 159].

2.2. Specificities of non-stoichiometric and/or biomimetic apatites

As mentioned previously, apatite compounds can exhibit different characteristics which strongly depend on their synthesis conditions. While low temperature synthesis processes (lower than 100 °C, typically close to room temperature) usually generate nanocrystalline non-stoichiometric apatites, also referred to as "biomimetic" [160-162], apatite samples prepared at higher temperatures are often close to stoichiometry (providing that precipitation is achieved in basic medium) as the thermal activation of ions allows for faster diffusion and greater crystallinity. When short heating periods are used for sample preparation at high temperature, apatites composed of nanosized crystals may sometimes be obtained, however, in most other cases, significantly larger crystals are formed.

The physicochemical and morphological features of biomimetic apatites have been explored in details in the last years thanks to technological evolutions of materials characterization techniques. They exhibit specific properties mainly related to their surface structure that exhibits non-apatitic features in the form of an ionic hydrated layer [163, 164]. From a chemical point of view, the composition of biomimetic apatites thus strongly differs from that of HA [165]. In comparison with stoichiometric HA (molar ratio of Ca/P equal to 1.67), which is the most stable and least soluble calcium phosphate at ambient conditions, biomimetic apatites present a non-stoichiometric composition (Ca/P lower than 1.67).

One important factor in the comprehension of apatites behaviour is the possible departure from stoichiometry. Non-stoichiometry is related to vacancies in M sites and Y sites (see Eq 1 in the *section 2.1*). Several types of non-stoichiometric apatites can be distinguished depending on the substituents and vacancies present in these structures. The non-stoichiometry starting from the HA composition may be explained on the basis of vacancies in both Ca and OH sites, concomitantly to the substitution of PO_4^{3-} ions by bivalent ions, like HPO_4^{2-} or CO_3^{2-} [160]. This incorporation of bivalent ions are mainly compensated by a complex defect associating of anionic and cationic vacancies, partially confirmed by Rietveld analysis [166]. Although some variations can be observed, such non-stoichiometric HA generally respond to the global chemical composition [165]:

$$Ca_{10-x}(PO_4)_{6-x}(HPO_4 \text{ or } CO_3)_x(OH \text{ or } ½\ CO_3)_{2-x} \quad (2)$$

with $0 \leq x \leq 2$. It can be noticed that carbonate ions may occupy different types of sites historically named as A and B, where sites A correspond to carbonate substitution in the monovalent anionic sites of the apatite structure (substitution of some OH^- ions in the case of HA) and sites B to trivalent anionic sites (substitution of some PO_4^{3-} ions).

The nanocrystalline character is another important feature to be taken into account when dealing with apatite compounds. HA generally exhibits typical rod or platelet like morphology (depending on the synthesis method), elongated along the c-axis of the hexagonal apatitic structure, and nanosize dimensions of the crystals allows increasing the extent of surface area being potentially activated, and therefore impact surface interaction [167]. For example, the mean crystallite dimensions of biomimetic apatites reach about 15-30 nm length and 6-9 nm width, as opposed to micron-sized crystals for sintered HA [161]. The crystallinity degree of these apatites is then rather low, and they are thus generally referred to as "poorly-crystalline" apatites in the literature [161, 164]. It may however be remarked that, in some cases, unsintered HA precipitated close to water boiling point may also be composed of nanosized crystals. Therefore, several approaches can be developed to modulate the surface area of apatitic samples.

In addition to the nanosized dimensions and nano-rods platelet morphology, biomimetic apatites exhibit on their surface a non-apatitic ionic and hydrated layer that provides very specific surface reactivity. The existence of this structured but non-apatitic surface layer was evidenced especially by spectroscopic techniques as Fourier Transform Infrared (FTIR) [168] and solid-state NMR spectroscopy [169] (see *section 3.1*). Such biomimetic apatite nanocrystals may then be described as an apatitic core (often non-stoichiometric) covered by an ionic and hydrated layer containing rather labile ions (Ca^{2+}, HPO_4^{2-}, CO_3^{2-} etc.) [161], as illustrated in **Figure 6**, that can take part to exchange or adsorption reactions. This hydrated layer should not be confused with a Stern double layer. Instead, this is the result of the precipitation process of biomimetic apatites. Moreover, the hydrated layer, particularly important in freshly precipitated apatites, progressively transforms into the more stable apatitic lattice upon ageing in aqueous solution and progressively disappears as the stable apatite domains (in the core of the crystals) develop with time, incorporating ions from the hydrated layer in the apatitic lattice (maturation) [163, 164, 170]. This "maturation" phenomenon can be slowed down when inhibitors of apatite crystal growth like Mg^{2+} or CO_3^{2-} are present in the hydrated layer but cannot be stopped [163]. The presence of this hydrated surface layer is responsible for most of the properties of biomimetic apatites, and in particular their high surface reactivity. The ionic substitution and molecular adsorption capabilities of the nanocrystals are greater than those of stoichiometric HA due to the high mobility of the mineral ions from the hydrated layer [161, 163], dependently on the composition of the hydrated layer and on the maturation stage (see *sections 3-4-1 and 3-4-2*).

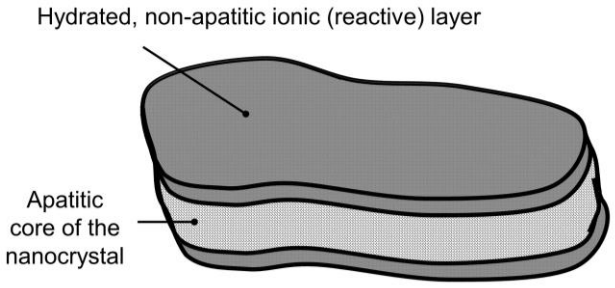


Figure 6: Schematic model of the peculiar structure of biomimetic apatite nanocrystals. Source: Stéphanie Sarda, Christophe Drouet.

In computational studies, the activities and description of apatite surfaces have been generally characterized using a slab or nanopore model. However, these models are not perfectly adapted for studying the processes occurring on apatite surfaces. More recently, the understanding of the structure of biomimetic nanocrystalline apatites has focused researchers' attention, revealing the coexistence on the nanocrystals of an ordered core and a disordered surface [171], in good agreement with experimental evidence. The interest of the molecular dynamics simulations is also to probe the impact of the temperature on the apatite structure and to quantify the disorder of the nanocrystals [171, 172]. To better understand the chemical composition of surface, DFT (density functional theory) calculations have been combined with NMR results and the estimation of chemical displacements was compared to experimental data, evidencing the impact of the atoms localization, as surface atoms exhibit a larger displacement compared to atoms from the bulk. The disorder observed for OH groups modifies the signal of P and allowed proposing a description of HA interfaces [128].

The distribution of acidic sites and basic sites on the apatitic surface depends on the apatite conditions of formation and characteristics such as Ca/P ratio and the presence of substituents. Ionic substitutions in the apatitic structure may indeed allow regulating the acidity and alkalinity of the crystal surface [173, 174] (see *section 3-2-2*). Thus, the tunable composition and surface properties of substituted (often non-stoichiometric) apatites have been widely used as acid-base catalyse for many classes of catalytic reactions (hydrolysis, alcoholysis, esterification etc.) [76, 95, 175]. However the excellent physico-chemical and surface properties of biomimetic (*i.e*. both non-stoichiometric, nanocrystalline and presenting a non-apatitic surface' layer) have essentially been exploited to-date for biomaterials applications [165], but have only recently developed in heterogeneous catalysis, which is thus still a domain to examine.

2.3. The relevance of apatites in catalysis

Bulk and/or surface composition to account for acid base properties?

The acid-base balance of the surfaces of hydroxyapatite and hydroxyapatite-modified systems are of primary interest for catalytic reaction mechanisms. The originality of the hydroxyapatite system is related to the fact that it can be used as acid catalysts (for examples: Friedel-Crafts [41], Diels Alder[25] dehydration [2, 56, 91, 94-99, 176], etc.), as basic catalysts (for examples: dehydrogenation of alcohol [90, 176], hydrogen transfer [7, 90], Knoevenhagel, [11, 15, 17, 60], Claisen-Schmidt [61, 62], Michael [47, 63, 64, 177], etc.), as well as bifunctional acid-base catalysts (for examples: Aldol reactions [178], and cascade reaction such as Guerbet reaction [8, 20, 59, 65-76]). Interestingly, the surface reactivity over hydroxyapatite is structure sensitive: both the crystallinity and the stoichiometry were found to influence the catalytic behavior. Despite being detrimental to the specific surface area, high crystallinity was reported to promote the performances of the system (even if only the surface is directly involved in the reaction) [179], indicating that the surface arrangement of the different active sites is also important, probably due to involvement of cooperating effects between different sites working as acid-base pairs in concerted mechanism or in successive elementary steps. Moreover, many catalytic results are discussed in line with the stoichiometry of the bulk material [66, 68, 94, 95, 99, 100, 105, 180-183] using the Ca/P bulk ratio that can be varied by the preparation conditions to account for the modulation of the acid-base properties: globally, the lower the Ca/P molar ratio the higher the acidity, and the higher the Ca/P molar ratio, the higher the basicity [20, 66, 70, 94, 95, 99, 105, 174, 182, 183]. This is illustrated in **Figure 7** on the basis of temperature programmed desorption (TPD) experiments of basic NH_3 and acid CO_2 molecules that are commonly used to quantify the total amount surface acid and base sites, respectively [99]. Similar tendencies were reported from the model conversion of isopropanol accounting for acid and base sites: a higher selectivity to acetone (basic dehydrogenation route) than in propylene (acidic dehydration route) is obtained as the Ca/P molar ratio increases [174]. However, from another model reaction, *i.e.* the basic conversion of 2-methylbut-3-yn-2-ol (MBOH) into acetone and acetylene reaction that is a very sensitive tool to probe basic reactivity [184], the situation appears more complex: the use of the Ca/P descriptor is valid at the first order when comparing an homogeneous series of compounds prepared in very similar conditions [185], but some inconsistencies with the Ca/P macroscopic ratio were encountered when considering samples prepared in different pH conditions, which was ascribed to very different carbonation contents [186].

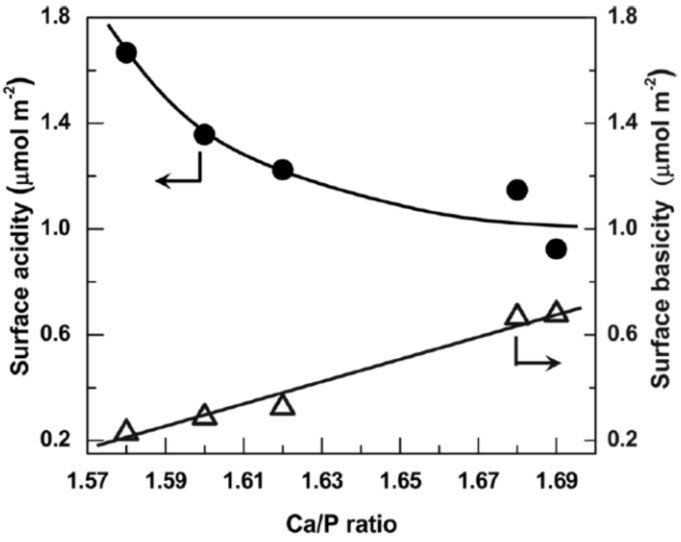


Figure 7: Influence of the Ca/P molar ratio on the surface density of acidic and basic sites probed by NH_3 and CO_2 TPD (temperature programmed desorption). Source: [99]. Adapted with permission of American Chemical Society.

In fact, the origin of the empirical relationships between bulk composition and surface reactivity is very questionable. Based on the simplified $Ca_{10-z}(HPO_4)_z(PO_4)_{6-z}(OH)_{2-z}.nH_2O$ ($0< z \leq 1$) which is the formula of non-stoichiometric apatites, it may roughly be explained on the one hand by the larger amount of HPO_4^{2-} (likely to account for the PO-H Brønsted acidity on the surface) that is associated to Ca^{2+} deficiency in under-stoichiometric compounds [66] and, on the other hand, to the higher concentration in basic OH^- in stoichiometric compounds [186]. Note that, by analogy with the case of CaO, the basicity was sometimes simply claimed to be associated to the presence of Ca^{2+} [66] which is a misinterpretation since the basic sites in CaO are O^{2-} and surface OH^- [187]. In addition, such a rapid explanation suffers from several limitations:

i) It completely skips the possible influence of cation content (Ca^{2+} or other ions in the case of substitution (co-precipitation or ion exchanged) or grafted complex) likely to provide by themselves Lewis acidity (quite weak of Ca^{2+}, but possibly stronger depending on the nature of hetero-cation involved) [49].

ii) There is a lack of data for so-called “over-stoichiometric” compounds, since the influence of bulk carbonation responsible for this over-stoichiometry is rarely discussed [68]. Moreover, high molar ratio of Cation/P values can result from synthesis carried out in the presence of a very large excess of cation (Ca(+Na)/P) precursor ratio up to 5.5 [174]: this particular case may correspond to highly Ca^{2+} doped materials with formation of CaO like

domains [68, 174]. In this later case, the acid-base properties are no more related to the apatite active phase only.

iii) Due to the complex general formula $Ca_{10-x-B}\square_{Ca\ x+B}(PO_4)_{6-x-B}(HPO_4)_x(CO_3)_{A+B}(OH)_{2-x-2A-B}$, $\square_{OH\ x+2A+B}$, where A and B account for A and B type carbonate contents and $\square$ stands for Ca and OH vacancies ($\square_{Ca}$ and $\square_{OH}$), some antagonistic compensating effects (Ca deficiency and B type carbonation) are hidden by the global Ca/P = (10–*x*–B)/(6–B) value [186]. In addition, the Ca/P ratio does not account for the A type carbonation. However, it greatly impacts the concentration in OH^-. This indicator was found to be a better bulk descriptor than the Ca/P molar ratio to account for basic properties, which directs to a key role played by OH^- in the basic properties [186].

iv) Correlation between the surface reactivity and the bulk Ca/P molar ratio value is quite surprising given the very different compositions between the surface and the bulk. The surface layer probed by XPS (X-ray photoelectron spectroscopy) analysis (depth ~ 10 nm) indicates that the surface Ca/P ratio is always significantly lower than the bulk one [66, 174, 188] even when considering crystalline terminations [189, 190]. Such a discrepancy between the bulk and surface Ca/P values seems to be specific of the hydroxyapatite system since it is not observed for the β-TCP tricalcium phosphate [66]. Consistently, Ospina et al. predicted from DFT simulations and HRTEM (High-resolution transmission electron microscopy) that surface terminations of crystalline hydroxyapatites particles can be enriched in phosphates species [191]. This is also confirmed by ion scattering spectroscopy (ISS) that enables to analyze the evolution of the Ca/P ratio of the first atomic surface layers thanks to a progressive scraping of the surface *via* He^+ bombardment (few Å probed) concluding to a gradient of concentration of calcium, with a progressive relative enrichment in calcium in the deepest layers: hence part of calcium tends to be relaxed in the sub-surface, rather than at the top surface [9, 189]. Interestingly, in the case of vanadium substituted $Ca_{10}(VO_4)_x(PO_4)_{6-x}(OH)_2$ stoichiometric apatite solid solution, a reverse tendency was observed, where vanadate groups are relaxed in the sub-surface leading to over exposure of calcium cations (surface Ca/(P+V) >2 for $x \geq 4$ whereas bulk Ca/(P+V) = 1.67) [9].

As mentioned above, surface characterization approach based on NH_3 and CO_2 TPD measurements is widely used. It leads to quite rough correlation tendencies between the total amount of acidic and basic sites probed with catalytic performances. For instance, in the case

of the production the acrylic acid from dehydration of lactic acid [99] or of the ethanol to n-butanol Guerbet conversion reaction [68] a volcano type dependence between the reaction rate and ratio between the amount of acid and basic sites was reported. This underlines the cooperation between acid and base sites in a concerted mechanism or in complex cascade network. The use of CO_2 to titrate the basic sites has however several drawbacks and caution should be taken : pretreatment has to be carefully done to desorb the surface carbonate ions prior to adsorption (the IR fingerprints of surface carbonate and hydrogencarbonate were discriminated from those of the bulk [192]) and blank experiment or limited temperature should be applied to avoid misleading interpretation due to high temperature bulk carbonate decomposition that would result in overestimating the amount of basic sites. In addition, CO_2 is known to react with the surfaces [94] and, especially, being also a soft Lewis base, it might interact with strong Lewis acid [193] (especially in the case of hydroxyapatites modified with strong Lewis acid cations). Recently, SO_2, which is a stronger acid molecule than CO_2, was reported to be more convenient to titrate all basic sites over hydroxyapatite [94]. Irrespectively of the accuracy of TPD characterization to quantify the acid and basic sites of HA, only the total amount of sites is probed (eventually discussed in terms of weak, medium or strong strengths), but it does not provide information on the chemical nature of the sites probed. When there are several types of basic or acid sites present on the surface (typical case of HA with Brønsted and Lewis acid sites), it is moreover questionable if the total amount or only a fraction is really involved for a given catalytic reaction.

All these considerations emphasize the need for refined surface characterizations, including *operando* approaches [75] to more precisely identify the nature of active species and rationalize the surface reactivity.

3. Advances in the characterization of structural and surface properties of hydroxyapatite: experimental and computational approaches

3.1. Structural and compositional characterization

The atomic Ca/P molar ratio, equal to 1.67 for stoichiometric (non-carbonated) apatite, is an important feature of the composition of apatitic compounds. For non-stoichiometric non-carbonated apatites (Ca/P lower than 1.67) where some HPO_4^{2-} ions substitute to PO_4^{3-}, the Ca/P molar ratio is directly related to the amount of cationic (and OH) vacancies. For non-stoichiometric carbonated apatites where CO_3^{2-} ions substitute PO_4^{3-} ions (B-type carbonate apatites), cationic vacancies are related to the Ca/(P+C) ratio. In more complex compositions for example with Sr^{2+} cationic substitution, the (Ca+Sr)/(P+C) molar ratio has in turn to be

taken into account to relate to the amount of vacancies [120]. In practice, depending on the preparation conditions, except careful attention devoted to the decarbonation of the precursor and base solutions, A and B-type carbonate, as well as bulk HPO_4^{2-} co-exist in the apatitic compounds resulting in complex general formula, $Ca_{10-x-B}\square_{Ca,x+B}(PO_4)_{6-x-B}(HPO_4)_x(CO_3)_{A+B}(OH)_{2-x-2A-B}\square_{OH,x+A+B}$ with antagonistic effects on the Ca/P ratio and huge impact of the amount of OH vacancies [186]. To determine these ratios, various chemical analyses can be used. The amount of calcium (and other substituting cations) can be determined using several techniques including atomic adsorption spectroscopy (AAS), inductively coupled plasma (ICP) emission spectroscopy, ionic chromatography, ionometry using specific electrodes, complexometry with a complexing agent as EDTA (ethylene diamine tetracetic acid), etc. [194]. The total phosphorus content (included in PO_4^{3-}, HPO_4^{2-}) can be titrated by ICP or ionic chromatography. However, to get the orthophosphate ions amount, titration by UV spectrophotometry of the phospho-vanado-molybdic acid complex is among the most used and most suitable. The amount of HPO_4^{2-}, related to non-stoichiometry, can be subsequently measured by difference using a second run of the same method after thermal conversion of HPO_4^{2-} into pyrophosphate ions [195]. For carbonate content titration, an accurate method is coulometry, exploiting an electrochemical cycle in acidic conditions. It can be noticed that FTIR spectroscopy can also be used to determine total carbonate content relatively to phosphate bands [196], but also apatitic and non apatitic PO_4^{3-} and HPO_4^{2-} content (in the case of biomimetic apatite), from mathematical decomposition of the ν_4 band related to the P-O bond of FTIR spectrum [197, 198]. Moreover, a very accurate technique for the determination of Ca/P molar ratio by X-Ray diffraction (XRD) has been developed (ISO standard 13779) for non-carbonated samples.

As previously detailed in *Section 2-1*, apatites generally crystallize in the hexagonal system ($P6_3/m$ space group) [115, 116] and XRD is an essential method for the characterization of HA and related compounds [199]. The peaks position in XRD patterns allows for the identification of apatitic calcium phosphates as recorded in the databases of diffraction peaks of hydroxyapatite (JCPDS file number 9-0432) (**Figure 8**). In addition to phase recognition, XRD can be used to estimate crystallographic parameters such as the unit-cell dimensions, mean crystallize dimensions and crystal strain parameters; and thereby evaluate the effects of ion substitutions on the structure. Substitution of calcium or phosphate ions by larger entities induces an increase of the unit-cell parameters; however, the replacement of a monovalent anion (*e.g.* OH^-) by a larger one induces an increase of the "a" parameter and a decrease of the "c"

parameter [120, 200]. Moreover, more elaborate treatments using Rietveld analysis of XRD data can be performed for more accurate determination of crystallite dimension, microstrains, unit-cell parameters and phase composition, but also structural information such as the atomic position of substituted ions or vacancies. Such data treatments have been performed for example to study the orientation of carbonate species and the location of vacancies in nonstoichiometric carbonate apatites [166] or the location strontium ions in Sr-containing apatites [151].

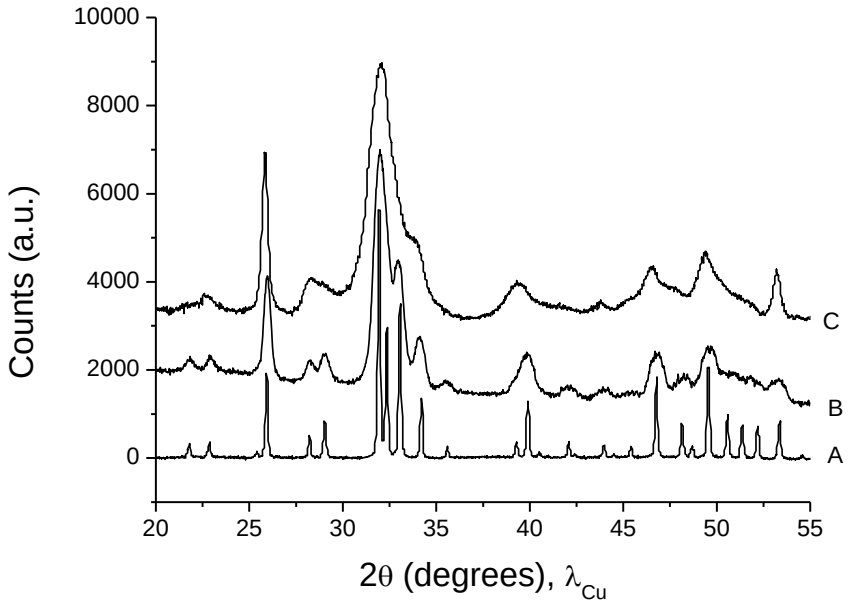


Figure 8: Typical XRD patterns for sintered stoichiometric HA (A), freeze-dried stoichiometric HA (B) and for biomimetic apatite (C) evidencing different degrees of crystallinity. Source: Stéphanie Sarda, Christophe Drouet.

Beside XRD, electron microscopy techniques are widely used for the determination of apatitic crystal morphology, their size and organization [120]. Indeed, apatitic calcium phosphates can show a variable morphology depending on their synthesis conditions. While precipitated amorphous calcium phosphates appear most generally as spherical units (diameter between 20 and 300 nm), well-crystallized apatites generally exhibit a rod/needle-like morphology with crystals elongated along the c axis of the hexagonal structure (**Figure 9**). Some approaches such as hydrothermal synthesis may lead to apatite crystals with a very high length/width ratio that can be considered as fibers [201].

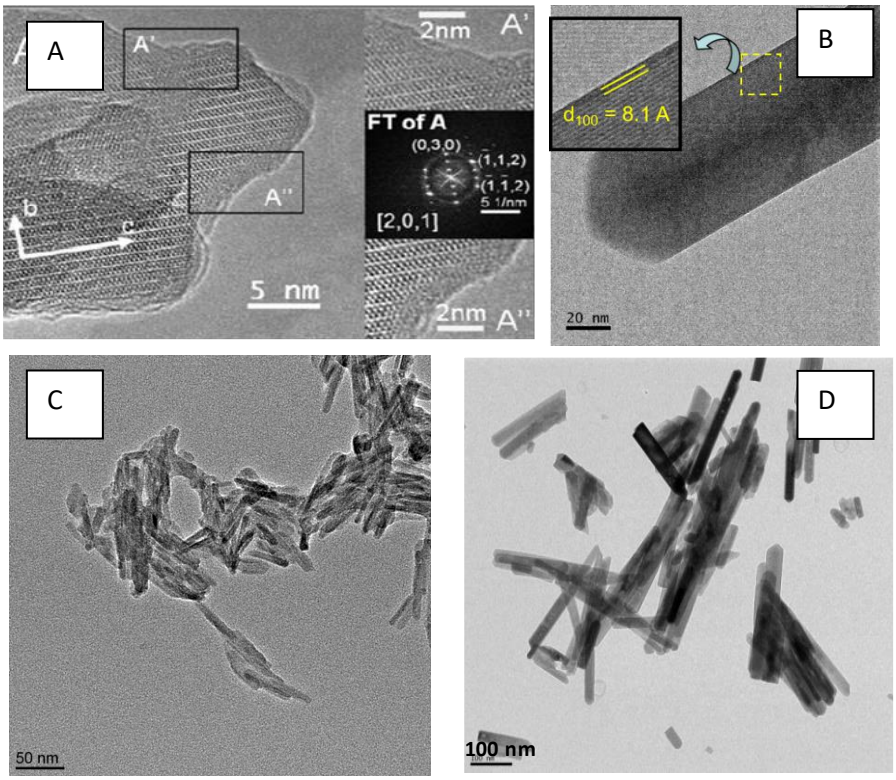


Figure 9: HRTEM pictures of (A) an apatite synthesized at 40 °C (Source: [202]. Adapted with permission of American Chemical Society), (B) a stoichiometric hydroxyapatite obtained by coprecipitation at 80 °C and high pH (after drying at 100 °C and thermal treatment under Ar flow at 350 °C) indicating it is crystalline up to the surface (Source: [190]. Adapted with permission of American Chemical Society), TEM observations of (C) a biomimetic nanocrystalline apatite synthesized at ambient temperature (aged in solution for 1 month) and freeze-dried, (D) typical rod like morphology of crystalline stoichiometric hydroxyapatite obtained by coprecipitation at 80 °C and high pH and dried at 100 °C (Source: [192]. Adapted with permission of American Chemical Society).

In addition to morphological and dimensional information, electron microscopy coupled with Energy Dispersive Spectrometry (EDS) or Wavelength Dispersive Spectrometry (WDS) can also be used for composition determination. These techniques are used for the determination of main elemental components of calcium phosphate compounds (as Ca, Mg, P, F). However, their accuracy depends on the stability and the characteristics of the apatitic sample (surface roughness, conditions of analyses, size) and the analysis of non-stoichiometric apatites remains difficult even with the use of adequate standards. Identification of phases at the microscopic level using electron diffraction, as selected area electron diffraction (SAED), can also be performed on calcium phosphates samples. HRTEM can also allow the identification of the

crystallographic planes, the determination of the d-spacings, the orientations of crystals, and the observation of crystal defects of apatitic compounds.

It should however be noticed that all of these beam techniques under vacuum can generate sample damages, as frequently observed with hydrated apatitic compounds, especially with biomimetic apatites and may ultimately lead to phase decomposition [203, 204]. Moreover, calcium phosphates are nonconductive compounds and it is often necessary to limit the charge effect *via* for example a coating with an electrically conductive layer. Working at low accelerating voltage at short working distance or under low vacuum should then be preferred, or the use of environmental microscopes to prevent the alteration of hydrated apatitic compounds. The use of cryogenic conditions during electron microscopy analyses can also be recommended.

In addition to electron microscopy, atomic force microscopy (AFM) may lead to complementary characterization details by allowing imaging the sample surface at the atomic scale, not only in ultrahigh vacuum but also in ambient air and even liquid environments [164]. AFM is based on the detection of a tip/sample surface interaction force, giving a map of surface topography [205]. Moreover *in situ* AFM can highlight the interaction of ions or molecules with HA surfaces in aqueous environments at the nanometer scale [206], as for example the interaction between HA in contact with citrate-containing solutions [207] or with proteins [208].

For surface assessments complementary to microscopy techniques, the specific surface area of the samples can be measured according to the BET (Brunauer−Emmett−Teller) method *via* nitrogen adsorption. However, since an outgassing initial stage is necessary to evacuate pre-adsorbed H_2O/CO_2 and other physisorbed species, care should be taken also when analysing hydrated (biomimetic) apatites so as to limit crystals degradation.

Spectroscopic techniques (FTIR, Raman, solid-state NMR etc.) are particularly useful for characterizing apatite compounds as they are in particular sensitive to the local environment of phosphate, carbonate and hydroxide ions. Vibrational spectroscopies (FTIR, Raman) appear in particular as interesting tools for the identification of such compounds. As explained previously, apatites may exhibit complex structures due to ion substitutions and vacancies and they can be poorly crystallized, which drastically limits the potential of XRD. Also, the principal advantage of vibrational spectroscopies over diffraction techniques is the identification of fine structural details, e.g. concerning the presence and location of PO_4^{3-},

HPO_4^{2-}, CO_3^{2-} or OH^- groups within the (nano)crystals or on the surface (see *section 3.4*). Moreover, these techniques are non-invasive and can adapt to a wide range of experimental conditions (temperature, wet conditions etc.).

Involving transitions between vibrational levels, these methods can particularly detect phosphate, carbonate, hydroxide ions and water molecules in apatites spectra (**Figure 10**). The PO_4^{3-} groups present four main vibration domains: ν_1 (around 950 cm^{-1}), ν_2 (400-470 cm^{-1}), ν_3 (1000-1150 cm^{-1}), ν_4 (500-620 cm^{-1}) and the main FTIR and Raman line positions of hydroxyapatite are summarized in **Table 1**. In addition to phosphate groups vibrations, several OH^- ion vibration bands can be distinguished: one domain corresponding to the stretching of the O-H bond (3400–3720 cm^{-1}) and a libration band, corresponding to a rotational energy level of the OH^- ion in the lattice (630–750 cm^{-1}) [120, 198]. The OH^- vibration and libration modes are very sensitive to the nature of the surrounding cations and to hydrogen bonding; it has for example been shown in fluoride- and chloride-containing apatites that the OH bands can be shifted compared to their position in hydroxyapatite [209]. As for water molecules, they exhibit three vibrational modes: the symmetric and antisymmetric stretching vibration, very close in energy and difficult to distinguish, giving a broad absorption band on FTIR spectra (3000–3700 cm^{-1}); and the H-O-H bending vibration displaying a narrower band at about 1640 cm^{-1}. Like OH^-, water molecules are very sensitive to hydrogen bonding. In addition to the characteristic fingerprints of OH running along the c channels (3570 cm^{-1}), or water molecules, lower intensive bands in the 3720-3640 cm^{-1} range, detected from self-supported pellet, are ascribed to ν_{PO-H} from bulk defective hydrogenphosphate (3657 cm^{-1}) and surface terminated phosphate groups [210] (*see section 3.4*).

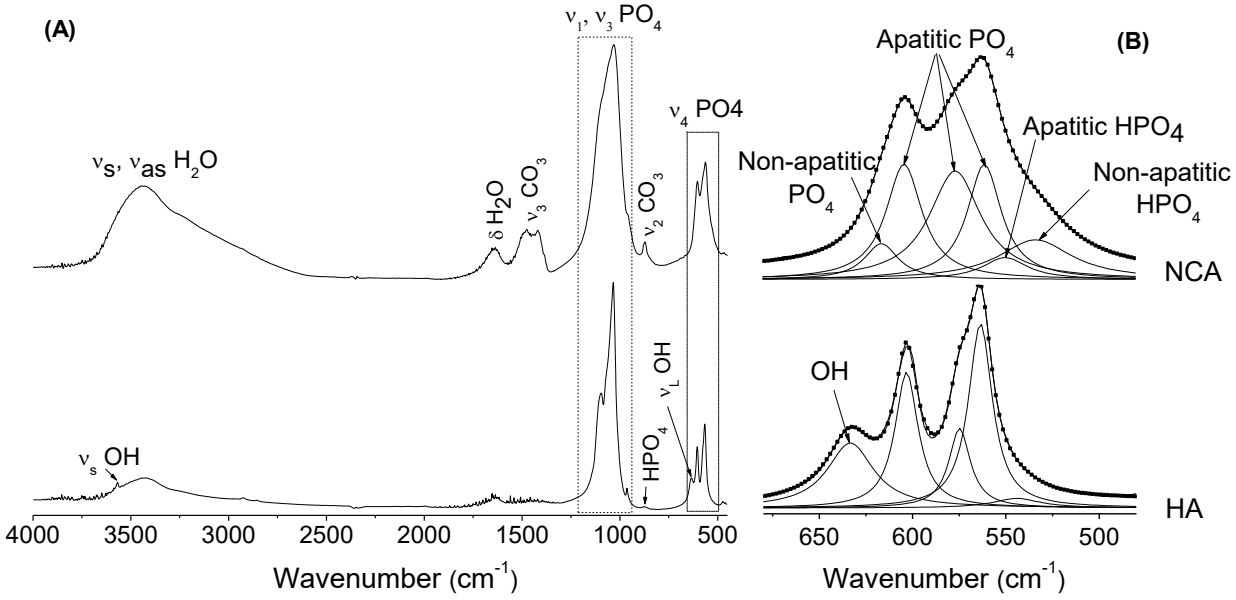


Figure 10: (A) FTIR spectra of well crystallized stoichiometric hydroxyapatite (HA) and biomimetic nanocrystalline carbonated apatite (NCA) (with 6 days of maturation) and (B) the corresponding decomposition in the ν_4 PO_4 domain. Both were prepared by double decomposition, filtered, washed and freeze dried. Source: [211]. Adapted with permission of Elsevier.

Table 1: FTIR and Raman line positions of phosphate ions in hydroxyapatite (cm^{-1}; m: medium, s: strong, sh: shoulder, v: very, w: weak). Sources: [212], [213]. Adapted with permission of Elsevier.

	FTIR (cm^{-1})	**Raman (cm^{-1})**
ν_3 PO_4	1092 s	
		1077 w
		1064 w
		1057 w
		1048 w
	1040 vs	1041 w
		1034 w
		1029 w
ν_1 PO_4		964 vs
	962 w	
ν_4 PO_4		614 w
	601 m	607 w
		591 w
	575 m,sh	580 w

	561 m		
ν_2 PO_4	472 vw		
	462 sh		
		448 w	
		433 w	

Ionic substitution in non-stoichiometric hydroxyapatites can also be evidenced by FTIR and Raman spectroscopies. For example, carbonate ions, present in biological apatites and in carbonate substituted synthetic apatites as explained in *section 2*, are active in four main vibrational domains: ν_1 (around 1050 cm^{-1}), ν_2 (820–900 cm^{-1}), ν_3 (1400–1550 cm^{-1}), and ν_4 (650–750 cm^{-1}) [120], (**Figure 10**). But A- and B-type carbonates give vibrations that essentially differ from each other, allowing for more in-depth carbonate analysis. Also, in biomimetic apatites, labile carbonates (LC type) can also be present, although their exact band location is still a matter of controversy. Several slight shifts can also be observed among carbonated apatites due to vacancies or water molecules or combination of the two main carbonate substitutions (A and B sites) [198, 214]. Moreover, besides bands ascribed to bulk A and B type carbonates, given the basic properties of HA, there are surface carbonates on crystalline HA surfaces. In the absence of *in situ* thermal treatment prior to IR spectrum recording, typically general case of KBr diluted samples, and their involvement in the ν_{CO} components has to be also considered to assign the various bulk and surface contributions (**Figure 11**) [192].

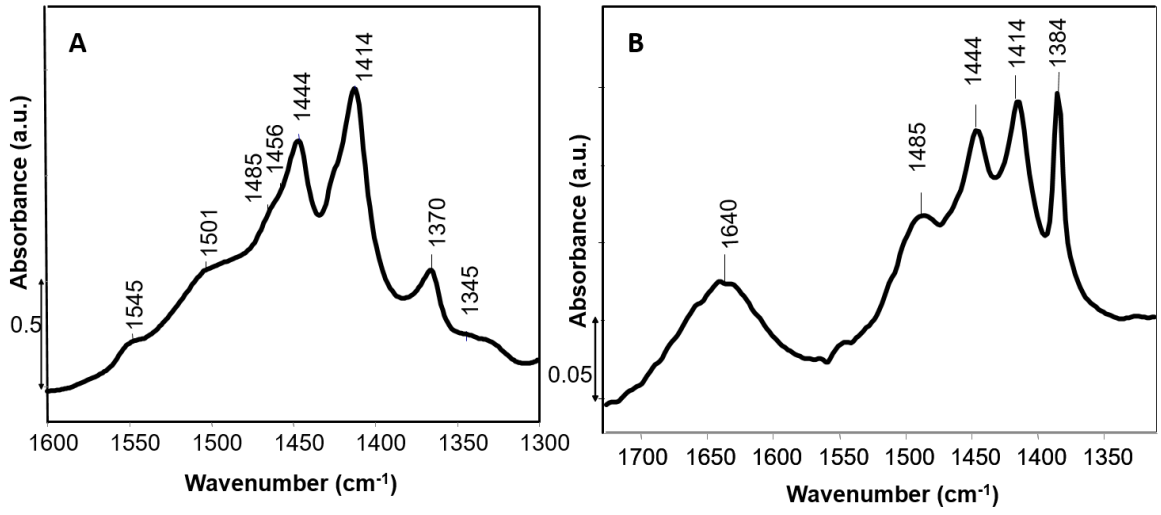


Figure 11: Comparison of FTIR spectra of a same crystalline hydroxyapatite sample recorded A) from self-supported pellet pretreated at 523 K and B) from dilution in KBr. Source: [192]. Adapted with permission of American Chemical Society.

As explained previously (s*ection 2.2*), one of the main properties of highly-reactive biomimetic apatites (whether biological or their synthetic analogues) is the presence of "non apatitic" environments of mineral ions (Ca^{2+}, HPO_4^{2-}, CO_3^{2-} etc.) in a structured metastable surface hydrated ionic layer surrounding an apatitic core (often itself non-stoichiometric) [168, 170]. For example, detailed analyses of the phosphate groups by FTIR reveal the presence of additional bands that cannot be attributed to phosphate groups in a regular apatitic environment and which are not present in stoichiometric hydroxyapatite; it is best observed in the $\nu_4\ PO_4$ vibration domain of FTIR spectra of biomimetic apatites where two shoulders can be found beside apatitic bands, respectively assigned to non-apatitic PO_4^{3-} ions (around 617 cm^{-1}) and non-apatitic HPO_4^{2-} ions (around 535 cm^{-1}), and FTIR spectra can be used to provide a sufficiently accurate evaluation of the amounts of such environments (**Fig. 10**) [161, 170]. This method may thus prove helpful in the characterization of upcoming catalysts based on biomimetic apatites, in order to evaluate the location of the acidic HPO_4^{2-} sites, keeping in mind that the non-apatitic HPO_4^{2-} ions are exposed on the nanocrystals surface.

Similar observations have been made for carbonated biomimetic apatites (and they have been confirmed by solid-state NMR measurements [215, 216]): a characteristic IR band around 866 cm^{-1} is clearly visible by FTIR in the $\nu_2\ CO_3$ vibration domain attributed to to the previously mentioned labile (non-apatitic) surface environments of carbonate ions, distinct from apatite domains, and incorporated in the surface hydrated layer, which can provide quantitative assessment of the amount of non-apatitic carbonate ions in the sample. Moreover, ^{13}C carbonate-containing solution allowed following carbonate species throw surface exchange reactions, and FTIR analysis confirmed the existence of different domains for carbonate ions inside the apatitic domains and on the surface in the hydrated layer [198]. In addition, X-ray absorption spectroscopy experiments have shown the existence of non-apatitic environments of calcium ions in the nanocrystals, not observed in well crystallised stoichiometric apatites [217].

It can be noticed that these non-apatitic features tend to progressively disappear during the ageing in solution (named "maturation process" as explained in *section 2.2*) due to the metastability of such poorly-crystallized non-stoichiometric apatites in solution, evolving towards stoichiometry in a thermodynamically-driven manner, leading to enhanced crystallinity and the progressive growth of the nanocrystals [218]. Moreover, vibrational spectroscopies used on wet samples (*i.e.* freshly precipitated) revealed the fine structuration of non-apatitic band which is lost upon drying [219], accompanied by a loss of reactivity of the nanocrystals on ageing related to the decrease of proportion of the unstable surface hydrated layer and its labile constituting surface ions [198]. It can finally be noticed that the alteration of the ionic

environments in the nanocrystals upon ageing can be evidenced by FTIR analysis upon experiments using isotopic substitutions experiments [198].

Complementary to vibrational spectroscopies, solid-state NMR (nuclear magnetic resonance) constitutes another very powerful technique for the characterization of apatitic compounds. This method allows for the exploration of the short-range environment of different nuclei possessing a magnetic moment, such as ^{1}H, ^{13}C, ^{31}P, ^{19}F, which can be present in (substituted) apatites [220, 221]. Despite exhibiting much more narrow signals than biomimetic apatites, crystalline stoichiometric or non-stoichiometric HA samples exhibit multicomponents ^{31}P and ^{1}H signals (**Figure 12**). They were identified by combining H-D exchanges procedures, specific NMR sequences including inversion recovery measurements, and 2 D Hetcor and DQSQ spectra [190]. Beside main signals associated to adsorbed water, structural phosphates and OH groups (including two resolved contributions related to up and down orientations of their related protons), additional NMR signals could be resolved. They were ascribed to the bulk defective hydrogenphosphate and to surface components (non-protonated and protonated surface terminating phosphate groups) and to surface OH emerging from the tunnel [190]. As for carbonated substituted apatites, NMR study of carbonate species confirmed the IR conclusions by evidencing the two main types of carbonate sites in the apatitic domain (A and B sites, see *section 2*.2), and a third one observed in biomimetic apatites and previously denoted as labile surface carbonates. Two-dimensional solid-state NMR analyses of carbonated apatites have also established the location of these labile carbonate species in the hydrated (surface) domain [216]. NMR spin diffusion experiments have then confirmed the concept of the hydrated layer rich in HPO_4^{2-} ions, proposed earlier on the basis of FTIR results [169]. In fluoride-containing carbonated apatites, ^{19}F solid-state NMR studies clearly showed the existence of two crystallographic sites corresponding to fluoride ions in monovalent sites and close to B-type carbonate ions [216]. Moreover, as FTIR and Raman spectroscopies, solid-state NMR appears particularly suitable concerning non-stoichiometric and low crystallinity apatites study, especially for biomimetic apatites characterization. As in vibrational spectroscopies, the presence of non-apatitic environments has been evidenced by solid-state NMR: in stoichiometric hydroxyapatite, ^{31}P solid state NMR shows a single peak at 2.3-2.9 ppm with respect to H_3PO_4 [222-224]; in contrast, in biomimetic apatite an asymmetrical broad ^{31}P peak is often observed [225, 226] involving HPO_4^{2-} ions in addition to PO_4^{3-}, suggesting phosphate environments different from those of stoichiometric HA, which was pointed out by 2D $^{1}H \leftrightarrow ^{31}P$ cross-polarization solid-state NMR analyses [225].

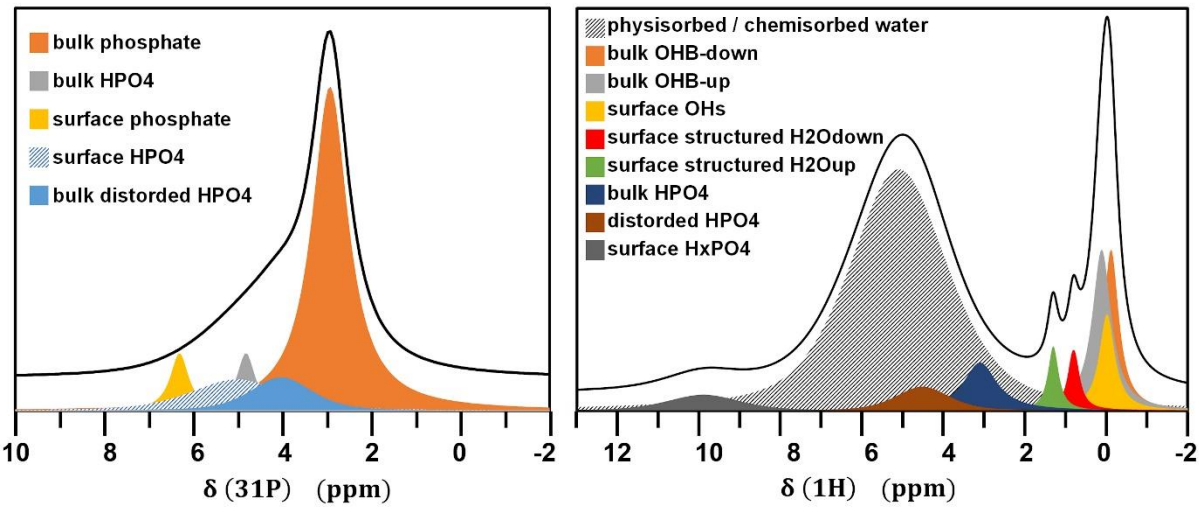


Figure 12: Typical multicomponent ^{31}P NMR (left) and ^{1}H spectra (right) of well crystallized hydroxyapatite sample. The different contributions are schematically reported. For the sake of clarity, unlike the positions of the different contributions, the relative intensities are not represented within a realistic manner. Source: [190]. Adapted with permission of American Chemical Society.

In addition to all the above-mentioned experimental techniques, in order to investigate the properties of such a large variety of solids, molecular simulations appear as another powerful tool and have allowed to elucidate/confirm the crystallographic structures of apatitic solids and their interfaces (see *section 2*), as well as adsorption performances and related energy values, electrical and mechanical properties. For that purpose, different levels of molecular simulations can be considered [113]: first-principles or DFT (density functional theory) calculations investigating the electronic distribution on the solids with a high precision but on a small number of atoms; and force field-based or classical simulations (such as energy minimization or molecular dynamics (MD) simulations) dealing with a large number of atoms but requiring the development of adapted force fields [227] in order to elucidate the thermodynamic and dynamical properties of the solids [138, 228, 229]. It becomes however evident that coupling experiments and simulations appears as a key approach to capture the global understanding of the various properties of the solids, due to the large variability of their chemical composition and related structural modifications [149].

3.2. Thermodynamic properties and thermal stability

Overview of apatites thermodynamics

Apatite thermodynamics have been the object of several studies, although addressing essentially end-member compositions. Standard thermodynamic properties of phosphate-bearing apatites with different substituents and degrees of stoichiometry have been recently reviewed (essentially based on experimental data) and analyzed. This allowed the development of the *Therm'AP* predictive thermodynamic model [230] as well as the related calculation freeware. This latter permitted one to estimate the standard formation enthalpy $\Delta H°_f$, entropy S° and Gibbs free energy $\Delta G_f°$ of phosphate apatites based on their chemical composition [231] (**Table 2**), with a relative uncertainty of the order of 0.5-1%. This approach was cross-validated on the basis of the Simple Salt Approximation (SSA) [232]. Lately, the *Therm'AP* model has also been extended to additional metal cations [233] (namely Ni^{2+}, Co^{2+}, Mn^{2+} and Fe^{2+}) that may also be relevant to the field of catalysis. Classical and quantum molecular simulations have also been used in a parallel way, to extract thermodynamic properties of apatites such as adsorption or formation enthalpy as a function of their composition. For instance, it has therefore been calculated that fluorapatite is more stable than HA [149, 234] and that the substitution of OH^- ions by F^- is exothermic while the substitution of F^- by Cl^- is strongly endothermic [146]. It has also been possible to calculate the impact of various substitutions (Sr^{2+} for Ca^{2+} or halogens for OH^-) and to compare the stability evolution [228, 235-237]. Only few data are available to-date on the thermodynamics of the surface of substituted apatites. For instance, ionic surface substitution was punctually investigated using MD simulations to understand the mechanisms occurring during the incorporation of Zn^{2+} and Sn^{2+} ions [238]. The comparison shows that adsorption of Zn^{2+} is preferred for the surfaces (010) while the adsorption of Sn^{2+} is weaker. Furthermore, the adsorption of cations appears favored by Ca2 sites.

Table 2: Gibbs free energy, enthalpy and entropy contributions of some constitutive ions in the apatite structure, as determined from the *Therm'AP* predictive approach. Sources: [230], [233]. Adapted with permission of Elsevier.

Contributing components in the apatite formula (298 K, 1 bar)	g_i (kJ.mol^{-1})	h_i (kJ.mol^{-1})	s_i (J.mol^{-1}.K^{-1})	***Contribution to the oxygen stoichiometry***
Energetic contributions per divalent cation				
Ca^{2+}	-740	-790	38.8	*+1*
Sr^{2+}	-740.9	-796.1	53	*+1*
Mg^{2+}	-634.3	-666.4	23.1	*+1*
Ba^{2+}	-739.4	-791.9	71.1	*+1*
Cu^{2+}	-134.6	-171	34.6	*+1*
Cd^{2+}	-262.4	-317	53.6	*+1*
Pb^{2+}	-236.2	-282.2	81	*+1*
Zn^{2+}	-344.5	-394.8	52.4	*+1*
Ni^{2+}	-221.8	-262.9	38.6	*+1*
Co^{2+}	-227.7	-266.9	53.3	*+1*
Mn^{2+}	-403.6	-446.8	60.7	*+1*
Fe^{2+}	-273.2	-308.5	61.3	*+1*
Energetic contributions per anion				
PO_4^{3-}	-816.15	-861.6	41.05	*+2.5*
OH^-	-140.8	-121.5	80.65	*–0.5*
F^-	-269.5	-237.2	68	*–0.5*
Cl^-	-103.5	-70	95.7	*–0.5*
Br^-	-90.5	-58	118.3	*–0.5*
Energetic contributions by other species				
H^+	-147.75	-187.85	66.2	
H_2O (hydration)	-234	-290	50.7	
P_2O_5	-1632.3	-1723.2	82.1	

An increasing departure from stoichiometry – *via* vacancies in cationic and monovalent anionic sites – has a direct decreasing effect on the overall thermodynamic stability (as followed

by the $\Delta G°_f$ value), which may be quantified from the chemical composition of the sample [230, 239]. In turn, this explains the increase in solubility of apatitic compounds departing from stoichiometry (see *3.3.1. subsection*). As far as solubility goes, however, the ionic contents of the solution have to be considered along with the nature of the apatitic phase itself (and pH), as the presence of some ionic species may modify the apatite solubility by affecting the ion activity product.

It may be noted that alkaline-earth apatites (Ca^{2+}, Sr^{2+}, Ba^{2+}, etc.) are globally more stable than transition (*e.g*. Mn, Fe, Co, etc.) or post-transition (*e.g*. Cd, Pb) metal apatites for a similar cation/P molar ratio and monovalent ion type (e.g. OH^-): Ca~Sr~Ba > Mg > Mn(II) > Zn > Cd ~ Fe(II) > Pb > Co(II) > Ni(II) > Cu. The effect of the incorporation of heavier cations like lanthanides was also scrutinized [240]. Overall, the thermodynamic properties of complex oxides like apatites not only depend on the radius and charge of the constituting ions, but also importantly on the affinity of the cation(s) for oxygen (shared by phosphate ions) and the elements own electronegativity [230]. However, it can be reminded that, in the presence of an aqueous medium (*e.g.* containing metal ions), the relative stability of the aqueous ions themselves has also to be considered when attempting to draw conclusions on the thermodynamic natural evolution path of the system. For example, while the Pb-HA solid phase ($\Delta G_{f,298}° \cong$ -7515 kJ/mol) is noticeably less stable than Ca-HA ($\Delta G_{f,298}° \cong$ -12634 kJ/mol), the incorporation of Pb^{2+} is still thermodynamically favored by the very low stability of aqueous lead ions ($\Delta G_{f,298}° \cong$ -24.43 kJ/mol) compared to the highly stable $Ca^{2+}_{(aq)}$ species ($\Delta G_{f,298}° \cong$ -553.58 kJ/mol) [230].

Biomimetic apatites described in *section 2.2* are an important subfamily of apatite compounds that exhibit a high (surface) reactivity that will be further developed in *section 3.4*, allowing in particular rapid surface ion exchange and a large adsorption capability. This reactivity is fairly directly related to the lower stability of these compounds – obtained at "low temperature" typically lower than 100°C – compared to high-temperature apatites. The hydrated ionic layer on the surface of the nanocrystals is in particular one key feature of such low-temperature apatites, as the presence of water plays a major role in ion mobility and apatite processing [241, 242]. Therefore, the relative metastability of biomimetic apatites can be exploited advantageously for applicative purposes for boosting apatite-based processes, as in catalysis. This increased reactivity can be tailored by controlling scrupulously the conditions of formation and post-treatment of such apatite nanocrystals, leading to more or less reactive crystals [239, 243]. Indeed, upon immersion in aqueous medium, nanocrystalline apatites

undergo a process known as “maturation” (ageing in solution) that has to be differentiated to regular Ostwald ripening and corresponds in fact to the evolution of the non-apatitic ionic environments from the hydrated surface domains to more stable apatitic environments composing the apatite nanocrystals core (see *section 2.2*). A mechanistic scheme has been proposed to identify the main stages of this process, which itself involves ion exchanges/equilibration with the surrounding solution [241]. If maturation is undergone in the presence of foreign ions, the latter may be more or less incorporated into the nanocrystals (e.g. [244]) depending on their affinity for the apatite structure and the stability of their aqueous species as mentioned above.

Thermal behavior

Apatite compounds are often subjected to post synthesis heat treatments whether during synthesis/production or processing in view of a wide range of applications. Also, the application itself may provide a heated environment as in several catalytic processes. Therefore, appreciating their thermal behavior is often necessary. Among phosphate compounds, stoichiometric apatites exhibit a rather high thermal stability. HA can for example be heated/sintered at 1200–1250 °C without major alteration of the structural features [120], albeit dehydroxylation into oxyapatite occurs toward high temperatures (> 850 °C in vacuum/dry atmosphere) [245] in a way that depends on experimental conditions such as water partial pressure (**Figure 13**, right side chart). Then, oxyapatite decomposes at higher temperatures into tricalcium phosphate (TCP) and tetracalcium phosphate (TTCP), itself decomposing further to CaO. In the process of hydroxy→oxyapatite transformation, vacancies are progressively created in the apatitic channels generating intermediate oxy/hydroxyapatites $Ca_{10}(PO_4)_6(OH)_{2-2x}O_x\square_x$, and the value of x can then influence the temperature of subsequent decomposition [246-248]. In stoichiometric HA, it may also be noted that surface phosphorus is often considered to be reactive and may form P-OH surface bonds that are dehydroxylated above 400 °C to form P-O-P surface groups [247].

In contrast, non-stoichiometric apatites follow a different thermal decomposition path. In link with the thermodynamic metastability features mentioned above, these compounds will evolve differently depending on their chemical composition (**Figure 13**, left chart for non-carbonated apatites and middle chart for carbonated apatites). In all cases, the hydrated layer progressively loses its water by *ca*. 200 °C, then HPO_4^{2-} and CO_3^{2-} decompositions occur upon further heating, ultimately giving rise to high-temperature phases like HA, β-TCP, calcium

pyrophosphate (typically β-$Ca_2P_2O_7$) or CaO following the indications given on the figure. The end-products and their relative amounts are dictated by the initial composition of the non-stoichiometric apatite sample considered. It may however be noticed that in the first stages of HPO_4^{2-} decomposition to pyrophosphates ions $P_2O_7^{4-}$, the latter remain in the apatite structure over a rather larger temperature range (typically up to at least 550 °C [249]) prior to witnessing the apatite structure collapse, thus potentially widening the temperature domain of use of these compounds for applicative purposes.

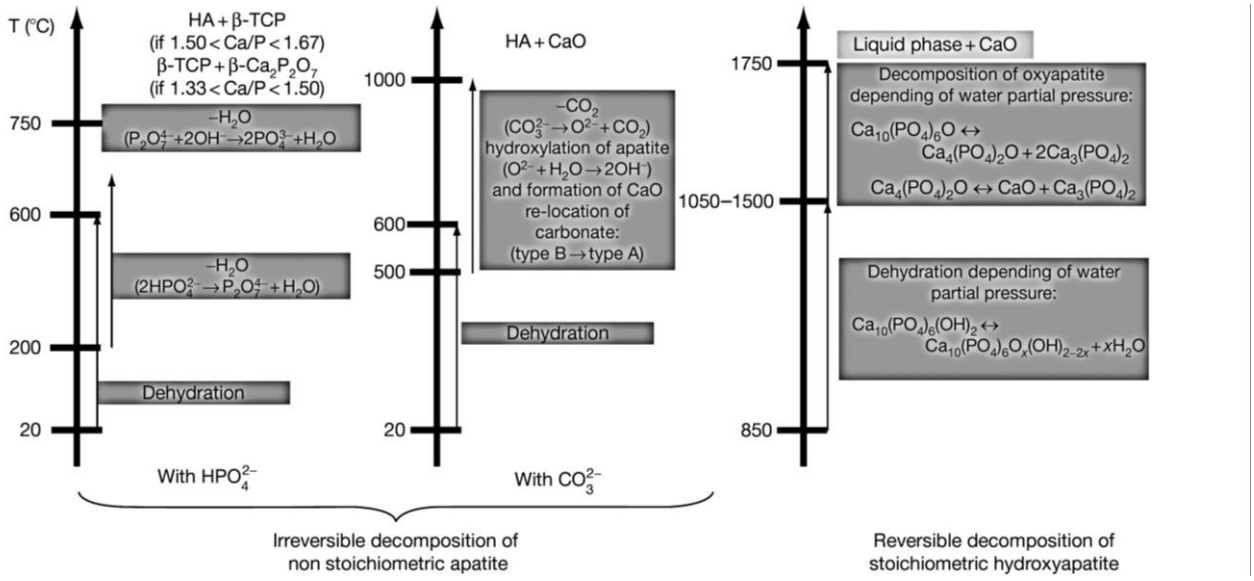


Figure 13: Thermal decomposition scheme of (non)stoichiometric apatites. Source: [120]. Adapted with permission of Elsevier.

As already mentioned in the above subsection, ion substitutions in the apatitic lattice are likely to modify the thermodynamic stability of the phase. It is thus bound to have direct effects on its thermal behavior. Substitution of the OH^- anions by F^- or Cl^- ions within the channels has for example the tendency to increase the apatite thermal stability typically in the order (fluorapatite) FA > (chlorapatite) ClA > HA [246]. Cationic substitutions may also modulate the thermal stability, as in the example of Mg-containing apatites for which decomposition temperatures are clearly down-shifted of several hundred degrees taking into account the stabilizing effect of phases such as β-TCP $(Ca,Mg)_3(PO_4)_2$ by Mg^{2+} ions [250].

3.3. Physico-chemical and interfacial properties

3.3.1. Solubility and evolution in solution

Solubility is one of the most important calcium phosphates properties since it will determine the meaning of some reactions such as their dissolution, precipitation, hydrolysis and phase transformations in aqueous environments. Solubility and interfacial properties of HA have been studied by several authors [115, 251, 252] and controversies remain numerous. The main reason is that the published values refer to products that are supposed to be pure, but contamination by various ions, even in low concentrations, can alter the stability of the crystal by creating significant stresses in the structure. Nevertheless, the solubility product (K_{sp}) of well-crystallised stoichiometric HA have been determined (- log K_{sp} = 116.8 at 25°C [120, 253]). Some studies show that the determination of K_{sp} as a function of the temperature (from 5 to 37°C) in a pH range from 3.7 to 6.7 is given by [253]:

$$\log K_{sp} = -8219.41 / T - 1.6657 - 0.098215\ T \quad (3)$$

where T is in Kelvin and K_{sp} in $(mol.L^{-1})^9$. This relation showed that there was a maximum in K_{sp} at about 16°C [115]. Moreover, above this point, the solubility of apatites has the particularity of being retrograde, *i.e.* beyond a specific temperature (16 °C in the case of stoichiometric HA), it decreases when the temperature increases [246].

In addition to temperature, the solubility of apatites may vary with pH as well as calcium and phosphate concentrations in solution. The simplest and most common solubility isotherms as a function of pH encountered in the literature correspond to that of **Figure 14** [115]; stoichiometric HA remains the least soluble calcium phosphate compound in a wide range of pH values up to 4. A more elaborated 3D diagram according to the pH, the calcium and phosphate concentrations has been proposed by Chow [254]. Several free software programs have been developed to calculate the various equilibria in solution and including solubility equilibria (Visual MINTEQ, MINEQL, PHREEQC etc.); these tools are very useful but not suitable for solutions with high solute concentrations. It must be mentioned that the presence of foreign ions in the composition of a phosphocalcic phase or in the surrounding solution may significantly affect the dissolution behaviour; for example, the presence of fluoride ions in the apatitic structure decreases the solubility, while the presence of carbonate or magnesium ions increases the solubility.

For the same composition, the phases with a lower density have the highest solubility in solution. These observations are related to the degree of cohesion of the phase structure by assuming that the electrostatic attraction between anions and cations within the structure is the main parameter responsible for the cohesion within the crystals of calcium phosphates. Thus, phosphocalcic apatites presenting smaller unit-cell dimensions have the highest cohesion forces

and the lowest solubilities; for example, fluorapatite is less soluble than HA, and calcium phosphate apatites less soluble than strontium phosphate apatites. Similarly, apatitic calcium phosphates with a high vacancies content should be more soluble than those with a low vacancies content [120].

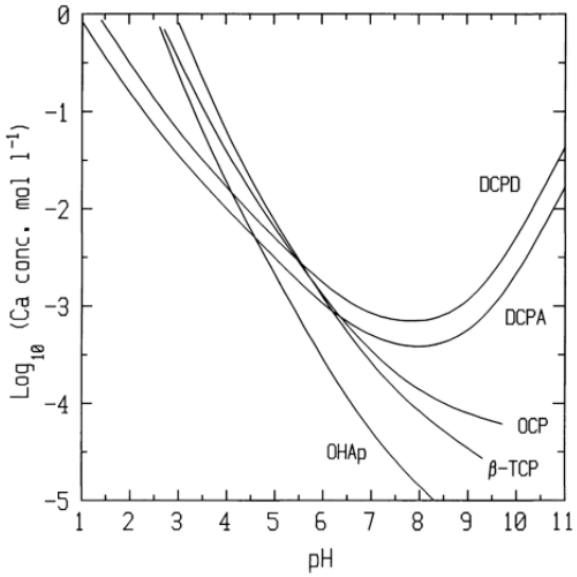


Figure 14: Solubility isotherms of calcium phosphates phases in the system $Ca(OH)_2$ – H_3PO_4 – H_2O at 37 °C. DCPA: dicalcium phosphate anhydrous; DCPD: dicalcium phosphate dihydrate; OCP: octacalcium phosphate; β-TCP: β – tricalcium phosphate; OHAp: stoichiometric hydroxyapatite. Source: [115]. Adapted with permission of Elsevier Science BV.

In addition to the considerations concerning stoichiometric HA, in the case of non-stoichiometric apatites and biomimetic apatites, some variability in the dissolution properties have been reported. Non-stoichiometric apatites show a higher solubility than stoichiometric apatites and the dissolution characteristic of the crystals depends on the composition of the samples, itself related to their conditions of formation [161, 255]. Moreover, the solubility of biomimetic apatites depends on the presence of vacancies: nanocrystals with low Ca/(P+C) ratios (where P represents phosphate ions and C the carbonate ions) present a high amount of cationic vacancies and a less cohesive solid with a higher solubility [161]. The amount of labile ("non-apatitic") surface species may also influence the solubility of the nanocrystals [251, 256]. The presence of crystal maturation inhibitors such as carbonate, magnesium or pyrophosphate, involves small apatitic crystals with high specific surface, rich in labile non-apatitic environments, which promote their dissolution [161]. It should be noted that non-stoichiometric apatites have the ability to mature like bone mineral, as previously explained (*Section 2-2*), and

may involve more stable and less soluble compounds upon ageing [161]. Moreover, unlike stoichiometric HA, the solubility product of biomimetic apatites could vary according to the amount of solid dissolved, leading to the concept of "Metastable Equilibrium Solubility" (MES) [163, 256-258]. Several explanations can be given for this observation, this behaviour could be related to the level of microstrains in the crystals [251], or to the variable surface composition and structure, and the existence of a hydrated layer [163].

3.3.2. Surface Charge

The surface charge of ionic solids in contact with solutions, at the origin of "zeta potential" (ζ-potential), is considered to be the result of preferential dissolution or adsorption of foreign ions or molecules from the solution, or else of the formation of complexes between lattice ions and species in the solution (which may either be formed at the solid/solution interface or in the solution and subsequently adsorb on the solid surface) [115, 120, 259].

The point of zero charge (pzc) defines the conditions of the solution (the pH value) for which the surface density of positive charges (contribution of cations) equals that of negative charges (anions) [120]. There exist a wide range of pzc values for stoichiometric HA reported in the literature [260, 261]; indeed, significant variations are observed between experimental and calculated values [259], which have been explained by substituted impurities, lattice defects or lack of equilibrium conditions in the experiments [259]. However, most of them are found in the range 6.4 and 8.5 [254]. HA surface involves at least three types of potential-determining ions (calcium, phosphate, and hydroxide or proton) [120, 259] and the pH of the solution can influence the solid surface charge by changing the distribution of proton and hydroxyl groups at the interface. To explain the surface behaviour of HA as a function of pH, Boix *et al.* [262] proposed models for HA surface using a mixture of a surface complexation model and a surface hydroxylation model (**Figure 15**).

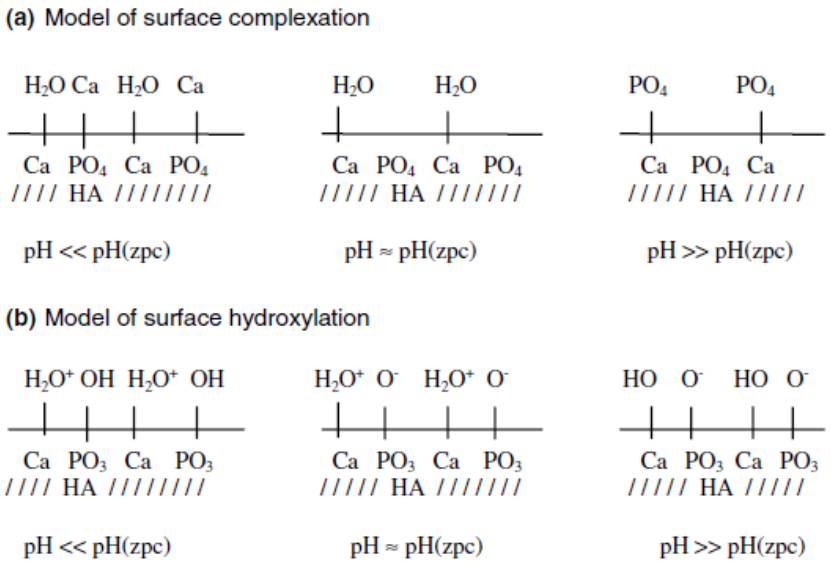


Figure 15: Models for HA surface proposed by Boix et al.: (a) model of surface complexation, (b) model of surface hydroxylation. Source: [262]. Adapted with permission of Elsevier.

For ionic solids such as apatitic calcium phosphates, the surface charge is closely related to the concentration of specific ions in the surrounding fluid that can interact with the surface of the solid, often called as "potential-determining". Under constant pH and ionic strength, a change in the calcium or phosphate concentrations can affect the surface charge of HA [120]. Indeed, an increase of calcium concentration will lead to more positive values of surface charge (adsorption of calcium ions on the surface of the solid), while an increase of phosphate concentration will lead to more negative surface charge [263]. Moreover, ionic substitutions and apatite composition also influence surface charge of apatitic compounds. For example, the pzc values of four apatite samples follow the following order: FA < HA< strontium-HA < barium-HA, which corresponds also to the order of increasing solubility [264]. The surface charge of silicated-HA appears more negative than that of HA, which can be related to the presence of tetravalent silicate ions on the apatitic surface instead of phosphate ions [265].

In addition, non-stoichiometry may also affect the surface charge of apatites; biomimetic apatites, more soluble than stoichiometric ones, have been found to exhibit greater zeta potential than stoichiometric HA [266]. However, in the case of nonstoichiometric biomimetic apatites, the existence of a non apatitic surface layer on the apatite nanocrystals (see previous *section 2-2*) leads to a more complex system which makes difficult to evaluate the amounts of phosphate or calcium ions actually exposed on the surface [165].

Finally, the presence of organic molecules adsorbed on the surface of apatite solids, including non-stoichiometric ones, can significantly modify their surface charge of the particles [264, 267]. For example, the adsorption of acetaminophen on HA leads to a surface noticeably more negatively charged compared to the unfunctionalized one [268], whereas the adsorption of amino acids [269] or an amine-terminated phospholipid [267] on calcium-deficient apatites leads to a more positive surface charge. The adsorption of organic molecules on apatitic surface can often be explained by the replacement of some surface ions by some charged/polarized end-groups of the organic molecule. For instance, molecules exposing negatively-charged functional groups may displace phosphate surface ions, while positively-charged groups may displace calcium ions [165]; however the affinity of such functional groups for the surface of the apatite has also a great influence on adsorption properties of organic molecules on the apatitic surface. The mechanism of adsorption and the role of the nature of organic molecules in the binding mechanisms are discussed *in Section 3-4*.

3.3.3. Interfacial tension

Surface/interfacial (free) energy or "tension" is another relevant parameter when addressing interactions between a solid surface and the surrounding medium. It may for example affect the adsorption capacities of a solid [270]. Also, in solution, it is linked to the stability of colloidal suspensions and impacts the crystal morphology and growth rate in solution [271]. In turn, interfacial tension plays a role in most theoretical dissolution kinetics models [272]. The surface energy of a solid is also directly related to its wettability (e.g. as a general trend, the higher the surface free energy, the better water wettability), and consequently to the surface roughness (an increase of surface roughness leads to an increase in apatite surface energy) [273]. However, data available in the literature on this matter are rather scarce for apatite compounds. Also, variability in reported values may be underlined, in part due to different measuring approaches or interfaces considered [271, 274, 275].

Surface tension can either be determined experimentally (typically from contact angle measurements or during HA dissolution or crystal growth experiments) or calculated from a simulation approach. Care should thus be taken when extracting or comparing data from literature, as experimental and simulation works generally refer to different thermodynamic states. When considering an apatite phase in contact with liquid water, the initial state is the apatite solid phase in equilibrium with its own vapor (described by $H_S°$ which is related to the surface tension of the solid $\gamma_S°$) while the final state is the solid-liquid interface (described by H_{SL} related to the γ_{SL} surface tension) [276, 277]. In enthalpy terms (a similar equation could

be written in terms of free energy), this can be described by way of the enthalpy of immersion ΔH_{imm} as follows:

$$\Delta H_{imm} = H_{SL} - H_S° \quad (4)$$

While in experimental studies, the value accessed is ΔH_{imm} or γ_{SL} thus referring to the solid in contact with liquid water, computational approaches rather calculate the $H_S°$ value.

From an experimental viewpoint, surface tension values (γ_{SL} referring to the apatite-liquid water interface) drawn from HA dissolution are generally lower than those determined from HA growth studies [278], which may be related to surface imperfections that may affect both approaches in a different way [279]. In some cases, the adsorption of impurities (e.g. foreign ions present in the medium) onto crystal faces may additionally alter the measured surface free energies of crystal faces, modifying the tendency for ions to be released from the crystal during dissolution experiments [272]. It is thus necessary to use well-established methodologies allowing the characterization of interfacial reactions in well-known reproducible conditions; and comparisons should probably be made on the basis of a common approach so as to limit undesirable bias.

As a general tendency, the surface tension of calcium phosphates seems to correlate rather well with their water solubility, the lowest surface tensions being noticed for the most soluble phases [120, 280]. Interfacial energies with respect to water for hydroxyl- and fluorapatite are generally considered around 9.0-9.3 and 17.1-18.5 mJ/m², respectively [280-282]. Since surface tension originates from the physical attractive force between the atoms composing the solid surface [283], ion substitutions in apatite are likely to modify the crystal surface energy. Heavier elements favor larger surface energy, as was evidenced for instance between barium- and strontium-chlorapatites surfaces [283]. Carbonation of HA (3 wt. % CO_3) was on the other hand reported to exhibit a surface energy of 9.0 mJ/m², close to (slightly lower than) that of HA [280]. However, changes were detected on the dispersive and polar components of surface energy, as the polar interaction energy with water was significantly lower on (A-type) carbonated apatite than on HA [284]. In non-stoichiometric apatites, carbonation was found to generate several significant modifications of apatite crystal features, obviously also affecting surface energy [285]. However, the surface energy of non-stoichiometric apatites has not yet been specifically addressed and is still a matter of discussion that will need further consideration. In the case of non-stoichiometric biomimetic apatites, since the nanocrystals exhibit a hydrated non-apatitic layer, their surface features such as surface energy are indeed expected to be deeply modified compared to the regular/stoichiometric

hydroxyapatite model: the surface layer is rich in HPO_4^{2-} ions (unless heavily carbonated) and in Ca^{2+} ions but exempt of OH^- ions (solely contained in the crystal core within the apatitic channels), a new model will thus have to be proposed to determine actual surface features.

From a modeling viewpoint, molecular simulations have also been used to calculate the surface energy [286] (referring to the solid in equilibrium with its own vapor) of various apatites and to determine from theoretical calculations the cleavage face or the morphology for crystal growth [287]. Indeed, one of the main goals of recent studies was to propose a description of surfaces (more realistic than bulk model [288] for applications dealing with surfaces). The relevance of involving surface OH groups has been pointed out. On stoichiometric apatite, the surfaces (010) terminated with OH groups have indeed been evidenced by calculations to be the most stable surfaces while the (001) and (010) surfaces terminated with calcium or phosphate groups have shown to be unreactive in presence of water [289]. The evaluation of the surface energy of different apatite compositions has also shown the impact of substitution. For example, in a carbonate-saturated HA, the surface energy was calculated as 900 mJ/m^2 compared to OH-saturated HA (750 mJ/m^2) using B3LYP [290]. To modify the adsorption properties, incorporation of ions is a possibility: considering different HAs (HA, HA substituted with Ag or Zn), the adhesion performance has been characterized by classical and quantum molecular simulations and the interactions between HA and Ti was found to be enhanced by doping with Zn or Ag [291]. In order to evaluate the activity of the apatite surfaces, an indirect approach considering water molecules as a probe has been envisaged [292, 293]. The adsorption properties for water on HA surfaces have also been evaluated using DFT calculations and showed that, depending on the surface ((001) or (010)), the interaction between water molecules and constituents was based on physisorption (~80 kJ/mol) on the (001) surface but on chemisorption with dissociation of H_2O and formation of Ca-OH and PO-H covalent bonds on the (010) HA surface [294]. Similar results led some authors to consider the (100) surface terminated by Ca^{2+} or phosphate groups as unstable since it strongly interacts with water [114]. It appears therefore that the different surfaces of the apatites present specific behaviours (in terms of hydrophilicity-hydrophobicity, stability, etc.), which can explain the differences observed during crystallization and the resulting morphology of the solids in the presence of external molecules [114, 288]. However, due to the limitation of DFT calculations and to investigate larger systems, adapted force-fields have to be developed to reproduce the interactions with water and then analyze the impact of the substitutions on the adsorption properties [295, 296] and characterize, especially in the case of apatitic nanoparticles, the

rearrangements of atoms at their surface, which can be accessed during simulations in the presence of water molecules [292].

3.4. Surface reactivity

3.4.1. Nature of acid and base sites.

Due to the lack of characterization tools for investigating the solid liquid interface, the surface termination of hydroxyapatite in liquid medium is an open question, and depends on the pKa values of the reactant molecules and products *versus* the pH of the aqueous medium. If recent developments propose methods for quantifying acid (or base) sites in liquid medium [297], the exact nature of sites in real operating conditions is still an unsolved question.

Although challenging, the identification of active sites working at solid gas interface for reactions implemented at moderate to high temperature conditions benefits of some *in situ* characterizations at solid gas interface. Among species likely to be present on the surface of hydroxyapatites, Ca^{2+} cations (or other coordinatively unsaturated cationic metallic centers depending on the target composition) can act as Lewis acid sites. However, surface relaxation processes may lead to some Ca^{2+} deficiency on the top surface [189]. To ensure the surface charge balance, terminated phosphate groups are protonated [210, 226, 298] and the resulting PO-H are likely to act as Brønsted sites. As far as basic sites are concerned, it is often implicitly assumed that PO_4^{3-} groups should be responsible for the basic properties of hydroxyapatite [97, 100], even if there is a lack of experimental proof for their direct involvement in catalytic reactions. Alternatively, OH^- emerging from the channels should be considered [186].

FTIR characterization may help in the identification of the active sites involved in the gas phase catalytic reactions. However, the main difficulty for investigating the active surface of hydroxyapatite comes from the fact that the same species are present both in the bulk and on the surface, only the latter species being likely to directly play a role in catalytic reactions. In a first step, spectroscopic fingerprints of surface species have to be discriminated from the bulk ones. The spectroscopic features of OH^- and HPO_4^{2-} originating from the bulk and from the surface could be discriminated using isotopic H–D gas phase exchanges successively implemented in mild conditions (180-200 °C) then at higher temperature (300 °C) to first selectively label the lone surface, then to achieve deep bulk deuteration, finally followed by a last surface reprotonation step (**Figure 16**) [210]. Once IR bands of vibrators located on the surface are identified, their behavior can be monitored via *in situ* adsorption of probe molecule

and even *operando* reaction conditions to complementarily characterize their acid (or basic) properties and discuss their involvement as active sites.

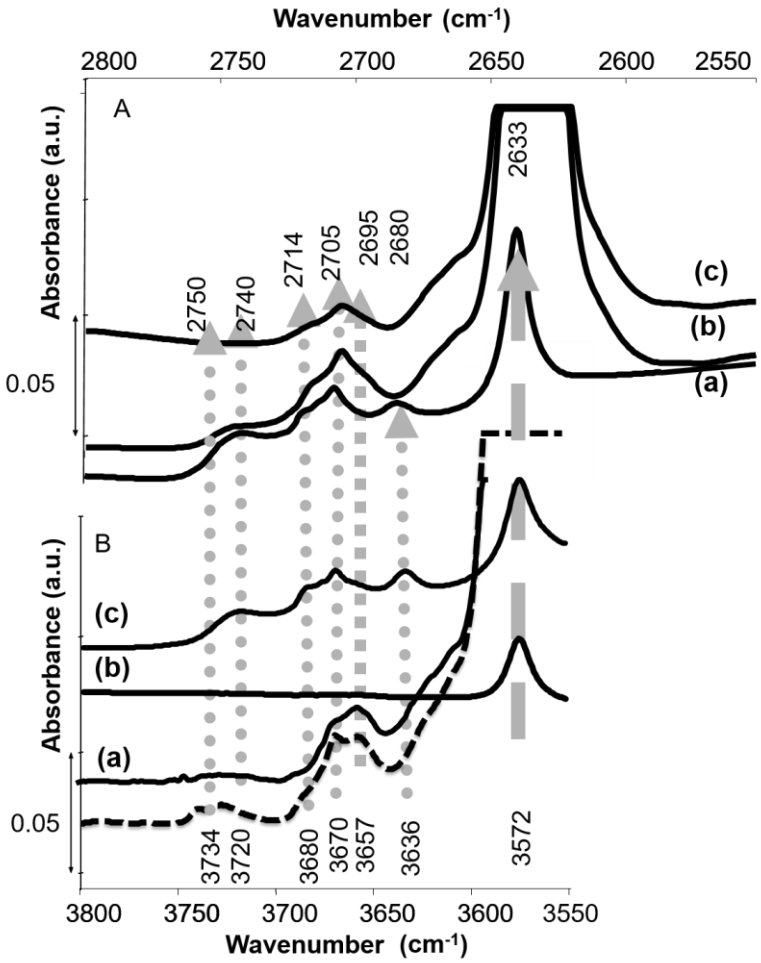


Figure 16: FTIR spectra on self-supported wafer of a HA: A) in the ν_{OD} region after surface deuteration (a spectrum), after bulk deuteration (b spectrum) and after surface protonation subsequent to a bulk deuteration (c spectrum); B) in the ν_{OH} region before deuteration (dotted line) after surface deuteration (a spectrum), after bulk deuteration (b spectrum), and after surface protonation subsequent to a bulk deuteration (c spectrum). To evidence the correspondence between the bands in the ν_{OD} and ν_{OH} regions (vertical arrows), the scale of the two frequencies axis has been adapted, taking into account the ν_{OH}/ν_{OD} ratio = 1.37. Source: [210]. Adapted with permission of Elsevier.

Acid sites

It was found that among the six IR ν_{PO-H} vibrators in the 3750-3600 cm^{-1} range, only that at 3657 cm^{-1} corresponds to bulk species, all the others at 3734, 3729, 3680, 3670 and 3636 cm^{-1} corresponding to surface species (**Figure 16**). Consistently, their perturbation upon

adsorption on the surface of basic gaseous probe molecules, typically CO probe molecule at 77K (that also generates vibration bands the 2200-2000 cm^{-1} range), confirmed their surface location as well their Brønsted acidic properties [189, 210]. Interestingly, the intensity of the perturbations (negative contribution in different spectra) does not follow that of the absolute bands which is indicative of a differentiation of the surface PO-H in terms of acidic strengths, accessibility and/or proximity with the neighboring basic sites [75, 192].

CO can also probe the presence of calcium cations. However, the top surface accessibility of CO adsorption experiments remained quite limited compared to that of PO-H [189]. Consistently, the lack of Lewis sites was also reported from gaseous pyridine adsorption [188]. Adsorption of evaporated glycine concludes to weak interaction through both H bonding between PO-H and the carboxyl group and between Ca^{2+} and the amino group [299]. The competitive involvement of cations or terminated PO-H sites may thus depend on the one hand on their affinity for interacting with the organic reactant and/or the involved mechanism, and on the other hand on the preferential surface exposure of one site over the other [189]. For instance, the higher efficiency of PO-H over Ca^{2+} acid sites was observed for ethanol or MBOH conversion in the gas phase by tuning the relative proportion of exposed PO-H and Ca^{2+} playing on the washing and drying procedures [189]. From *operando* studies, the unique selectivity of the hydroxyapatite system for the ethanol to n-butanol conversion was ascribed to the involvement of the weak PO-H Brønsted acid sites: when poisoned, the reaction stops to acetaldehyde, revealing that the selectivity is greatly dependent on the Brønsted or Lewis nature of the acidic sites involved [75]. Of course, in the case of modified hydroxyapatite, the acidic properties of the heteroatom may be determinant: for instance, the Lewis acidity associated with Ru bound complex promotes the Diels Alder reaction [25].

Basic sites

According to H-D exchange studies, the IR band at 3572 cm^{-1} was found to gather both the contributions of the main bulk OH located inside the channel and of the minor surface fraction emerging at the surface [210]. The involvement of the surface OH^- as basic partner in acid-base pair with neighboring acidic PO-H is evidenced by the simultaneous perturbation of their respective ν_{O-H} vibrator upon adsorption of acetylene [192] and its role as active sites is unambiguously shown from *operando* study [75] in the ethanol conversion to n-butanol. The ethanol conversion is directly dependent on the availability of the surface OH^-. At reverse, the involvement of O^{2-} of PO_4^{3-} for gas phase reaction still remains unproved, since the related IR

ν_{P-O} bands – whose saturation on self-supported wafer could be avoided upon dilution of the sample in diamond sample – were not perturbed upon adsorption of acetylene [192].

The role and identification of basic sites was also recently questioned for the activation of light alkanes, likely to occur *via* the hydrogen abstraction from the C-H bond. In the absence of any vanadyl group exposed on the surface in vanadate-modified hydroxyapatite, intrinsic basicity provided by the hydroxyapatite was proposed [9]. Obviously, the strength of the OH^- basic sites remains too weak for accounting for the vanadate or cobalt modified hydroxyapatites efficiency in oxidative dehydrogenation of propane or ethane [300, 301]. Thus, it was assumed that oxygen species derived from the abstraction of a hydrogen atom of the hydroxyl might be involved [50, 301]. This was recently confirmed by DRIFTS (Diffuse Reflectance Infrared Fourier Transform Spectroscopy) and NMR since upon thermal activation (up to 500°C), vanadate-substituted hydroxyapatites [302] progressively dehydrate to form a metastable vanadate-modified oxyhydroxyapatite active phase [9]. This process is assisted by a thermally-activated anisotropic proton conduction ability along the c axis [303] that finally leads to the surface exposure of strongly basic O^{2-} sites that are able to activate the C-H bond of light alkanes [9]. In the case of butan-2-ol oxidative dehydrogenation, it was found that low iron loading leading to Fe^{3+}-O-Ca^{2+} species (instead of Fe^{3+}-O-Fe^{3+} obtained at high iron loading) are favourable to catalytic performance since it avoids a drastic decrease of the basicity [48].

Note also that the fluoroapatite system was reported to exhibit modified basic properties compared to hydroxyapatite: the F^- homologous to OH^- inside the column could impact the acid-base balance, or may even be directly involved as basic sites [60, 63, 64, 78, 91].

3.4.2. Influence of substitution on surface reactivity

As mentioned in *section 2*, thanks to its peculiar flexibility, the apatite structure accepts both cationic (on Ca 1 and / or Ca 2 sites) and anionic (both on PO_4^{3-} and OH^- sites) substitutions. These substitutions abilities are not limited to ions of similar charges [39] (Ca^{2+} → Mg^{2+}, Sr^{2+}, Ba^{2+}, Co^{2+}, Ni^{2+}, Cu^{2+}, Zn^{2+}, Pb^{2+}, Cd^{2+}; [67, 70, 86, 185, 304-308] PO_4^{3-} →AsO_4^{3-}, VO_4^{3-};[302, 309, 310] OH^-→Cl^-, F^- [311]) but incorporation of ions of different charges is also reported (Ca^{2+} → Ln^{3+} [312]; PO_4^{3-}→ SiO_4^{4-} [313, 314]; CO_3^{2-}; OH^- → CO_3^{2-} [192, 303]). Although mostly associated to bulk modifications, such ability of hydroxyapatite structure to accommodate a wealth of cationic or anionic substitutions makes it a very attractive tunable support for a large class of multifunctional catalytic reactions. Various compositions of modified hydroxyapatites have been prepared incorporating the foreign ions in one pot coprecipitation approach [9, 185, 302] eventually followed by a hydrothermal treatment [49,

76, 309, 315] or by high temperature exchange reactions [316] (see *section 2*). Depending on the nature and content of the heteroatoms, the crystallinity, morphology [39], textural properties, surface relaxations [9] may also be greatly impacted. The bulk incorporation can be probed by XRD following the induced distortion of the crystalline cell. Recent literature focuses on DFT calculations and X-Ray absorption spectroscopy to more directly address the foreign atom location [317, 318]. As shown above, vibrational spectroscopies also allow for the identification of sites occupancies in substituted apatites through the position and/or shape of vibration bands; for cationic-substituted phosphate. IR vibration bands are globally shifted towards lower wavenumbers when a large cation replaces a smaller one (as strontium-calcium hydroxyapatite) [198]. Beside ionic radius and electronegativity, the spatial constrain also appears to be a key parameter to assess the preferential occupancy of divalent cations on Ca1 or Ca2 sites. This contributes to explain why the ability for M^{2+} (Mg^{2+}, Zn^{2+}, Cd^{2+} and Pb^{2+}) bulk doping is favored in the case of carbonated hydroxyapatites: by modifying the bond length and coordination number of Ca site, CO_3^{2-} enhances the solubility of foreign M^{2+} ions in the lattice [319]. In particular, the relaxation possibilities within the OH channels help the incorporation of many ions. Whereas the preference of Sr^{2+} for Ca1 site prevails for loading lower than 1 at%, for higher Sr^{2+} concentration Ca2 site appears progressively preferred, as visualized by the shift to a higher frequency of the IR ν_{OH} stretching mode [152]. At reverse, the related band shifts to lower frequency upon progressive Cd^{2+} incorporation is indicative of the higher covalent character of Cd-OH bonds [308]. Silicate incorporation is associated with OH loss [320] whereas vanadate substitution favors the oxyhydroxyapatite formation, as clearly evidenced not only during *in situ* thermal treatment (catalytic conditions) but also by the persistent loss in OH once back to room temperature, at least for high vanadium loading (after thermal treatment at 500 °C) [9]. Beside intrinsic properties provided by these new groups (redox in the case of vanadate), because those modifications impact the OH channels, they also influence the strength of basic sites. As an example, the rate of acetone condensation to mesityl oxide that is strongly dependent on the basicity is tuned depending on the nature of the divalent ion close to basic sites: typically, because too acidic partners within the acid-base pair, Mg^{2+} or Ca^{2+} bind acetone too strongly compared to Sr^{2+} that promotes the reaction [39]. Similarly, methanol dehydrogenation to formaldehyde also depends on the binding strength of methanol on the surface [96]. Moreover, by tuning the acid-base balance, the incorporation of Sr^{2+} and CO_3^{2-} promotes the selectivity in the Guerbet coupling of ethanol [68, 70]. Substituted vanadate anions increase the selectivity of acetaldehyde dimerization into crotonaldehyde [67] and generate strong basic sites able to activate the C-H bond of propane [9].

Despite these proven beneficial impacts on the catalytic performances observed for bulk-modified hydroxyapatite systems, it remains quite difficult to make a fair comparison with other systems since turn over frequencies (referring to activity per surface active site) cannot be accurately determined. Indeed, most introduced heteroatoms being located in the bulk (thus not directly involved as active sites) the quantification of surface active sites remains challenging. In addition, the formation of substituted hydroxyapatite solid solution by coprecipitation method is not always easy to establish, as other phosphate compounds [56, 321] and/or oxide particles [322] may competitively precipitate.

3.4.3. Low temperature ion immobilization and adsorption properties in aqueous media or wet conditions

In substituted apatites previously presented, the foreign mineral ions enter the apatite lattice; thus crystal surface is likely to present the same structure and composition than the apatitic core (although relaxation effects/surface energy considerations may lead to some extent to some differentiation in the surface composition [9]). On the contrary, modifications only of the surface of the crystals can be performed in aqueous media without affecting the apatitic structure, as the foreign species does not enter the apatitic domain, and concerns two types of surface phenomena: ion-immobilization and molecules functionalization. Surface modifications can involve several mechanisms, as for example dissolution and/or reprecipitation, or ionic exchange, depending on the nature of the foreign species, the characteristics of the apatitic support and the experimental conditions (pH, concentration, contact time, etc.) [120, 163, 316, 323]. Given the known influence of the apatite composition on the bioactivity of bone tissue [324] (Zn^{2+} enhances antibacterial properties [306, 318, 324], Sr^{2+} contributes to the activation of new bone tissue and reducing fracture risk [325], etc.), such properties are widely investigated for biomaterial applications, as drug delivery [326], or for adsorbents for heavy metals in environmental applications [327, 328], or else in chromatography column separations systems. The functionalization of hydroxyapatite support by controlled adsorption in aqueous medium is also obviously of particular interest for the development of new catalysts [329] since it is likely to introduce heteroatoms, complexes or grafted molecules specifically onto the surface. The understanding of the nature of interactions with the apatitic surface can provide fundamental tools to design performant multifunctional supported apatites.

In the catalysis community, the deposition of active ions, molecules or phase onto a support in aqueous medium is often referred to as wet impregnation (also called impregnation

in excess of solution since the support is stirred in the metal containing solution). Both the speciation in solution of these chemical entities (depending of the pH and concentration) and the charge of the surface govern the adsorption, and only species precursor in strong electrostatic interaction with the support remains after washing. It should be noted that although the zeta potential of apatites has been considered to play a major role in the adsorption process and most adsorption behaviors have been related to this surface parameter [120, 163], the correlation between this global physical parameter (describing the total surface charge of apatite particles) and chemical interactions in solution with specific ions or charged groups of molecules at an atomic level is not straightforward. It shall be considered that the global charge of a particle does not give any information on the local distribution of cations and anions on a mineral surface: for example, the adsorption of positively-charged molecules on a globally positive apatite surface and inversely negatively-charged molecules on a globally negative apatite surface has been described. Surface distribution of a metal on HA surface can be determined by techniques such as SEM-EDX, TEM-EDX.

The dynamical processes occurring at apatites surfaces are also key parameters and have been studied using classical molecular simulations. By this way, water diffusion has been investigated by MD simulations. It results that an anisotropic diffusion inside nanopores ranging from 20 Å to 240 Å is observed [330, 331], in which the molecules diffuse along the surface noticeably faster than perpendicularly to the surfaces. This observation is justified by the impact of the polarization effect of divalent cations [191, 290] as well as the hydration of the ions present at the (001) surfaces (confirmed by the evaluation of the activation energy for water diffusion close to 20-25 kJ/mol which is higher than in liquid water). Self-diffusion coefficients have also been calculated by MD simulations and the obtained values were found lower than self-diffusion in liquid water [332].

Surface ion immobilization

When applied to the case of hydroxyapatite support, adsorption of metal ions in excess of aqueous solution is often referred to as an "ion exchange procedure". The term "ion exchange" corresponds to a reaction specifically affecting the accessible ions on the surface of the apatitic crystals, and not to describe ion substitutions inside the apatite lattice (in this case, the word substitution is used instead of exchange). Several studies have investigated the ion exchange capability of HA with metal ions as Cd^{2+} or Zn^{2+} in solution [327, 328, 333]. However, the exact mechanism involved at the solid-liquid interface for such post-synthesis support modification is rarely precisely investigated in the catalysis community. This aspect is

better documented in the context of remediation to transition metal cations dissolved in wastewaters by hydroxyapatite used as low cost and eco-efficient adsorbent [334, 335] or in the biomedical and biomineralization fields [316]. From this literature, depending on the nature of the metal present in solution, its concentration, the pH solution and the surface charge [336], several immobilization mechanisms are likely to occur over hydroxyapatite: dissolution-precipitation [327], ionic exchange with Ca^{2+} [316], filling of surface cationic vacancies [150], and surface complexation (through surface hydroxyls, carbonates and/or hydrogenphosphates) [307]. The discrimination between these competitive processes should be made combining structural characterization (XRD, FTIR, Raman, SEM, TEM etc.) and quantitative analyses of both the composition of the modified surface (ICP *vs* XPS) and of the ions present in the solution at the end of the process (concentrations of consumed / remaining *vs* released ions).

Dissolution-precipitation mechanism may affect the whole bulk composition. This is typically the case for lead, since the formation of lead-doped hydroxyapatite potentially up to the end-member composition $Pb_{10}(PO_4)_6(OH)_2$ (resembling the pyromorphite phase $Pb_{10}(PO_4)_6Cl_2$) is obtained. Indeed, although the solid Pb-HA phase is significantly less thermodynamically stable than Ca-HA by itself [230, 231], the whole thermodynamic cycle involving also the aqueous species $Pb^{2+}_{(aq)}$ and $Ca^{2+}_{(aq)}$ – the former being significantly less stable than the latter – favors the formation of Pb-HA [307]. If such dissolution precipitation is limited (typically it should be minimized in neutral to basic medium), the deep surface layers composition may be affected and associated with surface restructuring. On the contrary, if any of the three other immobilization mechanisms is involved, the location of the heteroatoms is restricted to the top monolayer of the hydroxyapatite surface (in agreement between ICP-OES and XPS measurements [39]). According to Gervasini *et coll.*, the immobilization of copper in the excess of solution first proceeds *via* surface complexation (its affinity with the surface depends on the B or AB-type carbonation and its interaction strength with the surface decreases as the involved surface anions goes from OH^- to CO_3^{2-} then to HPO_4^{2-}), then ion exchange with Ca^{2+} cations becomes active at long contact time [307]. From DFT, the substitution of Zn^{2+} on Ca^{2+} site in aqueous medium is less energetically favorable than Zn^{2+} occupation on Ca vacancy site [150]. Zn-bound hydroxyapatite was found very effective as a co-catalyst together with a Lewis base in coupling of CO_2 and epoxides [337]. The occupancy of Ca vacancy site is also invoked in the generation of monomeric La complexes active for Michael reactions [64] or Pd^{II} complexes grafted onto the surface of hydroxyapatite of different stoichiometries active for Heck or Suzuki reactions [42]. These Pd^{II} grafted complexes easily transformed into Pd^0 particles with narrow size distribution active in selective oxidation of alcohols [42].

Interestingly, despite the use of chloride precursor (for the preparation of Ru or Co modified hydroxyapatite), most studies conclude to the absence of surface Cl^- substitution for OH^- observed at solid liquid interface, at least for low Ru loading [26, 338, 339]. This has to be related to the lower thermodynamic stability of chlorapatite compared to HA, even in the presence of large Cl^- contents in solution (this is why in bone the apatite phase, yet in the presence of ubiquitous dissolved NaCl, does not get chlorinated). At reverse, in gas phase catalytic reaction, typically partial oxidation of methane [181, 340] or oxidative-coupling reaction [340] operating at high temperature (700 °C) in the presence of tetrachloromethane in the feedstock, surface and even bulk chlorination occurs, resulting in the formation of chloroapatite. Such modification would promote the selectivity in CO [340].

The possibility to rapidly and reversibly immobilize mineral ions by ion exchange process on apatitic surface was firstly studied by Neuman et al. for carbonate-HPO_4^{2-} exchanges in biological apatites [341], later, highlighted by spectroscopic studies and solid state NMR [198]. Note that concerning well-crystallized stoichiometric apatites, low temperature ion surface immobilization reactions described in aqueous media in most instances involve a dissolution-reprecipitation process [316] (as for example fluoride uptake by HA); the surface ion exchange property is particularly relevant for biomimetic apatites, which display a metastable and non-apatitic hydrated ionic layer, highly reactive, rich in labile ionic species able to rapidly and reversibly be exchanged by ions in solution. Several types of adsorption sites have been described on apatitic surface, such as carbonate/hydrogenphosphate, Mg/Ca or Sr/Ca [198, 316]. Analysis of the solid and of the solution ion concentrations confirms that the reactions occur by the replacement of ions of the solid by ions in the solution. By the titration of the remaining solution during adsorption (supernatant), the ion exchange isotherms can be obtained by plotting the quantity of species adsorbed as a function of the remained (equilibrated) concentration in solution. The adsorption isotherms on apatitic surface may often be satisfyingly described by the Langmuir model (for example for Sr^{2+} on non-stoichiometric apatite in **Figure 17**) [244]. The adsorption parameters K and N, representing the affinity constant to the apatitic surface and the maximum amount adsorbed (at a given temperature), respectively, are deduced from Langmuir equation and depends on the nature of foreign species and on the composition of the apatite and its maturation stage. For example, for identical solution concentrations, the exchange rate of Sr^{2+} ions is always larger than that of Mg^{2+} ions for a given maturation stage of the nanocrystals studied. It can be noticed that some monovalent cations like Na^+ and K^+ could not, in contrast, be incorporated in these conditions [161]. All these exchange reactions are very fast (the equilibrium is reached within few minutes) and

irreversible with respect to dilution or simple washing. It has been shown that the quantity of ions exchanged decreased when the maturation time of the nanocrystals used increased, which can be interpreted as a decrease of the amount of potentially exchangeable ions in the hydrated surface layer [162]. However, when a maturation period (ageing) occurs after the exchange, several types of ions in the hydrated layer shall be distinguished: ions like Mg^{2+}, for which only a limited number can enter the HA lattice and remain essentially exchangeable in the surface during maturation through ion exchange reactions; and on the contrary ions like Sr^{2+} which can replace calcium ions in the apatitic structure and thus, during the maturation, the growing of apatitic domain progressively incorporates such ions and the amount of this exchangeable ions constantly decreases as the maturation time increases after a primary exchange reaction [316]. Carbonate ions show an intermediate behavior. The incorporation of foreign species from the hydrated layer into the apatitic core of the nanocrystals during maturation can be studied typically by vibrational spectroscopy experiments using isotopic substitution. For example, solution exchange experiments involving ^{13}C-labeled carbonate have been used to follow carbonate species from the hydrated layer during the ageing of nanocrystalline apatites using FTIR spectroscopy [198]. Moreover, such experiments evidenced that only surface species were exchanged and that the apatitic core was not altered during the exchange experiments [162].

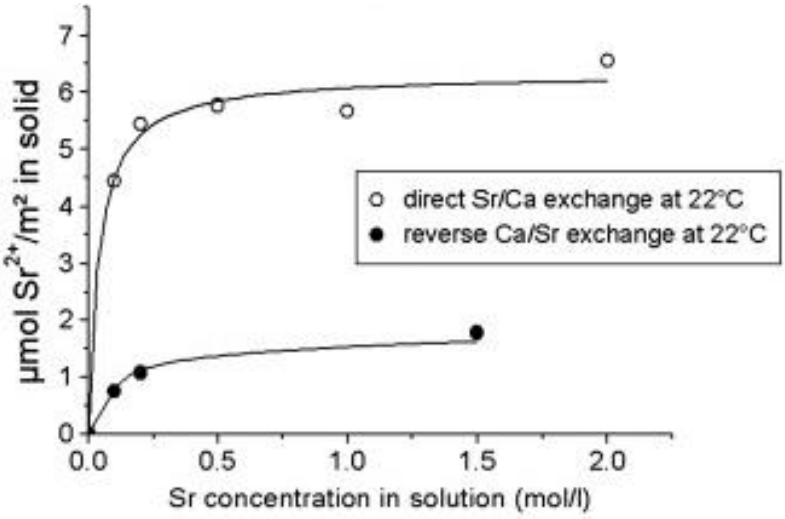


Figure 17: Sr^{2+} uptake on non-stoichiometric apatite after direct and inverse exchange with Ca^{2+}. Source: [244]. Adapted with permission of Elsevier.

Regardless of the mechanisms involved, such preparation of metal modified hydroxyapatite in excess of solution has many advantages: easy to implement, possible quantification of metal deposited on the surface by elementary analysis, absence of metal

leaching [26, 28, 342] due to irreversible immobilization ascribed to strong metal-support interaction, and finally high metal dispersion obtained [42]. Depending on the metal loading, the immobilized ion may remain isolated, resulting in atomically dispersed species, or be a nucleation point for the growth of highly dispersed nanoclusters or nanoparticles. Note that Ca^{2+} exchange process was also suggested by several authors to be the initial stage of metal deposition by incipient wetness impregnation (the volume of the metal-containing solution that is added onto the catalyst support is precisely adapted to its pore volume). In addition, in this later case, larger particle sizes are expected than with the exchange in excess of solution. In particular, the exchangeability properties (or involving other single atom or monomeric complex immobilization mechanisms) in aqueous medium provide a unique opportunity to get the active species atomically dispersed for low metal loading [18, 337, 343]. Such single atom catalysts are of great interest in heterogeneous catalysis as they are stable and durable [18]. The dispersion of cobalt onto ion-exchanged hydroxyapatite surface in the form of isolated Co^{2+} species for 0.2wt % loading was evidenced by magnetic measurements. However, for higher metal loading, Co_xO_y clustered entities then Co_3O_4 nanoparticles are formed at higher cobalt loading, resulting in a decreased basicity, and hence in the decay of specific activity in the 2-butanol and ethane dehydrogenation reactions [304, 344].

The Ni hydroxyapatite system also illustrates how crucial is the preparation method towards nickel dispersion for the control of selectivity and stability of the catalyst. This parameter is a very critical point for the challenging methane dry reforming reaction to avoid deactivation due to coke formation on nanoparticles. Large-size nickel particles (200 nm) supported over hydroxyapatite obtained by incipient wetness impregnation [103] were responsible for irreversible deactivation due to their densification and core-shell carbon formation. Coke deposition was comparatively more limited when nickel and cobalt were simultaneously co-impregnated on the support [104]. Although the co-precipitated Ni-Sr hydroxyapatite system led to promising results for the dry reforming of methane, the simultaneous presence of other nickel phosphate phases makes the origin of fine Ni particles (few nm), formed onto the surface of the spent catalyst, difficult to explain [321]. Recently, Ni deposited by exchange in excess of solution onto a cerium-doped hydroxyapatite previously prepared by co-precipitation led to very well dispersed Ni species, as deduced from aberration-corrected high angle annular dark field scanning transmission electron microscopy [18]. Cerium would prevent Ni sintering, resulting in the formation of particles of only 10 nm for 10 wt% Ni loading. Furthermore, for lower loading, 0.5 wt%, atomically dispersed Ni atoms could be stabilized as revealed by the absence of Ni-Ni bond detected by EXAFS. Such isolated Ni atoms

were found intrinsically coke-resistant due to their unique ability to only activate the first C-H bond in methane. It is proposed that cerium doping induces strong metal-support interaction which stabilizes Ni single atoms towards sintering resulting in highly stable and performant system for the dry reforming of methane [18].

Adsorption of molecules

As for ions adsorption, the adsorption of molecules on apatite particles affects only the surface of the crystals. In most cases, typically on high-temperature hydroxyapatite compounds or on biomimetic apatites with adsorbing molecule with only a low affinity for apatite surfaces, the adsorption process corresponds to a regular adsorptive event, with the "simple" positioning of the molecule on the crystal surface, establishing essentially electrostatic bonds with the ions constitutive of the surface. However, in some favorable cases involving biomimetic apatites when the adsorbing molecule exposes at least one high-affinity end-group (often anionic end-groups such as phosphate or phosphonate), the adsorption of the molecule was shown to be simultaneously accompanied by an ion exchange process, where the relevant end-group displaces surface ions (e.g. HPO_4^{2-}) for an actual anchoring of the molecule onto the surface hydrated layer. Several publications have indeed pointed out this effect showing, for example, that the adsorption of molecules with negative functional groups is generally related to a phosphate (or carbonate) ions release in the solution, evidencing such a concomitant ionic exchange reaction [323, 345, 346]. It may be remarked however that this cannot be *a priori* extended to all molecules containing a phosphate or phosphonate end-group, as other studies have shown the absence of simultaneous ion exchange even on biomimetic apatites [347, 348], and the overall molecular geometry/conformation also probably plays a key role in the molecule/support affinity, which will have to be further investigated by simulation methods.

Adsorption isotherms give essential information on the molecule/apatite interaction. They can be obtained by measuring the concentration of species in solution and in the solids during adsorption process. As for ion exchange, the adsorption of molecules on apatites is generally well represented by a Langmuir-type isotherm (although in certain cases other models such as Sips/Hill lead to a better fit), even in the case of a concomitant ion exchange involving the replacement of mineral ions of the apatite surface by molecular ions from the solution. In the case of such ion exchange simultaneous to adsorption, contrarily to general adsorption cases, no desorption should be expected here by simple dilution of the adsorbent solution (or even upon washing of the apatitic support), except for a low release due dissolution of the support. As for ions exchange, the number of ions displaced (*e.g.* phosphates) per adsorbed

molecule depends then on the characteristics of the apatitic surface [346, 349, 350] (**Figure 18**). Whether the adsorption event is associated or not to an ion exchange, the maturation stage and apatite composition play a significant role in the adsorption process, which is particularly relevant for biomimetic apatites. The Langmuir affinity constant also varies according to the characteristics of the apatite substrate, and the amount adsorbed at saturation appears higher for immature nanocrystals with a well-developed hydrated layer and decreases with the maturation time.

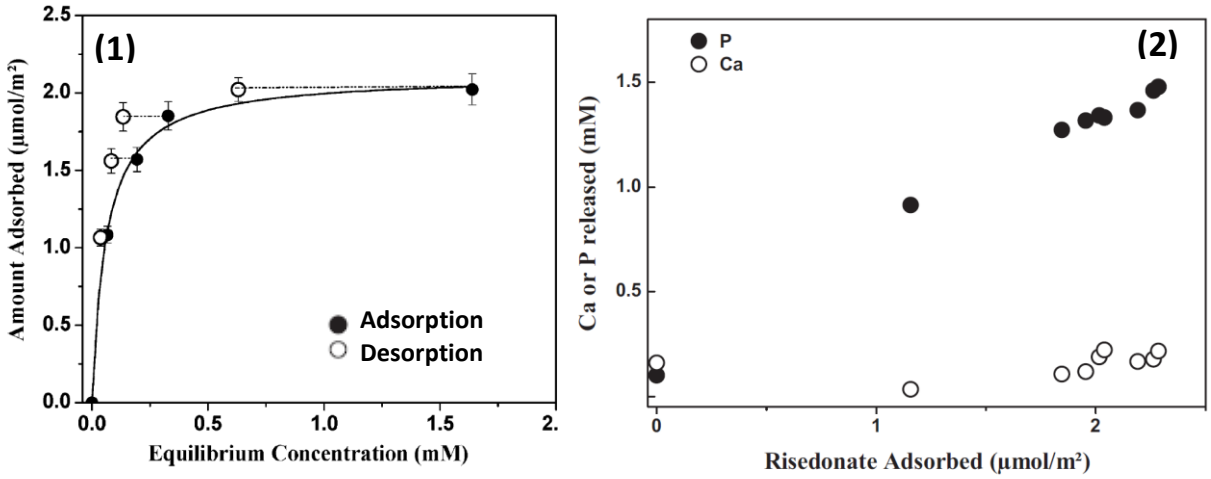


Figure 18: (1) Adsorption and desorption isotherms of bisphosphate molecules (risedronate) on stoichiometric HA at pH = 7.4 and T = 37 °C; the dashed lines indicate that no risedronate desorbs upon dilution. (2) Variation of the phosphate and calcium concentrations in the solution versus the amount of risedronate absorbed. Source: [326]. Adapted with permission of John Wiley and Sons.

Moreover, the nature of the functional end-groups of the molecule exposed is one of the key parameters to be taken into account when considering the interaction with a calcium phosphate surface. In case of adsorption with concomitant ion exchange, the number of (phosphate) ions displaced per adsorbed molecule has been determined by several authors and it appears dependent on the characteristics of the apatitic surface as well as the nature of the molecules adsorbed [346, 349, 350]. Phosphate esters and phosphonate, silicate and sulfate, and similar groups especially interact strongly with apatite surfaces. In general, carboxylate groups present a lower affinity, except when they are associated in polyacids [349, 351]. For example, the very high affinity of phosphoserine for apatite surface compared to that of serine can be related to the existence of the phosphate group which can strongly interact with the apatite surface, whereas the carboxyl group of serine itself presents only a moderate interaction with

HA surface. Thus, adsorption of serine can be described by a Freundlich-type isotherm like that of other simple molecules weakly interacting with apatite surfaces such as glycine or acetic acid, for example [350, 352]. Positively-charged groups (like $–NH_3^+$) can also adsorb on apatites but generally less strongly than negatively-charged ones.

It can be noticed that, as for ions exchanges, several phenomena can be considered as competitive reactions: the possible precipitation of calcium (or phosphate) salts with the adsorbing molecules, the dissolution equilibrium of the apatite and the surface, or hydrolysis reactions of the support. These events do not generally give a Langmuir-type isotherm with a typical saturation domain. The analysis of the solid phase by XRD, spectroscopic analysis or electron microscopy generally evidences new phases formation [211].

4. Conclusions

Apatitic calcium phosphates, such as HA, appear as excellent candidates of new class of greener catalytic materials offering numerous advantages for versatile applications in catalysis: tunable surface properties, recyclability and high thermal stability. These bio-inspired and eco-compatible materials offer the possibility of generating diverse chemical compositions, degrees of crystallinity and particle morphologies, depending on their mode of preparation (stoichiometric or non-stoichiometric, nanocrystalline or not, substituted or not, surface-grafted or not), thus providing samples with different features of relevance to catalysis. This chapter provides fundamental tools to help understanding the behavior of apatite-based catalysts, based on advances in the characterization of their structural and surface properties, through both experimental and computational approaches, to study their structure as well as their thermodynamic and physicochemical properties and surface reactivity. Based on the characteristics of the apatitic support, it is possible to improve performances by simply adjusting certain parameters to better fit the required application. Heterogeneous catalysis on apatites requires a good understanding of solid catalysts, including of their preparation methods and thorough characterization. Studying structure-properties-reactivity relationships is essential to provide a multi-scale description from microscopic to macroscopic scales, evaluate application performances and optimize their catalytic perspectives.

References

1. Bett JAS, Christner LG, Hall WK. (1967). Studies of the Hydrogen Held by Solids. XII. Hydroxyapatite Catalysts. *J Amer Chem Soc*. 89(22):5536-41.

2. Bett JAS, Hall WK. (1968). The microcatalytic technique applied to a zero order reaction: The dehydration of 2-butanol over hydroxyapatite catalysts. *J Catal*. 10:108-13.

3. Bett JAS, Christner LG, Hall WK. (1969). Infrared studies of hydroxyapatite catalysts. Adsorbed carbon dioxide, 2-butanol, and methyl ethyl ketone. *J Catal*.332-6.

4. Fihri A, Len C, Varma RS, Solhy A. (2017). Hydroxyapatite: A review of syntheses, structure and applications in heterogeneous catalysis. *Coordination Chemistry Reviews*. 347:48-76.

5. Nayak B, Samant A, Misra PK, Saxena M. (2019). Nanocrystalline hydroxyapatite: a potent material for adsorption, biological and catalytic studies. *Materials Today: Proceedings*. 9:689-98.

6. Ibrahim M, Labaki M, Giraudon J-M, Lamonier J-F. (2020). Hydroxyapatite, a multifunctional material for air, water and soil pollution control: A review. *Journal of hazardous materials*. 383:121139.

7. Imizu Y, Kadoya M, Abe H, Itoh H, Tada A. (1982). High-temperature evacuated hydroxyapatite as a base catalyst for the isomerization of 1-butene. *Chem Lett*. 3:414-6.

8. Scalbert J, Thibault-Starzyk F, Jacquot R, Morvan D, Meunier F. (2014). Ethanol condensation to butanol at high temperatures over a basic heterogeneous catalyst: How relevant is acetaldehyde self-aldolization? *J Catal*. 311:28-32.

9. Petit S, Thomas C, Millot Y, Krafft JM, Laberty-Robert C, Costentin G. (2020). Activation of C-H Bond of Propane by Strong Basic Sites Generated by Bulk Proton Conduction on V-Modified Hydroxyapatites for the Formation of Propene. *ChemCatChem*. 12 2506–21.

10. Han YF, Phonthammachai N, Ramesh K, Zhong Z, White T. (2008). Removing organic compounds from aqueous medium via wet peroxidation by gold catalysts. *Envron Sci Technol*. 42:908-12.

11. Zhang Y, Zhao Y, Xia C. (2009). Basic ionic liquids supported on hydroxyapatite-encapsulated γ-Fe2O3 nanocrystallites: An efficient magnetic and recyclable heterogeneous catalyst for aqueous Knoevenagel condensation. *J Mol Catal A*. 306(1):107-12.

12. Lv C, Liang H, Chen H, Wu L. (2019). Hydroxyapatite supported Co3O4 catalyst for enhanced degradation of organic contaminants in aqueous solution: Synergistic visible-light photo-catalysis and sulfate radical oxidation process. *Microchemical Journal*. 149:103959.

13. Mitsudome T, Mikami Y, Mori H, Arita S, Mizugaki T, Jitsukawa K, et al. (2009). Supported silver nanoparticle catalyst for selective hydration of nitriles to amides in water. *ChemCommun*. 22:3258-60.

14. Hara T, Kanai S, Mori K, Mizugaki T, Ebitani K, Jisukawa K, et al. (2006). Highly efficient C-C bond forming reactions in aqueous media catalyzed by monomeric vanadate species in an apatite framework. *J Org Chem*. 71:7455-62.

15. Sebti Sd, Tahir R, Nazih R, Saber A, Boulaajaj Sd. (2002). Hydroxyapatite as a new solid support for the Knoevenagel reaction in heterogeneous media without solvent. *Appl Catal A*. 228(1):155-9.

16. Ichihara J, Yamaguchi S, Nomoto T, Nakayama H, Iteya K, Naitoh N, et al. (2002). Keggin-type polyacid clusters on apatite: characteristic catalytic activities in solvent-free oxidation. *Tetrahedron Lett*. 43(46):8231-4.

17. Pillai KM, Singh S, Jonnalagadda S. (2010). Solvent-free Knoevenagel condensation over cobalt hydroxyapatite. *Synthetic Commun*. 40:3710–5.

18. Akri M, Shu Zhao S, Li X, Zang K, Lee AF, Isaacs MA, et al. (2019). Atomically dispersed nickel as coke-resistant active sites for methane dry reforming. *Nat Communic*. 10(1):1-10.

19. Sugiyama S, Hashimoto T, Morishita Y, Shigemoto N, Hayashi H. (2004). Effects of calcium cations incorporated into magnesium vanadates on the redox behaviors and the catalytic activities for the oxidative dehydrogenation of propane. *Appl Catal A*. 270(1-2):253-60.

20. Tsuchida T, Sakuma S, Takeguchi T, Ueda W. (2006). Direct Synthesis of n-Butanol from Ethanol over Nonstoichiometric Hydroxyapatite. *Ind Eng Chem Res*. 45:8634-42.

21. Wang Y, Chen B-b, Crocker M, Zhang Y-j, Zhu X-b, Shi C. (2015). Understanding on the origins of hydroxyapatite stabilized gold nanoparticles as high-efficiency catalysts for formaldehyde and benzene oxidation. *Catal Communic*. 59:195-200.

22. Tang H, Wei J, Liu F, Qiao B, Pan X, Li L, et al. (2016). Strong Metal–Support Interactions between Gold Nanoparticles and Nonoxides. *J Americ Chem Soc*. 138(1):56-9.

23. Boukha Z, Ayastuy JL, González-Velasco JR, Gutiérrez-Ortiz MA. (2018). Water-gas shift reaction over a novel Cu-ZnO/HAP formulation: Enhanced catalytic performance in mobile fuel cell applications. *Appl Catal A*. 566:1-14.

24. Yamaguchi K, Mori K, Mizugaki T, Ebitani K, Kaneda K. (2000). Creation of a Monomeric Ru Species on the Surface of Hydroxyapatite as an Efficient Heterogeneous Catalyst for Aerobic Alcohol Oxidation. *J Americ Chem Soc*. 122(29):7144-5.

25. Mori K, Hara T, Mizugaki T, Ebitani K, Kaneda K. (2003). Hydroxyapatite-Bound Cationic Ruthenium Complexes as Novel Heterogeneous Lewis Acid Catalysts for Diels−Alder and Aldol Reactions. *J Americ Chem Soc*. 125(38):11460-1.

26. Opre Z, Ferri D, Krumeich F, Mallat T, Baiker A. (2006). Aerobic oxidation of alcohols by organically modified ruthenium hydroxyapatite. *J Catal*. 241(2):287-95.

27. Yan B, Zhang Y, Chen G, Shan R, Ma W, Liu C. (2016). The utilization of hydroxyapatite-supported CaO-CeO2 catalyst for biodiesel production. *Energy Conversion and Management*. 130:156-64.

28. Pang Y, Kong L, Chen D, Yuvaraja G, Mehmood S. (2020). Facilely synthesized cobalt doped hydroxyapatite as hydroxyl promoted peroxymonosulfate activator for degradation of Rhodamine B. *J Hazard Mater*. 384:121447.

29. Maaten B, Moussa J, Desmarets C, Gredin P, Beaunier P, Kanger T, et al. (2014). Cu-modified hydroxy-apatite as catalyst for Glaser–Hay CC homo-coupling reaction of terminal alkynes. *Journal of Molecular Catalysis A: Chemical*. 393:112-6.

30. Boukha Z, Kacimi M, Pereira MFR, Faria JL, Figueiredo JL, Ziyad M. (2007). Methane dry reforming on Ni loaded hydroxyapatite and fluoroapatite. *Appl Catal A*. 317(2):299-309.

31. Zahmakıran M, Tonbul Y, Özkar S. (2010). Ruthenium(0) nanoclusters supported on hydroxyapatite: highly active, reusable and green catalyst in the hydrogenation of aromatics under mild conditions with an unprecedented catalytic lifetime. *Chem Commun*. 46:4788-90.

32. Gruselle M. (2015). Apatites: A new family of catalysts in organic synthesis. *J Organometal Chem*. 793:93-101.

33. Bilakanti V, Boosa V, Velisoju VK, Gutta N, Medak S, Akula V. (2017). Role of Surface Basic Sites in Sonogashira Coupling Reaction over Ca5(PO4)3OH Supported Pd Catalyst: Investigation by Diffuse Reflectance Infrared Fourier Transform Spectroscopy. *J Phys Chem C*. 121(40):22191-8.

34. Essamlali Y, Amadine O, Larzek M, Len C, Zahouily M. (2017). Sodium modified hydroxyapatite: Highly efficient and stable solid-base catalyst for biodiesel production. *J Enconman*. 149:355-67.

35. Li C, Xu G, Liu X, Zhang Y, Fu Y. (2017). Hydrogenation of Biomass-Derived Furfural to Tetrahydrofurfuryl Alcohol over Hydroxyapatite-Supported Pd Catalyst under Mild Conditions. *Ind Eng Chem Res*. 56(31):8843-9.

36. Xu G, Zhang Y, Fu Y, Guo Q. (2017). Efficient Hydrogenation of Various Renewable Oils over Ru-HAP Catalyst in Water. *ACS Catal*. 7(2):1158-69.

37. Chaudharya R, Dhepe PL. (2017). Solid base catalyzed depolymerization of lignin into low molecular weight products†. *Green Chem*. 19:778–88.

38. Gao T, Yin Y, Fang W, Cao Q. (2018). Highly dispersed ruthenium nanoparticles on hydroxyapatite as selective and reusable catalyst for aerobic oxidation of 5-hydroxymethylfurfural to 2,5-furandicarboxylic acid under base-free conditions. *J Mol Catal*. 450:55-64.

39. Ho CR, Zheng S, Shylesh S, Bell AT. (2018). The mechanism and kinetics of methyl isobutyl ketone synthesis from acetone over ion-exchanged hydroxyapatite. *J Catal*. 365:174-83.

40. Peeters A, Claes L, Geukens I, Stassen I, De Vos D. (2014). Alcohol amination with heterogeneous ruthenium hydroxyapatite catalysts. *Appl Catal A*. 469:191-7.

41. Sebti S, Tahir R, Nazih R, Boulaajaj S. (2001). Comparison of different Lewis acid supported on hydroxyapatite as new catalysts of Friedel–Crafts alkylation. *Appl Catal A*. 218:25-30.

42. Mori K, Yamaguchi K, Hara T, Mizugaki T, Ebitani K, Kaneda K. (2002). Controlled Synthesis of Hydroxyapatite-Supported Palladium Complexes as Highly Efficient Heterogeneous Catalysts. *J Amer Chem Soc*. 124(39):11572-3.

43. Venugopal A, Scurrell MS. (2003). Hydroxyapatite as a novel support for gold and ruthenium catalysts. Behaviour in the water gas shift reaction *Appl Catal A*. 245(1):137-47.

44. Wuyts S, De Vos DE, Verpoort F, Depla D, De Gryse R, Jacobs PA. (2003). A heterogeneous Ru–hydroxyapatite catalyst for mild racemization of alcohols. *J Catal*. 219(2):417-24.

45. Mori K, Hara T, Mizugaki T, Ebitani K, Kaneda K. (2004). Hydroxyapatite-Supported Palladium Nanoclusters: A Highly Active Heterogeneous Catalyst for Selective Oxidation of Alcohols by Use of Molecular Oxygen. *J Amer ChemSoc*. 126(34):10657-66.

46. Solhy A, Clark JH, Tahir R, Sebti S, Larzek M. (2006). Transesterifications catalysed by solid, reusable apatite–zinc chloride catalysts. *Green Chem*. 8:871-4.

47. Tahir R, Banert K, Solhy A, Sebti S. (2006). Zinc bromide supported on hydroxyapatite as a new and efficient solid catalyst for Michael addition of indoles to electron-deficient olefins. *J Mol Catal*. 246(1-2):39-42.

48. Khachani M, Kacimi M, Ensuque A, Piquemal JY, Connan C, Bozon-Verduraz F, et al. (2010). Iron–calcium–hydroxyapatite catalysts: Iron speciation and comparative performances in butan-2-ol conversion and propane oxidative dehydrogenation. *Appl Catal A*. 388:113-23.

49. Matsuura Y, Onda A, Ogo S, Yanagisawa K. (2014). Acrylic acid synthesis from lactic acid over hydroxyapatite catalysts with various cations and anions. *Catal Today*. 226:192-7.

50. Sugiyama S, Osaka T, Hirata Y, Sotowa KI. (2006). Enhancement of the activity for oxidative dehydrogenation of propane on calcium hydroxyapatite substituted with vanadate. *Appl Catal A*. 312:52-8.

51. Chlala D, Giraudon JM, Nuns N, Lancelot C, Vannier R-N, Labaki M, et al. (2016). Active Mn species well dispersed on Ca2+ enriched apatite for total oxidation of toluene. *Appl Catal B*. 184:87-95.

52. Tounsi H, Djemal S, Petitto C, Delahay G. (2011). Copper loaded hydroxyapatite catalyst for selective catalytic reduction of nitric oxide with ammonia. *Appl Catal B*. 107(1):158-63.

53. Dasireddy VDBC, Friedrich HB, Singh S. (2013). Studies towards a mechanistic insight into the activation of n-octane using vanadium supported on alkaline earth metal hydroxyapatites. *Appl Catal A*. 467:142-53.

54. Dasireddy VDBC, Singh S, Friedrich HB. (2013). Activation of n-octane using vanadium oxide supported on alkaline earth hydroxyapatites. *Appl Catal A*. 456:105-17.

55. Dasireddy VDBC, Singh S, Friedrich HB. (2014). Vanadium oxide supported on non-stoichiometric strontium hydroxyapatite catalysts for the oxidative dehydrogenation of n-octane. *J Mol Catal A*. 395:398-408.

56. Carvalho DC, Pinheiro LG, Campos A, Millet ERC, de Sousa FF, Filho JM, et al. (2014). Characterization and catalytic performances of copper and cobalt-exchanged hydroxyapatite in glycerol conversion for 1-hydroxyacetone production. *Appl Catal A Gen*. 471:39-49.

57. Jemal J, Petitto C, Delahay G, Ksibi Z, Tounsi H. (2015). Selective catalytic reduction of NO by NH3 over copper-hydroxyapatite catalysts: effect of the increase of the specific surface area of the support. *Reac Kinet Mech Cat*. 114:185-96.

58. Campisi S, Galloni MG, Bossola F, Gervasini A. (2019). Comparative performance of copper and iron functionalized hydroxyapatite catalysts in NH3-SCR. *Catal Communic*. 123:79-85.

59. Moteki T, Flaherty DW. (2016). Mechanistic Insight to C−C Bond Formation and Predictive Models for Cascade Reactions among Alcohols on Ca- and Sr-Hydroxyapatites. *ACS Catal*. 6:4170-83.

60. Smahi A, Solhy A, El Badaoui H, Amoukal A, Tikad A, Maizi M, et al. (2003). Potassium fluoride doped fluorapatite and hydroxyapatite as new catalysts in organic synthesis. *ApplCatalA: Gen*. 250:151-9.

61. Sebti S, Solhy A, Tahir R, Smahi A. (2002). Modified hydroxyapatite with sodium nitrate: an efficient new solid catalyst for the Claisen-Schmidt condensation. *Appl Catal A*. 235(1-2):273-81.

62. Solhy A, Tahir R, Sebti S, Skouta R, Bousmina M, Zahouily M, et al. (2010). Efficient synthesis of chalcone derivatives catalyzed by re-usable hydroxyapatite. *Appl Catal A*. 374(1):189-93.

63. Mori K, Oshiba M, Hara T, Mizugaki T, Ebitani K, Kaneda K. (2005). Michael reaction of 1,3-dicarbonyls with enones catalyzed by a hydroxyapatite-bound La complex. *Tetrahedron Lett*. 46(25):4283-6.

64. Mori K, Oshiba M, Hara T, Mizugaki T, Ebitani K, Kaneda K. (2006). Creation of monomeric La complexes on apatite surfaces and their application as heterogeneous catalysts for Michael reactions. *New J Chem*. 30:44-52.

65. Tsuchida T, Yoshioka T, Sakuma S, Takeguchi T, Ueda W. (2008). Synthesis of Biogasoline from Ethanol over Hydroxyapatite Catalyst. *Ind Eng Chem Res*. 47:1443-52.

66. Tsuchida T, Kubo J, Yoshioka T, Sakuma S, Takeguchi T, Ueda W. (2008). Reaction of ethanol over hydroxyapatite affected by Ca/P ratio of catalyst. *J Catal*. 259(2):183-9.

67. Ogo S, Onda A, Yanagisawa K. (2011). Selective synthesis of 1-butanol from ethanol over strontium phosphate hydroxyapatite catalysts. *Appl Catal A*. 402(1):188-95.

68. Silvester L, Lamonier JF, Faye, J., Capron M, Vannier RN, Lamonier C, et al. (2015). Reactivity of ethanol over hydroxyapatite-based Ca-enriched catalysts with various carbonate contents. *Catal Sci Technol*. 5:2994-3006.

69. Hanspal S, Young ZD, Shou H, Davis RJ. (2015). Multiproduct steady-state isotopic transient kinetc analysis of the ethanol coupling reaction over hydroxyapatite and magneisa. *ACS Catal*. 5:1737-46.

70. Silvester L, Lamonier JF, Lamonier C, Capron M, Vannier RN, Mamede AS, et al. (2017). Guerbet Reaction over Strontium-Substituted Hydroxyapatite Catalysts Prepared at Various (Ca+Sr)/P Ratios. *ChemCatChem*. 9:2250 – 61.

71. Hanspal S, Young D, Prillaman JT, Davis RJ. (2017). Influence of surface acid and base sites on the Guerbet coupling of ethanol to butanol over metal phosphate catalysts. *J Catal*. 352:182-90.

72. Young ZD, Davis RJ. (2018). Hydrogen transfer reactions relevant to Guerbet coupling of alcohols over hydroxyapatite and magnesium oxide catalysts. *Catal Sci Technol*. 8:1722-9.

73. Wu X, Fang G, Tong Y, Jiang D, Liang Z, Leng W, et al. (2018). Catalytic Upgrading of Ethanol to n-Butanol:Progress in Catalyst Development. *ChemSusChem*. 11:71-85.

74. Cimino S, Lisi L, Romanucci S. (2018). Catalysts for conversion of ethanol to butanol: Effect of acid-base and redox properties. *Catal Today*. 304:58-63.

75. Ben Osman M, Krafft JM, Thomas C, Yoshioka T, Kubo J, Costentin G. (2019). Importance of the Nature of the Active Acid / Base Pairs of Hydroxyapatite Involved in the Catalytic Transformation of Ethanol to n-Butanol Revealed by Operando DRIFTS. *ChemCatChem* 11(6):1765-78.

76. Ogo S, Onda A, Iwasa Y, Hara K, Fukuoka A, Yanagisawa K. (2012). 1-Butanol synthesis from ethanol over strontium phosphate hydroxyapatite catalysts with various Sr/P ratios. *Journal of catalysis*. 296:24-30.

77. Masuyama Y, Yoshikawa K, Suzuki N, Hara K, Fukuoka A. (2011). Hydroxyapatite-supported copper(II)-catalyzed azide–alkyne [3+2] cycloaddition with neither reducing agents nor bases in water. *Tetrahedron Lett*. 52(51):6916-8.

78. Choudary BM, Sridhar C, Kantam ML, Venkanna GT, Sreedhar B. (2005). Design and Evolution of Copper Apatite Catalysts for N-Arylation of Heterocycles with Chloro- and Fluoroarenes. *J Amer Chem Soc*. 127(28):9948-9.

79. Kanai H, Nakao M, Imamura S. (2003). Selective photoepoxidation of propylene over hydroxyapatite–silica composites. *Catal Communic*. 4(8):405-9.

80. Opre Z, Mallat T, Baiker A. (2007). Epoxidation of styrene with cobalt-hydroxyapatite and oxygen in dimethylformamide: A green technology? *J Catal*. 245(2):482-6.

81. Singh SJ, Sreekanth B. (2008). Selective oxidation of n-pentane over V2O5 supported on hydroxyapatite *Catal Lett*. 126(1-2):200-6.

82. Boucetta C, Kacimi M, Ensique J, Y., Bonzon-Verduraz F, Ziyad M. (2009). Oxidative dehydrogenation of propane over chromium-loaded calcium hydroxyapatite. *Appl Catal A*. 356:201-10.

83. Dasireddy VDBC, Singh S, Friedrich HB. (2012). Oxidative dehydrogenation of n-octane using vanadium pentoxide-supported hydroxyapatite catalysts. *Appl Catal A*. 421-422:58-69.

84. Chlala D, Giraudon JM, Nuns N, Labaki M, Lamonier JF. (2017). Highly Active Noble-Metal-Free Copper Hydroxyapatite Catalysts for the Total Oxidation of Toluene. *ChemCatChem*. 9:2275-83.

85. Aellach B, Ezzamarty A, Leglise J, Lamonier C, Lamonier JF. (2010). Calcium-deficient and stoichiometric hydroxypatite promoted by cobalt for the catalytic removal of oxygenated volatile organic compounds. *Catal Lett*. 135:197-206.

86. More RK, Lavande NR, More PM. (2019). Copper supported on Co substituted hydroxyapatite for complete oxidation of diesel engine exhaust and VOC. *Molecul Catal*. 474:110414.

87. Dominguez MI, Romero-Sarria F, Centeno MA, Odriozola JA. (2009). Gold/hydroxyapatite catalysts. Synthesis, characterization and catalytic activity to CO oxidation. *Appl Catal B*. 87:245-51.

88. Chlala D, Labaki M, Giraudon J-M, Gardoll O, Denicourt-Nowicki A, Roucoux A, et al. (2016). Toluene total oxidation over Pd and Au nanoparticles supported on hydroxyapatite. *CR Chimie*. 19(4):525-37.

89. Sun Y-P, Fu H-Y, Zhang D-l, Li R-X, Chen H, Li X-J. (2010). Complete hydrogenation of quinoline over hydroxyapatite supported ruthenium catalyst. *Catal Communic*. 12(3):188-92.

90. Kibby CL, Hall WK. (1973). Dehydrogenation of alcohols and hydrogen transfer from alcohols to ketones over hydroxyapatite catalysts. *J Catal*. 31(1):65-73.

91. Boukha Z, Kacimi M, Ziyad M, Ensuque A, Bozon-Verduraz F. (2007). Comparative study of catalytic activity of Pd loaded hydroxyapatite and fluoroapatite in butan-2-ol conversion and methane oxidation. *J Mol Catal*. 270(1):205-13.

92. Zaccheria F, Scotti N, Ravasio N. (2018). The Role of Copper in the Upgrading of Bioalcohols. *ChemCatChem*. 10:1526-35.

93. Goulas KA, Song Y, Johnson GR, Chen JP, Gokhale AA, Grabow LC, et al. (2018). Selectivity tuning over monometallic and bimetallic dehydrogenation catalysts: effects of support and particle size. *Catal SciTech*. 8(1):314-27.

94. Stošić D, Bennici S, Sirotin S, Calais C, Couturier JL, Dubois JL, et al. (2012). Glycerol dehydration over calcium phosphate catalysts: Effect of acidic–basic features on catalytic performance. *Appl Catal A*. 447-448:124-34.

95. Ghantani VC, Lomate ST, Dongare MK, Umbarkar SB. (2013). Catalytic dehydration of lactic acid to acrylic acid using calcium hydroxyapatite catalysts. *Green Chem*. 15(5):1211-7.

96. Sugiyama S, Moffat JB. (2002). Cation Effects in the Conversion of Methanol on Calcium, Strontium, Barium and Lead Hydroxyapatites. *Catal Lett*. 81(1-2):77-81.

97. Cheikhi N, Kacimi M, Rouimi M, Ziyad M, Liotta LF, Pantaleo G, et al. (2005). Direct synthesis of methyl isobutyl ketone in gas-phase reaction over palladium-loaded hydroxyapatite. *J Catal*. 232(2):257-67.

98. Rahmanian A, Ghaziaskar HS. (2013). Continuous dehydration of ethanol to diethyl ether over aluminum phosphate–hydroxyapatite catalyst under sub and supercritical condition. *J Supercritical Fluids*. 78:34-41.

99. Yan B, Tao LZ, Liang Y, Xu BQ. (2014). Sustainable Production of Acrylic Acid: Catalytic Performance of Hydroxyapatites for Gas-Phase Dehydration of Lactic Acid. *ACS Catal*. 4(6):1931-43.

100. Miao D, Cavusoglu G, Lichtenberg H, Yu J, Xu H, Grunwaldt JD, et al. (2017). Water-gas shift reaction over platinum/strontium apatite catalysts. *Appl Catal B*. 202:587-96.

101. Schiavoni M, Campisi S, Carniti P, Gervasini A, Delplanche T. (2018). Focus on the catalytic performances of Cu-functionalized hydroxyapatites in NH3-SCR reaction. *Appl Catal A*. 563:43-53.

102. Ogo S, S. M, Sekine Y. (2017). Coke Resistance of Sr-Hydroxyapatite Supported Co Catalyst for Ethanol Steam Reforming. *Chem Lett*. 46:729–32.

103. Rego de Vasconcelos B, Pham Minh D, Sharrock P, Nzihou A. (2018). Regeneration study of Ni/hydroxyapatite spent catalyst from dry reforming. *Catal Today*. 310:107-15.

104. Phan TS, Sane AR, Rêgo de Vasconcelos B, Nzihou A, Sharrock P, Grouset D, et al. (2018). Hydroxyapatite supported bimetallic cobalt and nickel catalysts for syngas production from dry reforming of methane. *Appl Catal B*. 224:310-21.

105. Boukha Z, Yeste MP, Cauqui MÁ, González-Velasco JR. (2019). Influence of Ca/P ratio on the catalytic performance of Ni/hydroxyapatite samples in dry reforming of methane. *Appl Catal A*. 580:34-45.

106. Kaneda K, Mizugaki T. (2009). Development of concerto metal catalysts using apatite compounds for green organic syntheses. *Energy Environ Sci*. 2:655-73.

107. Sugiyama S. (2007). Approach Using apatite to stiudies on energy and environment. *Phosphorus Res Bull*. 21:1-8.

108. Kuwahara Y, Ohmichi T, Kamegawa T, Mori K, Yamashita H. (2009). A novel synthetic route to hydroxyapatite–zeolite composite material from steel slag: investigation of synthesis mechanism and evaluation of physicochemical properties. *J Mater Chem*. 19:7263-72.

109. Gorbanev YY, Kegnæs S, Riisager A. (2011). Selective Aerobic Oxidation of 5-Hydroxymethylfurfural in Water Over Solid Ruthenium Hydroxide Catalysts with Magnesium-Based Supports. *Catal Lett*. 141:1752-60.

110. Wang QN, Weng XF, Zhou BC, Lv SP, Miao S, Zhang D, et al. (2019). Direct, Selective Production of Aromatic Alcohols from Ethanol Using a Tailored Bifunctional Cobalt−Hydroxyapatite Catalyst. *ACS Catal*. 9:7204−16.

111. Nishimura S, Mizuhori K, Ebitani K. (2016). Reductive amination of furfural toward furfurylamine with aqueous ammonia under hydrogen over Ru-supported catalyst. *Res Chem Interm*. 42(1):19-30.

112. Lovón-Quintana JJ, Rodriguez-Guerrero JK, Valença PG. (2017). Carbonate hydroxyapatite as a catalyst for ethanol conversion to hydrocarbon fuels. *Appl Catal A:*. 542:136-45.

113. De Leeuw N. (2010). Computer simulations of structures and properties of the biomaterial hydroxyapatite. *Journal of Materials Chemistry*. 20(26):5376-89.

114. Zhao W, Xu Z, Yang Y, Sahai N. (2014). Surface energetics of the hydroxyapatite nanocrystal–water interface: a molecular dynamics study. *Langmuir*. 30(44):13283-92.

115. Elliott JC. (1994). *Structure and Chemistry of the Apatites and other Calcium Orthophosphates*. Amsterdam: Elsevier Science BV.

116. White TJ, ZhiLi D. (2003). Structural derivation and crystal chemistry of apatites. *Acta Crystallographica Section B*. 59(1):1-16.

117. Ptáček P. (2016). Introduction to apatite In *Apatites and their Synthetic Analogues-Synthesis, Structure, Properties and Applications*: IntechOpen.

118. Ma G, Liu XY. (2009). Hydroxyapatite: hexagonal or monoclinic? *Crystal Growth and Design*. 9(7):2991-4.

119. Kay MI, Young RA, Posner AS. (1964). Crystal structure of hydroxyapatite. *Nature*. 204:1050-2.

120. Rey C, Combes C, Drouet C, Grossin D. (2011). Bioactive Ceramics: Physical Chemistry. In *Comprehensive biomaterials*, Elsevier, editor. p. 187-221.

121. De Leeuw N. (2001). Local ordering of hydroxy groups in hydroxyapatite. *Chemical Communications*. (17):1646-7.

122. Almora-Barrios N, Grau-Crespo R, Leeuw NHd. (2013). A computational study of magnesium incorporation in the bulk and surfaces of hydroxyapatite. *Langmuir*. 29(19):5851-6.

123. Balachandran PV, Rajan K. (2012). Structure maps for AI4AII6 (BO4) 6X2 apatite compounds via data mining. *Acta Crystallographica Section B: Structural Science*. 68(1):24-33.

124. Habelitz S, Pascual L, Durán A. (1999). Nitrogen-containing apatite. *Journal of the European Ceramic Society*. 19(15):2685-94.

125. Corno M, Rimola A, Bolis V, Ugliengo P. (2010). Hydroxyapatite as a key biomaterial: quantum-mechanical simulation of its surfaces in interaction with biomolecules. *Physical Chemistry Chemical Physics*. 12(24):6309-29.

126. Slepko A, Demkov AA. (2011). First-principles study of the biomineral hydroxyapatite. *Physical Review B*. 84(13):134108.

127. Šupová M. (2015). Substituted hydroxyapatites for biomedical applications: a review. *Ceramics international*. 41(8):9203-31.

128. Chappell H, Duer M, Groom N, Pickard C, Bristowe P. (2008). Probing the surface structure of hydroxyapatite using NMR spectroscopy and first principles calculations. *Physical Chemistry Chemical Physics*. 10(4):600-6.

129. Opre Z, van Bokhoven JA, Baiker A. (2007). Catalytic oxidation over transition metal containing hydroxyapatites.

130. Goldenberg JE, Wilt Z, Schermerhorn DV, Pasteris JD, Yoder CH. (2015). Structural effects on incorporated water in carbonated apatites. *American Mineralogist*. 100(1):274-80.

131. Uskoković V. (2015). The Role of Hydroxyl Channel in Defining Selected Physicochemical Peculiarities Exhibited by Hydroxyapatite. *RSC Adv*. 5:36614-33.

132. Wang J. (2015). Incorporation of iodine into apatite structure: a crystal chemistry approach using Artificial Neural Network. *Frontiers in Earth Science*. 3:20.

133. Markovic S, Veselinovic L, Lukic MJ, Karanovic L, Bracko I, Ignjatovic N, et al. (2011). Synthetical bone-like and biological hydroxyapatites: a comparative study of crystal structure and morphology. *Biomed Mater*. 6(4):045005.

134. Rey C. (2020). Apatite Channels and Zeolite-Like Properties. In *Hydroxyapatite and Related Materials*, Paul W. Brown BC, editor. Boca Raton: CRC Press. p. 257-62.

135. Sugiyama S, Osaka T, Hirata Y, Sotowa K-I. (2006). Enhancement of the activity for oxidative dehydrogenation of propane on calcium hydroxyapatite substituted with vanadate. *Applied Catalysis A: General*. 312:52-8.

136. Yashima M, Kubo N, Omoto K, Fujimori H, Fujii K, Ohoyama K. (2014). Diffusion Path and Conduction Mechanism of Protons in Hydroxyapatite. *The Journal of Physical Chemistry C*. 118(10):5180-7.

137. Camargo CL, Resende NS, Perez CA, Abreu CR, Salim VM, Tavares FW. (2018). Molecular dynamics simulation and experimental validation by X-ray data of hydroxyapatite crystalline structures. *Fluid Phase Equilibria*. 470:60-7.

138. Mostafa NY, Brown PW. (2007). Computer simulation of stoichiometric hydroxyapatite: Structure and substitutions. *Journal of Physics and Chemistry of Solids*. 68(3):431-7.

139. Zahn D, Hochrein O. (2008). On the composition and atomic arrangement of calcium-deficient hydroxyapatite: An ab-initio analysis. *Journal of Solid State Chemistry*. 181(8):1712-6.

140. Sun J, Song Y, Wen G, Wang Y, Yang R. (2013). Softening of hydroxyapatite by vacancies: a first principles investigation. *Materials Science and Engineering: C*. 33(3):1109-15.

141. Ulian G, Valdrè G, Corno M, Ugliengo P. (2014). DFT investigation of structural and vibrational properties of type B and mixed AB carbonated hydroxylapatite. *American Mineralogist*. 99(1):117-27.

142. Astala R, Stott M. (2005). First principles investigation of mineral component of bone: CO3 substitutions in hydroxyapatite. *Chemistry of Materials*. 17(16):4125-33.

143. Fleet ME, Liu X. (2007). Coupled substitution of type A and B carbonate in sodium-bearing apatite. *Biomaterials*. 28(6):916-26.

144. Ren F, Lu X, Leng Y. (2013). Ab initio simulation on the crystal structure and elastic properties of carbonated apatite. *Journal of the mechanical behavior of biomedical materials*. 26:59-67.

145. Peroos S, Du Z, de Leeuw NH. (2006). A computer modelling study of the uptake, structure and distribution of carbonate defects in hydroxy-apatite. *Biomaterials*. 27(9):2150-61.

146. De Leeuw N. (2002). Density functional theory calculations of solid solutions of fluor-and chlorapatites. *Chemistry of materials*. 14(1):435-41.

147. Jay EE, Rushton MJ, Grimes RW. (2012). Migration of fluorine in fluorapatite–a concerted mechanism. *Journal of Materials Chemistry*. 22(13):6097-103.

148. Sugiyama S, Sugimoto N, Hirata Y, Nakagawa K, Sotowa K-I. (2008). Oxidative dehydrogenation of propane on vanadate catalysts supported on various metal hydroxyaptites. *Phosphorus Research Bulletin*. 22:13-6.

149. Wang M, Wang Q, Lu X, Wang K, Ren F. (2017). Computer simulation of ions doped hydroxyapatite: a brief review. *Journal of Wuhan University of Technology-Mater Sci Ed*. 32(4):978-87.

150. Ma X, Ellis DE. (2008). Initial stages of hydration and Zn substitution/occupation on hydroxyapatite (0001) surfaces. *Biomaterials*. 29(3):257-65.

151. Bigi A, Boanini E, Capuccini C, Gazzano M. (2007). Strontium-substituted hydroxyapatite nanocrystals. *Inorganica Chimica Acta*. 360(3):1009-16.

152. Terra J, Dourado ER, Eon J-G, Ellis DE, Gonzalez G, Rossi AM. (2009). The structure of strontium-doped hydroxyapatite: an experimental and theoretical study. *Physical Chemistry Chemical Physics*. 11(3):568-77.

153. Matsunaga K, Inamori H, Murata H. (2008). Theoretical trend of ion exchange ability with divalent cations in hydroxyapatite. *Physical Review B*. 78(9):094101.

154. Wang Q, Li P, Tang P, Ge X, Ren F, Zhao C, et al. (2019). Experimental and simulation studies of strontium/fluoride-codoped hydroxyapatite nanoparticles with osteogenic and antibacterial activities. *Colloids and Surfaces B: Biointerfaces*. 182:110359.

155. Li P, Jia Z, Wang Q, Tang P, Wang M, Wang K, et al. (2018). A resilient and flexible chitosan/silk cryogel incorporated Ag/Sr co-doped nanoscale hydroxyapatite for osteoinductivity and antibacterial properties. *Journal of Materials Chemistry B*. 6(45):7427-38.

156. Shang S, Zhao Q, Zhang D, Sun R, Tang Y. (2019). Molecular dynamics simulation of the adsorption behavior of two different drugs on hydroxyapatite and Zn-doped hydroxyapatite. *Materials Science and Engineering: C*. 105:110017.

157. Kasamatsu S, Sugino O. (2018). First-principles investigation of polarization and ion conduction mechanisms in hydroxyapatite. *Physical Chemistry Chemical Physics*. 20(13):8744-52.

158. Wang Q, Tang P, Ge X, Li P, Lv C, Wang M, et al. (2018). Experimental and simulation studies of strontium/zinc-codoped hydroxyapatite porous scaffolds with excellent osteoinductivity and antibacterial activity. *Applied Surface Science*. 462:118-26.

159. Ishisone K, Jiraborvornpongsa N, Isobe T, Matsushita S, Wakumura M, Oshikiri M, et al. (2020). Experimental and theoretical investigation of WOx modification effects on the photocatalytic activity of titanium-substituted hydroxyapatite. *Applied Catalysis B: Environmental*. 264:118516.

160. Rey C, Combes C, Drouet C, Glimcher M. (2009). Bone mineral: update on chemical composition and structure. *Osteoporosis International*. 20(6):1013-21.

161. Eichert D, Drouet C, Sfihi H, Rey C, Combes C. (2007). Nanocrystalline apatite-based biomaterials: synthesis, processing and characterization. *Biomaterials Research Advances*.93-143.

162. Rey C, Combes C, Drouet C, Lebugle A, Sfihi H, Barroug A. (2007). Nanocrystalline apatites in biological systems: characterisation, structure and properties. *Materialwissenschaft und Werkstofftechnik*. 38(12):996-1002.

163. Rey C, Combes C, Drouet C, Cazalbou S, Grossin D, Brouillet F, et al. (2014). Surface properties of biomimetic nanocrystalline apatites; applications in biomaterials. *Progress in Crystal Growth and Characterization of Materials*. 60(6):3e73.

164. Gómez-Morales J, Iafisco M, Delgado-López JM, Sarda S, Drouet C. (2013). Progress on the preparation of nanocrystalline apatites and surface characterization: Overview of fundamental and applied aspects. *Progress in Crystal Growth and Characterization of Materials*. 59(1):1-46.

165. Drouet C, Gomez-Morales J, Iafisco M, Sarda S, Rimondini L, Bianchi C, et al. (2012). Calcium phosphate surface tailoring technologies for drug delivering and tissue engineering. *Surface Tailoring of Inorganic Materials for Biomedical Applications*.43-111.

166. Wilson RM, Elliott JC, Dowker SE, Rodriguez-Lorenzo LM. (2005). Rietveld refinements and spectroscopic studies of the structure of Ca-deficient apatite. *Biomaterials*. 26(11):1317-27.

167. Kim HM, Rey C, Glimcher MJ. (1995). Isolation of calcium-phosphate crystals of bone by non-aqueous methods at low temperature. *Journal of Bone and Mineral Research*. 10(10):1589-601.

168. Eichert D, Sfihi H, Combes C, Rey C. (2004). Specific characteristics of wet nanocrystalline apatites. Consequences on biomaterials and bone tissue. *Key Engineering Materials*. 254:927-30.

169. Jäger C, Welzel T, Meyer Zaika W, Epple M. (2006). A solid state NMR investigation of the structure of nanocrystalline hydroxyapatite. *Magn Reso Chem*. 44(6):573-80.

170. Rey C, Combes C, Drouet C, Sfihi H, Barroug A. (2007). Physico-chemical properties of nanocrystalline apatites: Implications for biominerals and biomaterials. *Materials Science and Engineering: C*. 27(2):198-205.

171. Wu H, Xu D, Yang M, Zhang X. (2016). Surface structure of hydroxyapatite from simulated annealing molecular dynamics simulations. *Langmuir*. 32(18):4643-52.

172. Xie Q, Xue Z, Gu H, Hu C, Yang M, Wang X, et al. (2018). Molecular Dynamics Exploration of Ordered-to-Disordered Surface Structures of Biomimetic Hydroxyapatite Nanoparticles. *The Journal of Physical Chemistry C*. 122(12):6691-703.

173. Lu Y, Dong W, Ding J, Wang W, Wang A. (2019). Hydroxyapatite Nanomaterials: Synthesis, Properties, and Functional Applications. In *Nanomaterials from Clay Minerals*: Elsevier. p. 485-536.

174. Silvester L, Lamonier JF, Vannier RN, Lamonier C, Capron M, Mamede AS, et al. (2014). Structural, textural and acid-base properties of carbonates-containing hydroxyapatites. *J Mater Chem A*. 2:11073-90.

175. Solhy A, Amer W, Karkouri M, Tahir R, El Bouari A, Fihri A, et al. (2011). Bi-functional modified-phosphate catalyzed the synthesis of α-α′-(EE)-bis (benzylidene)-cycloalkanones: Microwave versus conventional-heating. *Journal of Molecular Catalysis A: Chemical*. 336(1-2):8-15.

176. Monma H. (1982). Catalytic Behavior of Calcium Phosphates for Decompositions of 2-Propanol and Ethanol. *J Catal*. 75:200-3.

177. Gruselle M, Kanger T, Thouvenot R, Flambard A, Kriis K, Mikli V, et al. (2011). Calcium hydroxyapatites as efficient catalysts for the michael C–C bond formation. *ACS Catalysis*. 1(12):1729-33.

178. Rodrigues EG, Keller TC, Mitchell S, Pérez-Ramírez J. (2014). Hydroxyapatite, an exceptional catalyst for the gas-phase deoxygenation of bio-oil by aldol condensation. *Green Chem*. 16:4870-4.

179. Wang J-D, Liu J-K, Lu Y, Hong D-J, Yang X-H. (2014). Catalytic performance of gold nanoparticles using different crystallinity HAP as carrier materials. *Mater Res Bull*. 55:190-7.

180. Kibby CL, Hall WK. (1973). Studies of acid catalyzed reactions: XII. Alcohol decomposition over hydroxyapatite catalysts. *J Catal*. 29(1):144-59.

181. Sugiyama S, Minami T, Moriga T, Hayashi H, Koto K, Tanaka M, et al. (1996). Surface and bulk properties, catalytic activities and selectivities in methane oxidation on near-stoichiometric calcium hydroxyapatites. *J Mater Chem*. 6(3):459-64.

182. Matsumura Y, Moffat JB. (1996). Methanol adsorption and dehydrogenation over stoichiometric and non-stoichiomet ric h ydroxyapa tit e cat alysts. *J Chem SOC, Faraday Trans*. 92:1981-4.

183. Tsuchida T, Kubo J, Yoshioka T, Sakuma S, Takeguchi T, Ueda W. (2009). Influence of preparation factors on Ca/P ratio and surface basicity of hydroxyapatite catalysts. *J Jap Petrol Inst*. 52(2).

184. Lauron-Pernot H. (2006). Evaluation of Surface Acido-Basic Properties of Inorganic-Based Solids by Model Catalytic Alcohol Reaction Networks

Catal Rev. 48:315-61.

185. Diallo-Garcia S, Laurencin D, Krafft JM, Casale S, Smith ME, Lauron-Pernot H, et al. (2011). Influence of Magnesium Substitution on the Basic Properties of Hydroxyapatites. *J Phys Chem C*. 115:24317-27.

186. Ben Osman M, Krafft JM, Millot Y, Averseng F, Yoshioka T, Kubo J, et al. (2016). Molecular Understanding of the Bulk Composition of Crystalline Nonstoichiometric Hydroxyapatites: Application to the Rationalization of Structure–Reactivity Relationships. *Eur J Inorg Chem*. 17:2709-20.

187. Petitjean H, Krafft JM, Che M, Lauron Pernot H, Costentin G. (2010). Basic reactivity of CaO: investigating active surface sites under realistic conditions. *Phys Chem Chem Phys*. 12:14740 - 8

188. Tanaka H, Watanabe T, Chikazawa M. (1997). FTIR and TPD studies on the adsorption of pyridine, n-butylamine and acetic acid on calcium hydroxyapatite. *J Chem Soc Faraday Trans*. 93(24):4377-81.

189. Ben Osman M, Diallo Garcia S, Krafft JM, Methivier C, Blanchard J, Yoshioka T, et al. (2016). Control of calcium accessibility over hydroxyapatite by post precipitation steps: influence on the catalytic reactivity toward alcohols. *Phys Chem Chem Phys*. 18:27837–47.

190. Ben Osman M, Diallo-Garcia S, Herledan V, Yoshioka T, Kubo K, Millot Y, et al. (2015). Discrimination of Surface and Bulk Structure of Crystalline Hydroxyapatite Nanoparticles by NMR. *J Phys Chem C* 119:23008-20.

191. Ospina C, Terra J, Ramirez A, Farina M, Ellis DE, Rossi A. (2012). Experimental evidence and structural modeling of nonstoichiometric (0 1 0) surfaces coexisting in hydroxyapatite nano-crystals. *Colloids and Surfaces B: Biointerfaces*. 89:15-22.

192. Diallo-Garcia S, Ben Osman M, Krafft JM, Casale S, Thomas C, Kubo J, et al. (2014). Identification of Surface Basic Sites and Acid-Base Pairs of Hydroxyapatite. *J Phys Chem C*. 118(24):12744-57.

193. Bolis V, Magnacca G, Cerrato G, Morterra C. (2001). Microcalorimetric and IR-spectroscopic study of the room temperature adsorption of CO2 on pure and sulphated t-ZrO2. *Thermochim Acta*. 379:147–61.

194. Charlot G. (1974). *Chimie analytique quantitative*. Masson et Cie ed. Paris.

195. Gee A, Deitz VR. (1953). Determination of phosphate by differential spectrophotometry. *Analytical Chemistry*. 25(9):1320-4.

196. Rey C, Collins B, Goehl T, Dickson IR, Glimcher MJ. (1989). The carbonate environment in bone mineral: a resolution-enhanced Fourier transform infrared spectroscopy study. *Calcified Tissue International*. 45(3):157-64.

197. Combes C, Rey C, Mounic S. (2000). Identification and evaluation of HPO4 ions in biomimetic poorly crystalline apatite and bone mineral. *Key Engineering Materials*. 192:143-6.

198. Rey C, Marsan O, Combes C, Drouet C, Grossin D, Sarda S. (2014). Characterization of calcium phosphates using vibrational spectroscopies. In *Advances in calcium phosphate biomaterials*: Springer. p. 229-66.

199. Ducheyne P, Van Raemdonck W, Heughebaert J, Heughebaert M. (1986). Structural analysis of hydroxyapatite coatings on titanium. *Biomaterials*. 7(2):97-103.

200. Howie R. (1974). (D.) McConnell. Apatite: its crystal chemistry, mineralogy, utilization, and geologic and biologic occurrences. Applied Mineralogy, Volume 5. Vienna and New York (Springer-Verlag), 1973. xvi+ III pp., 17 figs. Price $314 (DM 47; $14.90). *Mineralogical Magazine*. 39(305):617-8.

201. Ioku K, Yamauchi S, Fujimori H, Goto S, Yoshimura M. (2002). Hydrothermal preparation of fibrous apatite and apatite sheet. *Solid State Ionics*. 151(1-4):147-50.

202. Sakhno Y, Bertinetti L, Iafisco M, Tampieri A, Roveri N, Martra G. (2010). Surface hydration and cationic sites of nanohydroxyapatites with amorphous or crystalline surfaces: a comparative study. *The Journal of Physical Chemistry C*. 114(39):16640-8.

203. Bres E, Hutchison J, Senger B, Voegel J-C, Frank R. (1991). HREM study of irradiation damage in human dental enamel crystals. *Ultramicroscopy*. 35(3-4):305-22.

204. Suvorova E, Buffat P-A. (2001). Size effect in X-ray and electron diffraction patterns from hydroxyapatite particles. *Crystallography Reports*. 46(5):722-9.

205. Wiesendanger R. (1994). *Scanning probe microscopy and spectroscopy: methods and applications*: Cambridge University Press.

206. Siedlecki CA, Marchant RE. (1998). Atomic force microscopy for characterization of the biomaterial interface. *Biomaterials*. 19(4):441-54.

207. Jiang W, Pan H, Cai Y, Tao J, Liu P, Xu X, et al. (2008). Atomic force microscopy reveals hydroxyapatite− citrate interfacial structure at the atomic level. *Langmuir*. 24(21):12446-51.

208. Wallwork ML, Kirkham J, Zhang J, Smith DA, Brookes SJ, Shore RC, et al. (2001). Binding of matrix proteins to developing enamel crystals: an atomic force microscopy study. *Langmuir*. 17(8):2508-13.

209. Engel G, Klee W. (1972). Infrared spectra of the hydroxyl ions in various apatites. *Journal of Solid State Chemistry*. 5(1):28-34.

210. Diallo-Garcia S, Ben Osman M, Krafft JM, Boujday S, Costentin G. (2014). Discrimination of infra red fingerprints of bulk and surface POH and OH of hydroxypatites. *Catal Today*. 226:81–8.

211. Errassifi F, Sarda S, Barroug A, Legrouri A, Sfihi H, Rey C. (2014). Infrared, Raman and NMR investigations of risedronate adsorption on nanocrystalline apatites. *Journal of Colloid and Interface Science*. 420(0):101-11.

212. Fowler B, Moreno E, Brown W. (1966). Infra-red spectra of hydroxyapatite, octacalcium phosphate and pyrolysed octacalcium phosphate. *Archives of Oral Biology*. 11(5):477-92.

213. Penel G, Leroy N, Van Landuyt P, Flautre B, Hardouin P, Lemaitre J, et al. (1999). Raman microspectrometry studies of brushite cement: in vivo evolution in a sheep model. *Bone*. 25(2):81S-4S.

214. Barroug A, Rey C, Trombe J, editors. Precipitation and formation mechanism of type AB carbonate apatites analogous to dental enamel. Advanced Materials Research; 1994: Trans Tech Publ.

215. Beshah K, Rey C, Glimcher M, Schimizu M, Griffin R. (1990). Solid state carbon-13 and proton NMR studies of carbonate-containing calcium phosphates and enamel. *Journal of Solid State Chemistry*. 84(1):71-81.

216. Fraissard J, Lapina O. (2012). *Magnetic resonance in colloid and interface science*: Springer Science & Business Media.

217. Eichert D, Salome M, Banu M, Susini J, Rey C. (2005). Preliminary characterization of calcium chemical environment in apatitic and non-apatitic calcium phosphates of biological interest by X-ray absorption spectroscopy. *Spectroc Acta Pt B-Atom Spectr*. 60(6):850-8.

218. Cazalbou S, Combes C, Eichert D, Rey C, Glimcher MJ. (2004). Poorly crystalline apatites: evolution and maturation in vitro and in vivo. *Journal of bone and mineral metabolism*. 22(4):310-7.

219. Eichert D, Combes C, Drouet C, Rey C, editors. Formation and evolution of hydrated surface layers of apatites. Key Engineering Materials; 2005: Trans Tech Publ.

220. Yesinovski JP, Eckert H. (1987). Hydrogen environments in calcium phosphates: 1H MAS NMR at high spinning speeds. *J Am Chem Soc*. 109:6274-82.

221. Yesinowski JP. (1998). Nuclear magnetic resonance spectroscopy of calcium phosphates. In *Calcium phosphates in biological and industrial systems*: Springer. p. 103-43.

222. Pourpoint F, Gervais C, Bonhomme-Coury L, Azais T, Coelho C, Mauri F, et al. (2007). Calcium phosphates and hydroxyapatite: Solid-state NMR experiments and first-principles calculations. *Applied Magnetic Resonance*. 32(4):435-57.

223. Aue W, Roufosse A, Glimcher M, Griffin R. (1984). Solid-state phosphorus-31 nuclear magnetic resonance studies of synthetic solid phases of calcium phosphate: potential models of bone mineral. *Biochemistry*. 23(25):6110-4.

224. Miquel J, Facchini L, Legrand A, Rey C, Lemaitre J. (1990). Solid state NMR to study calcium phosphate ceramics. *Colloids and surfaces*. 45:427-33.

225. Wu Y, Glimcher M, Rey C. (1994). Unique protonated group in bone mineral not present in synthetic calcium phosphates–Identification by phosphorous-31 solid state NMR spectroscopy. *J Mol Biol*. 244:423-35.

226. Jarlbring M, Sandström DE, Antzutkin ON, Forsling W. (2006). Characterization of active phosphorus surface sites at synthetic carbonate-free fluorapatite using single-pulse 1H, 31P, and 31P CP MAS NMR. *Langmuir*. 22(10):4787-92.

227. Lin T-J, Heinz H. (2016). Accurate force field parameters and pH resolved surface models for hydroxyapatite to understand structure, mechanics, hydration, and biological interfaces. *The Journal of Physical Chemistry C*. 120(9):4975-92.

228. Yuan Z, Li S, Liu J, Kong X, Gao T. (2018). Structural, electronic, dynamical and thermodynamic properties of $Ca_{10}(PO_4)_6(OH)_2$ and $Sr_{10}(PO_4)_6(OH)_2$: First-principles study. *International Journal of Hydrogen Energy*. 43(29):13639-48.

229. Cheng X, Wu H, Zhang L, Ma X, Zhang X, Yang M. (2017). Hydroxyl migration disorders the surface structure of hydroxyapatite nanoparticles. *Applied Surface Science*. 416:901-10.

230. Drouet C. (2015). A comprehensive guide to experimental and predicted thermodynamic properties of phosphate apatite minerals in view of applicative purposes. *the Journal of Chemical Thermodynamics*. 81:143-59.

231. 231. Drouet C, Alphonse P. ThermAP additive model for applied predictive thermodynamics. Therm'AP free calculation program, www.christophedrouet.com/thermAP (2015).

232. Glasser L. (2019). Apatite Thermochemistry: The Simple Salt Approximation. *Inorganic Chemistry*. 58(19):13457-63.

233. Drouet C. (2019). Applied predictive thermodynamics (ThermAP). Part 2. Apatites containing Ni^{2+}, Co^{2+}, Mn^{2+}, or Fe^{2+} ions. *The Journal of Chemical Thermodynamics*. 136:182-9.

234. Li C-X, Duan Y-H, Hu W-C. (2015). Electronic structure, elastic anisotropy, thermal conductivity and optical properties of calcium apatite Ca5(PO4)3X (X=F, Cl or Br). *Journal of Alloys and Compounds*. 619:66-77.

235. Wang Q, Li P, Tang P, Ge X, Ren F, Zhao C, et al. (2019). Experimental and simulation studies of strontium/fluoride-codoped hydroxyapatite nanoparticles with osteogenic and antibacterial activities. *Colloids and Surfaces B: Biointerfaces*. 182:110359.

236. Cruz FJAL, Canongia Lopes JN, Calado JCG, Minas da Piedade ME. (2005). A Molecular Dynamics Study of the Thermodynamic Properties of Calcium Apatites. 1. Hexagonal Phases. *The Journal of Physical Chemistry B*. 109(51):24473-9.

237. Cruz FJAL, Canongia Lopes JN, Calado JCG. (2006). Molecular Dynamics Study of the Thermodynamic Properties of Calcium Apatites. 2. Monoclinic Phases. *The Journal of Physical Chemistry B*. 110(9):4387-92.

238. Garley A, Hoff SE, Saikia N, Jamadagni S, Baig A, Heinz H. (2019). Adsorption and Substitution of Metal Ions on Hydroxyapatite as a Function of Crystal Facet and Electrolyte pH. *The Journal of Physical Chemistry C*. 123(27):16982-93.

239. Rollin-Martinet S, Navrotsky A, Champion E, Grossin D, Drouet C. (2013). Thermodynamic basis for evolution of apatite in calcified tissues. *American Mineralogist*. 98(11-12):2037-45.

240. Hosseini SM, Drouet C, Al-Kattan A, Navrotsky A. (2014). Energetics of lanthanide-doped calcium phosphate apatite. *American Mineralogist*. 99(11-12):2320-7.

241. Drouet C, Aufray M, Rollin-Martinet S, Vandecandelaère N, Grossin D, Rossignol F, et al. Nanocrystalline apatites: The fundamental role of water. American Mineralogist2018. p. 550.

242. Wopenka B, Pasteris JD, Yoder CH. (2014). Molecular water in nominally unhydrated carbonated hydroxylapatite: The key to a better understanding of bone mineral†. *American Mineralogist*. 99(1):16-27.

243. Vandecandelaere N, Rey C, Drouet C. (2012). Biomimetic apatite-based biomaterials: on the critical impact of synthesis and post-synthesis parameters. *Journal of Materials Science: Materials in Medicine*. 23(11):2593--606.

244. Drouet C, Carayon M-T, Combes C, Rey C. (2008). Surface enrichment of biomimetic apatites with biologically-active ions Mg2+ and Sr2+: A preamble to the activation of bone repair materials. *Materials Science and Engineering: C*. 28(8):1544-50.

245. Trombe JC, Montel G. (1978). Some features of the incorporation of oxygen in different oxidation state in the apatitic lattice-1 On the existence of calcium and strontium oxyapatites. *J Inorg Nucl Chem*. 40:15-21.

246. Tõnsuaadu K, Gross KA, Plūduma L, Veiderma M. (2012). A review on the thermal stability of calcium apatites. *Journal of Thermal Analysis and Calorimetry*. 110(2):647-59.

247. Tanaka H, Chikazawa M, Kandori K, Ishikawa T. (2000). Influence of thermal treatment on the structure of calcium hydroxyapatite. *Physical Chemistry Chemical Physics*. 2(11):2647-50.

248. Wang T, Dorner-Reisel A, Müller E. (2004). Thermogravimetric and thermokinetic investigation of the dehydroxylation of a hydroxyapatite powder. *Journal of the European Ceramic Society*. 24(4):693-8.

249. Heughebaert JC. (1977). Contribution à l'étude de l'évolution des othophosphates de calcium précipités amorphes en orthophosphates apatitiques. Institut National Polytechnique de Toulouse, Toulouse, France.

250. Cacciotti I, Bianco A, Lombardi M, Montanaro L. (2009). Mg-substituted hydroxyapatite nanopowders: Synthesis, thermal stability and sintering behaviour. *Journal of the European Ceramic Society*. 29(14):2969-78.

251. Baig A, Fox J, Young R, Wang Z, Hsu J, Higuchi W, et al. (1999). Relationships among carbonated apatite solubility, crystallite size, and microstrain parameters. *Calcified Tissue International*. 64(5):437-49.

252. Brown WE, Chow LC, Mathew M. (1983). Thermodynamics of hydroxyapatite surfaces. *Croatica Chemica Acta*. 56(4):779-87.

253. McDowell H, Gregory T, Brown W. (1977). Solubility of Ca5 (P04) 3OH in the System Ca (OH) 2-H3P04-H20 at 5, 15, 25, and 37 C. *J Res Natl Bur Stand Sec A*. 81:273-781.

254. Chow LC, Eanes E. (2001). Solubility of calcium phosphates. *Monographs in oral science*. 18:94-111.

255. LeGeros RZ. (1993). Biodegradation and bioresorption of calcium phosphate ceramics. *Clinical materials*. 14(1):65-88.

256. Baig AA, Fox JL, Hsu J, Wang Z, Otsuka M, Higuchi WI, et al. (1996). Effect of Carbonate Content and Crystallinity on the Metastable Equilibrium Solubility Behavior of Carbonated Apatites. *Journal of Colloid and Interface Science*. 179(2):608-17.

257. Hsu J, Fox JL, Higuchi WI, Powell GL, Otsuka M, Baig A, et al. (1994). Metastable equilibrium solubility behavior of carbonated apatites. *Journal of colloid and interface science*. 167(2):414-23.

258. Chhettry A, Wang Z, Hsu J, Fox JL, Baig AA, Barry AM, et al. (1999). Metastable equilibrium solubility distribution of carbonated apatite as a function of solution composition. *Journal of colloid and interface science*. 218(1):57-67.

259. Chander S, Fuerstenau D. (1984). Solubility and interfacial properties of hydroxyapatite: a review. In *Adsorption on and surface chemistry of hydroxyapatite*: Springer. p. 29-49.

260. El Shafei GM, Moussa NA. (2001). Adsorption of some essential amino acids on hydroxyapatite. *Journal of colloid and interface science*. 238(1):160-6.

261. Wu L, Forsling W, Schindler PW. (1991). Surface complexation of calcium minerals in aqueous solution: 1. Surface protonation at fluorapatite—water interfaces. *Journal of Colloid and Interface Science*. 147(1):178-85.

262. Boix T, Gomez-Morales J, Torrent-Burgues J, Monfort A, Puigdomènech P, Rodriguez-Clemente R. (2005). Adsorption of recombinant human bone morphogenetic protein rhBMP-2m onto hydroxyapatite. *Journal of inorganic biochemistry*. 99(5):1043-50.

263. Misra DN. (1984). *Adsorption on and surface chemistry of hydroxyapatite*: Springer.

264. Saleeb F, De Bruyn P. (1972). Surface properties of alkaline earth apatites. *Journal of Electroanalytical Chemistry and Interfacial Electrochemistry*. 37(1):99-118.

265. Botelho C, Lopes M, Gibson IR, Best S, Santos J. (2002). Structural analysis of Si-substituted hydroxyapatite: zeta potential and X-ray photoelectron spectroscopy. *Journal of Materials Science: Materials in Medicine*. 13(12):1123-7.

266. Ducheyne P, Pollack S, Kim C. (1991). HA powder were reported before." The calcium-deficient HA had a Ca/Pratio of 1.58, a specific. *Electromagnetics in Medicine and Biology*.49.

267. Bouladjine A, Al-Kattan A, Dufour P, Drouet C. (2009). New advances in nanocrystalline apatite colloids intended for cellular drug delivery. *Langmuir*. 25(20):12256-65.

268. Mangood A, Malkaj P, Dalas E. (2006). Hydroxyapatite crystallization in the presence of acetaminophen. *Journal of crystal growth*. 290(2):565-70.

269. Palazzo B, Walsh D, Iafisco M, Foresti E, Bertinetti L, Martra G, et al. (2009). Amino acid synergetic effect on structure, morphology and surface properties of biomimetic apatite nanocrystals. *Acta Biomaterialia*. 5(4):1241-52.

270. dos Santos EA, Farina M, Soares GA, Anselme K. (2008). Surface energy of hydroxyapatite and beta-tricalcium phosphate ceramics driving serum protein adsorption and osteoblast adhesion. *J Mater Sci Mater Med*. 19(6):2307-16.

271. Wu W, Nancollas GH. (1999). Determination of interfacial tension from crystallization and dissolution data: a comparison with other methods. *Advances in Colloid and Interface Science*. 79:229-79.

272. Tang R, Wu W, Haas M, Nancollas G. (2001). Kinetics of Dissolution of beta-tricalcium phosphate. *Langmuir*. 17:3480-5.

273. Wang X, Zhang Q. (2020). Insight into the Influence of Surface Roughness on the Wettability of Apatite and Dolomite. *Minerals*. 10:114.

274. Rakovan J. (2020). Growth and Surface Properties of Apatite. *Reviews in Mineralogy and Geochemistry*. 48(1):51-86.

275. Tung D MSaS. (2001). Interfacial properties of hydroxyapatite, fluorapatite and octacalcium phosphate. In, Eanes LCCED, editor.: Karger. p. 112-29.

276. Médout-Marère V, Belarbi H, Thomas P, Morato F, Giuntini JC, Douillard JM. (1998). Thermodynamic Analysis of the Immersion of a Swelling Clay. *Journal of Colloid and Interface Science*. 202(1):139-48.

277. Douillard JM. (1996). What Can Really Be Deduced from Enthalpy of Immersional Wetting Experiments? *Journal of Colloid and Interface Science*. 182(1):308-11.

278. Dorozhkin SV. (2012). Dissolution mechanism of calcium apatites in acids: A review of literature. *World journal of methodology*. 2(1):1-17.

279. Christoffersen J, Christoffersen MR, Johansen T. (1996). Kinetics of growth and dissolution of fluorapatite. *Journal of Crystal Growth*. 163(3):295-303.

280. Tang R, Henneman ZJ, Nancollas GH. (2003). Constant composition kinetics study of carbonated apatite dissolution. *J Cryst Growth*. 249:614-24.

281. Nancollas GH. (2000). The Control of Mineralization on Natural and Implant Surfaces. In, Scheid PLPCTKRLC, editor.: Materials Research Society, Warrendale (PA, USA). p. 99-108.

282. Wu WaN. (1999). Determination of interfacial tension from crystallization and dissolution data: a comparison with other methods. *Advances in Colloid and Interface Science*. 79:229-79.

283. Suzuki T, Hirose G, Oishi S. (2004). Contact angle of water droplet on apatite single crystals. *Materials Research Bulletin*. 39(1):103-8.

284. Redey SA, Nardin M, Bernache-Assolant D, Rey C, Delannoy P, Sedel L, et al. (2000). Behavior of human osteoblastic cells on stoichiometric hydroxyapatite and type A carbonate apatite: Role of surface energy. *Journal of Biomedical Materials Research*. 50:353-64.

285. Deymier AC, Nair AK, Depalle B, Qin Z, Arcot K, Drouet C, et al. (2017). Protein-free formation of bone-like apatite: New insights into the key role of carbonation. *Biomaterials*. 127:75-88.

286. Fleche JL. (2002). Thermodynamical functions for crystals with large unit cells such as zircon, coffinite, fluorapatite, and iodoapatite from ab initio calculations. *Physical Review B*. 65(24):245116.

287. Xie J, Zhang Q, Mao S, Li X, Shen Z, Li L. (2019). Anisotropic crystal plane nature and wettability of fluorapatite. *Applied Surface Science*. 493:294-307.

288. Wang X, Zhang L, Liu Z, Zeng Q, Jiang G, Yang M. (2018). Probing the surface structure of hydroxyapatite through its interaction with hydroxyl: a first-principles study. *RSC Advances*. 8(7):3716-22.

289. Zeglinski J, Nolan M, Thompson D, Tofail SA. (2014). Reassigning the most stable surface of hydroxyapatite to the water resistant hydroxyl terminated (010) surface. *Surface science*. 623:55-63.

290. Peccati F, Bernocco C, Ugliengo P, Corno M. (2018). Properties and Reactivity toward Water of A Type Carbonated Apatite and Hydroxyapatite Surfaces. *The Journal of Physical Chemistry C*. 122(7):3934-44.

291. Sun JP, Song Y. (2018). Strengthening Adhesion of the Hydroxyapatite and Titanium Interface by Substituting Silver and Zinc: A First Principles Investigation. *ACS Applied Nano Materials*. 1(9):4940-54.

292. Wang X, Wu H, Cheng X, Yang M, Zhang L. (2020). Probing the surface activity of hydroxyapatite nanoparticles through their interaction with water molecules. *AIP Advances*. 10(6):065217.

293. Lou Z, Zeng Q, Chu X, Yang F, He D, Yang M, et al. (2012). First-principles study of the adsorption of lysine on hydroxyapatite (100) surface. *Applied Surface Science*. 258(11):4911-6.

294. Corno M, Busco C, Bolis V, Tosoni S, Ugliengo P. (2009). Water Adsorption on the Stoichiometric (001) and (010) Surfaces of Hydroxyapatite: A Periodic B3LYP Study. *Langmuir*. 25(4):2188-98.

295. Hauptmann S, Dufner H, Brickmann J, Kast SM, Berry RS. (2003). Potential energy function for apatites. *Physical Chemistry Chemical Physics*. 5(3):635-9.

296. de Leeuw NH. (2004). A computer modelling study of the uptake and segregation of fluoride ions at the hydrated hydroxyapatite (0001) surface: introducing a Ca10(PO4)6(OH)2 potential model. *Physical Chemistry Chemical Physics*. 6(8):1860-6.

297. Carniti P, Gervasini A. (2013). Liquid-solid adsorption properties: Measurement of the effective surface acidity of solid catalysts. In *Calorimetry and Thermal Methods in Catalysis*: Springer. p. 543-51.

298. Wilson RM, Elliot JC, Dowker SEP. (2003). Formate incorporation in the structure of Ca-deficient apatite: rietveld structure refinement. *JSolid State Chem*. 174:132-40.

299. Hill IM, Hanspal S, Young ZD, Davis RJ. (2015). DRIFTS of Probe Molecules Adsorbed on Magnesia, Zirconia, and Hydroxyapatite Catalysts. *J Phys Chem C*. 119:9186−97.

300. Elkabouss K, Kacimi M, Ziyad M, Bozon-Verduraz F. (2005). Catalytic behaviour of cobalt exchanged hydroxyapatite in the oxidative dehydrogenation of ethane. *J Phys IV*. 123:313-7.

301. Sugiyama S, Hayashi H. (2003). Role of hydroxide groups in hydroxyapatite catalysis for the oxidative dehydrogenation of alkanes. *Int J Modern Physics B*. 17:1476-81.

302. Petit S, Gode T, Thomas C, Dzwigaj S, Millot Y, Brouri D, et al. (2017). Incorporation of Vanadium in the Framework of Hydroxyapatites: Importance of the Vanadium Content and pH Conditions during the Precipitation Step. *Phys Chem Chem Phys*. 19:9630 – 40.

303. Tanaka Y, Kikuchi M, Tanaka K, Hashimoto K, Hojo J, Nakamura M, et al. (2010). Fast Oxide Ion Conduction Due to Carbonate Substitution in Hydroxyapatite. *J Am Ceram Soc, .* 93(11):3577-9.

304. Elkabouss K, Kacimi M, Ziyad M, Ammar S, Bozon-verduraz F. (2004). Cobalt-exchanged hydroxyapatite catalysts: magnetic studied, spectroscopic investigations, performance in 2-butanol and ethane oxidative dehydrogenations. *J Catal*. 226:16-24.

305. Sugiyama S, Matsumoto H, Hayashi H, Moffat JB. (2000). Sorption and ion-exchange properties of barium hydroxyapatite with divalent cations. *Colloids Surf A*. 169(1):17-26.

306. Matsunaga K, Murata H, Mizoguchi T, Nakahira A. (2010). Mechanism of incorporation of zinc into hydroxyapatite. *Acta Biomaterialia*. 6(6):2289-93.

307. Campisi S, Castellano C, Gervasini A. (2018). Tailoring the structural and morphological properties of hydroxyapatite materials to enhance the capture efficiency towards copper(II) and lead(II) ions. *New J Chem*. 42:4520.

308. Terra J, Gonzalez GB, Rossi AM, Eon JG, Ellis DE. (2010). Theoretical and experimental studies of substitution of cadmium into hydroxyapatite. *Phys Chem Chem Phys*. 12(47):15490-500.

309. Ogo S, Onda A, Yanagisawa K. (2008). Hydrothermal synthesis of vanadate-substituted hydroxyapatites, and catalytic properties for conversion of 2-propanol. *Appl Catal A*. 348:129-34.

310. Zhu Y, Zhang X, Long F, Liu H, Qian M, He N. (2009). Synthesis and characterization of arsenate/phosphate hydroxyapatite solid solution. *Materials Letters*. 63(13):1185-8.

311. Hughes JM, Cameron M, Crowley KD. (1989). Structural variations in natural F, OH, and Cl apatites. *Am Mineral*. 74:870–6.

312. Kaur K, Singh KJ, Anand V, Islam N, Bhatia G, Kalia N, et al. (2017). Lanthanide (=Ce, Pr, Nd and Tb) ions substitution at calcium sites of hydroxyl apatite nanoparticles as fluorescent bio probes: Experimental and density functional theory study. *Ceram Int*. 43(13):10097-108.

313. Gibson LR, Skakle JMS, inventors Silicate- substituted hydroxyapatite. patent W02010079316A1. 2010.

314. Solonenko AP, Golovanova OA. (2014). Silicate Substituted Carbonated Hydroxyapatite Powders Prepared by Precipitation from Aqueous Solutions. *Russian Journal of Inorganic Chemistry*. 59(11):1228-36.

315. Onda A, Ogo S, Iwasa Y, Matsuura Y, Yanagisawa K. (2013). Conversion of Ethanol into 1-Butanol over Strontium Phosphate Apatite Catalysts. *ABC-7*.

316. Cazalbou S, Eichert D, Ranz X, Drouet C, Combes C, Harmand MF, et al. (2005). Ion exchanges in apatites for biomedical application. *J Mater Sci-Mater Med*. 16(5):405-9.

317. Tõnsuaadu K, Gruselle M, Villain F, Thouvenot R, Peld M, Mikli V, et al. (2006). A new glance at ruthenium sorption mechanism on hydroxy, carbonate, and fluor apatites: Analytical and structural studies. *Journal of colloid and interface science*. 304(2):283-91.

318. Tang Y, Chappell HF, Dove MT, Reeder RJ, Lee YJ. (2009). Zinc incorporation into hydroxylapatite. *Biomaterials*. 30(15):2864-72.

319. Saito T, Yokoi T, Nakamura A, Matsunaga K. (2020). Formation energies and site preference of substitutional divalent cations in carbonated apatite. *J Amer Ceram Soc*. 103(9):5354-64.

320. Mostafa NY, Hassan MH, Abd Elkader OH. (2011). Preparation and Characterization of Na1,SiO44 ,andCO32- Co-Substituted Hydroxyapatite. *J Am Ceram Soc*. 94(5):1594-0.

321. Lee SJ, Jun JH, Lee S-H, Yoon KJ, Lim TH, Nam S-W, et al. (2002). Partial oxidation of methane over nickel-added strontium phosphate. *Appl Catal A*. 230(1):61-71.

322. Qu Z, Sun Y, Chen D, Wang Y. (2014). Possible sites of copper located on hydroxyapatite structure and the identification of active sites for formaldehyde oxidation. *Journal of Molecular Catalysis A: Chemical*. 393:182-90.

323. Errassifi F, Menbaoui A, Autefage H, Benaziz L, Ouizat S, Santran V, et al. Adsorption on apatitic calcium phosphates: application to drug delivery. In: Soc AC, editor. 8th Pacific Rim Conference on Ceramic and Glass Technology; Vancouver, Canada2010. p. 159-74.

324. Bootchanont A, Sailuam W, Sutikulsombat S, Temprom L, Chanlek N, Kidkhunthod P, et al. (2017). Synchrotron X-ray Absorption Spectroscopy study of local structure in strontium-doped hydroxyapatite. *Ceram Int*. 43(14):11023-7.

325. Bazin D, Daudon M, Chappard c, Rehr JJ, Thiaudière D, Reguer S. (2011). The status of strontium in biological apatites: an XANES investigation. *J Synchrotron Rad*. 18:912-8.

326. Al-Kattan A, Errassifi F, Sautereau AM, Sarda S, Dufour P, Barroug A, et al. (2010). Medical Potentialities of Biomimetic Apatites through Adsorption, Ionic Substitution, and Mineral/Organic Associations: Three Illustrative Examples. *Adv Eng Mater*. 12(7):B224-B33.

327. Chen X, Wright JV, Conca JL, Peurrung LM. (1997). Effects of pH on heavy metal sorption on mineral apatite. *Environmental Science & Technology*. 31(3):624-31.

328. Xu Y, Schwartz FW, Traina SJ. (1994). Sorption of Zn2+ and Cd2+ on hydroxyapatite surfaces. *Environmental Science & Technology*. 28(8):1472-80.

329. Michelot A, Sarda S, Audin C, Deydier E, Manoury E, Poli R, et al. (2015). Spectroscopic characterisation of hydroxyapatite and nanocrystalline apatite with grafted

aminopropyltriethoxysilane: nature of silane–surface interaction. *Journal of Materials Science*. 50(17):5746-57.

330. Prakash M, Lemaire T, Caruel M, Lewerenz M, de Leeuw NH, Di Tommaso D, et al. (2017). Anisotropic diffusion of water molecules in hydroxyapatite nanopores. *Physics and Chemistry of Minerals*. 44(7):509-19.

331. Honorio T, Lemaire T, Di Tommaso D, Naili S. (2019). Anomalous water and ion dynamics in hydroxyapatite mesopores. *Computational Materials Science*. 156:26-34.

332. Lemaire T, Pham T, Capiez-Lernout E, de Leeuw NH, Naili S. (2015). Water in hydroxyapatite nanopores: possible implications for interstitial bone fluid flow. *Journal of biomechanics*. 48(12):3066-71.

333. Viipsi K, Sjöberg S, Tõnsuaadu K, Shchukarev A. (2013). Hydroxy-and fluorapatite as sorbents in Cd (II)–Zn (II) multi-component solutions in the absence/presence of EDTA. *Journal of hazardous materials*. 252:91-8.

334. Mignardi S, Corami A, Ferrini V. (2013). Immobilization of Co and Ni in Mining-Impacted Soils Using Phosphate Amendments. *Water Air Soil Pollut*. 224:1447.

335. Chen X, Wright JV, Conca JL, Peurrung LM. (1997). Evaluation of heavy metal remediation using mineral apatite. *Water, Air, and Soil Pollution* 98:57-78.

336. Vila M, Sánchez-Salcedo S, Vallet-Regí M. (2012). Hydroxyapatite foams for the immobilization of heavy metals: From waters to the human body. *Inorganica Chimica Acta*. 393:24-35.

337. Mori K, Mitani Y, Hara T, Mizugaki T, Ebitani K, Kaneda K. (2005). A single-site hydroxyapatite-bound zinc catalyst for highly efficient chemical fixation of carbon dioxide with epoxides. *Chemical Communications*. (26):3331-3.

338. Mondelli C, Ferri D, Baiker A. (2008). Ruthenium at work in Ru-hydroxyapatite during the aerobic oxidation of benzyl alcohol: An in situ ATR-IR spectroscopy study. *J Catal*. 258(1):170-6.

339. Opre Z, Grunwaldt JD, Maciejewski M, Ferri D, Mallat T, Baiker A. (2005). Promoted Ru–hydroxyapatite: designed structure for the fast and highly selective oxidation of alcohols with oxygen. *J Catal*. 230:406-19.

340. Sugiyama S, Minami T, Hayashi H, Tanaka M, Shigemoto N, Moffat JB. (1996). Enhancement of the selectivity to carbon monoxide with feedstream doping by tetrachloromethane in the oxidation of methane on stoichiometric calcium hydroxyapatite. *Journal of the Chemical Society, Faraday Transactions*. 92(2):293-9.

341. Neuman W, Toribara T, Mulryan B. (1956). The Surface Chemistry of Bone. IX. Carbonate: Phosphate Exchange1. *Journal of the American Chemical Society*. 78(17):4263-6.

342. Yamaguchi K, Mori K, Mizugaki T, Ebitani K, Kaneda K. (2000). Creation of a monomeric Ru species on the surface of hydroxyapatite as an efficient heterogeneous catalyst for aerobic alcohol oxidation. *Journal of the American Chemical Society*. 122(29):7144-5.

343. Akri M, El Kasmi A, Batiot-Dupeyrat C, Qiao B. (2020). Highly Active and Carbon-Resistant Nickel Single-Atom Catalysts for Methane Dry Reforming. *Catalysts*. 10(6):630.

344. El Kabouss K, Kacimi M, Ziyad M, Ammar S, Ensuque A, Piquemal JY, et al. (2006). Cobalt speciation in cobalt oxide-apatite materials: structure–properties relationship in catalytic oxidative dehydrogenation of ethane and butan-2-ol conversion. *J Mater Chem*. 16:2453-63.

345. Josse S, Faucheux C, Soueidan A, Grimandi G, Massiot D, Alonso B, et al. (2005). Novel biomaterials for bisphosphonate delivery. *Biomaterials*. 26(14):2073-80.

346. Mukherjee S, Huang C, Guerra F, Wang K, Oldfield E. (2009). Thermodynamics of bisphosphonates binding to human bone: a two-site model. *Journal of the American Chemical Society*. 131(24):8374-5.

347. Choimet M, Tourrette A, Drouet C. (2015). Adsorption of nucleotides on biomimetic apatite: The case of cytidine 5′ monophosphate (CMP). *Journal of colloid and interface science*. 456:132-7.

348. Hammami K, El Feki H, Marsan O, Drouet C. (2015). Adsorption of nucleotides on biomimetic apatite: The case of adenosine 5′ monophosphate (AMP). *Applied Surface Science*. 353:165-72.

349. Pascaud P, Errassifi F, Brouillet F, Sarda S, Barroug A, Legrouri A, et al. (2014). Adsorption on apatitic calcium phosphates for drug delivery: interaction with bisphosphonate molecules. *Journal of Materials Science: Materials in Medicine*. 25(10):2373-81.

350. Benaziz L, Barroug A, Legrouri A, Rey C, Lebugle A. (2001). Adsorption of O-Phospho-L-Serine and L-Serine onto Poorly Crystalline Apatite. *Journal of Colloid and Interface Science*. 238(1):48-53.

351. Barroug A, Legrouri A, Rey C. (2008). Exchange reactions at calcium phosphates surface and applications to biomaterials. *Key Engineering Materials*. 361-363:79-82.

352. Misra DN. (1998). Interaction of some alkali metal citrates with hydroxyapatite: Ion-exchange adsorption and role of charge balance. *Colloids and Surfaces A: Physicochemical and Engineering Aspects*. 141(2):173-9.